A NETWORK MODEL OF THE HUMAN AQUEOUS OUTFLOW SYSTEM

by

DAVID BENEDICT YAN

B.A.Sc., Engineering Science
University of Toronto
(1986)

SUBMITTED TO THE DEPARTMENT OF
MECHANICAL ENGINEERING
IN PARTIAL FULFILLMENT OF THE REQUIREMENTS
FOR THE DEGREE OF

MASTER OF SCIENCE IN MECHANICAL ENGINEERING

at the

MASSACHUSETTS INSTITUTE OF TECHNOLOGY

May, 1988

Signature of Author: _____

Department of Mechanical Engineering
May 6, 1988

Certified by: _____

Professor Roger D. Kamm
Department of Mechanical Engineering
Thesis Supervisor

Certified by: _____

Dr. Mark C. Johnson
Department of Mechanical Engineering
Thesis Supervisor

Accepted by: _____

Professor Ain. A. Sonin
Department Graduate Committee

A NETWORK MODEL OF THE HUMAN AQUEOUS OUTFLOW SYSTEM

by

DAVID B. YAN

Submitted to the Department of Mechanical Engineering
on May 6, 1988 in partial fulfillment of the
requirements for the Degree of
Master of Science in Mechanical Engineering

ABSTRACT

The outflow system of the human eye consists of three distinct regions: the trabecular meshwork, Schlemm's canal and the collector channels. As aqueous humor passes through this network from the anterior chamber to the episcleral venous system, its fluid pressure typically drops 7 mmHg in normal eyes and up to 40 mmHg in glaucomatous eyes. This study investigates the interactions between the three regions of the outflow system which determine the flow distribution and, consequently, the intraocular pressure. The outflow system is modeled as a network of resistors geometrically arranged to correspond to the anatomical orientation of the outflow regions. Schlemm's canal is modeled as an elliptic channel with a porous, compliant inner wall and a rigid, impermeable outer wall. Experiments were performed to obtain pressure-resistance measurements on enucleated human eyes in the 10-100 mmHg pressure range to study the flow behavior of the outflow system when Schlemm's canal is in a highly collapsed state. Based on a comparison of the model to data accumulated in this study and results reported in the literature, the following conclusions are reached:

1. A network model of the entire aqueous outflow system including a porous, compliant inner wall of Schlemm's canal was constructed and numerically solved. The predictions are consistent with experimental observations and previous numerical results.

2. The experimental pressure-resistance curve for enucleated human eyes was extended to the 50-100 mmHg range. Results indicate that resistance continues to increase linearly with pressure in this range.

3. A one-third power law model of the septae compression was proposed and tested. This model successfully produces a linear relationship between pressure and resistance in agreement with the experimental data.

Thesis Supervisor: Roger Kamm
Associate Professor of
Mechanical Engineering

Acknowledgements

I would like to extend my sincere appreciation to my thesis supervisor, Professor Roger Kamm, whose invaluable guidance and support made this project possible. I would also like to thank Dr. Mark Johnson, who taught me the finer points of how to contribute as an engineer working in ophthalmic research. Together, they have helped me come a long way in making the change from aerospace to biomedical engineering.

I would like to thank the members of the Fluids lab for their friendship during my stay at MIT, and the members of the Howe lab at Mass. Eye & Ear for their help in setting up my experiments.

Finally, I would like to express my warmest thanks to my parents and my girlfriend Rosemary for their endless devotion and support.

Contents

1 Introduction

1.1 Anatomy of the Aqueous Outflow System

Aqueous humor is produced in the ciliary epithelium by a combination of secretion and ultrafiltration at a rate of about 2 μl/min [5]. The aqueous humor then leaves the ciliary body and enters the posterior chamber, from which it proceeds to flow between the iris and the anterior surface of the lens until it reaches the pupil. Once through the pupil, the aqueous humor proceeds to flow radially in the anterior chamber towards the chamber angle. The function served by the circulation of aqueous humor via this pathway is to provide nutrients to the lens, vitreous body, and the cornea.

Upon reaching the chamber angle, the aqueous humor exits from the anterior chamber via two routes. The first route, commonly referred to as the conventional outflow pathway, consists of the trabecular meshwork, Schlemm's canal and the collector channel regions. The aqueous humor can also exit from the anterior chamber via the anterior surface of the ciliary muscle, the suprachoroid and out through the sclera. This route is called the uveoscleral or unconventional pathway, and is of secondary importance as it accounts for only 5-20% of the total drainage at normal intraocular pressure [5]. Uveoscleral outflow does not change significantly as IOP increases, and thus carries a smaller fraction of the total drainage at higher pressures [6]. Since this route plays only a minimal role in determining the IOP, it will not be considered in the context of this study.

The first structure encountered by aqueous humor entering the conventional outflow pathway is the trabecular meshwork, which can be divided into 4 layers: uveal meshwork, corneoscleral meshwork, juxtacanalicular tissue (JCT) and the endothelial lining of Schlemm's canal.

The uveal meshwork is a forward extension of the ciliary muscle [5]; the openings through this meshwork are large and the flow resistance of this layer can be considered negligible [7,12].

The second layer underlying the uveal meshwork is the corneoscleral meshwork, which consists of several flattened, perforated sheets of connective tissue extending between the scleral spur and the cornea. The aqueous humor must travel a long, tortuous path between the meshwork sheets, with the dimensions of the intratrabecular spaces decreasing in the deeper layers of the meshwork [5].

The next layer in the trabecular region is the JCT, which consists of loose connective tissue containing collagen and elastin fibres, ground substance and endothelial-type cells. It is believed that the JCT is the primary site of flow resistance in the trabecular region [7]. The mechanism responsible for this flow resistance is not currently known but for the purposes of this study, it is sufficient to determine the magnitude of the resistance in the entire meshwork region. Since the thickness of the JCT and endothelial lining is much smaller than the thickess of the corneoscleral meshwork or the characteristic circumferential dimension of Schlemm's canal, the precise distribution of the flow resistance within these negligible dimensions need not be determined.

The final layer traversed by the aqueous humor before entering the lumen of Schlemm's canal is the endothelial lining of the inner wall. The mechanism by which fluid passes through the endothelial lining has not been precisely determined, but pores and giant vacuoles have been observed and are thought to be responsible for the passage of aqueous humor through this layer. By counting the number of pores lining the inner wall surface and calculating the resistance of each pore, Bill & Svedbergh [7] determined that no more than 10% of the total outflow resistance could reside in the endothelial lining.

After passing through the endothelial lining, the aqueous humor enters the lumen of Schlemm's canal and moves circumferentially along the canal until it reaches a collector channel (CC) opening in the outer wall. Schlemm's canal has the appearance of a highly elongated ellipse in cross-section, with the endothelial lining acting as the inner wall and the sclera comprising the outer wall. The outer wall is relatively rigid and stationary, maintaining the width of the canal constant as the

system is pressurized. In contrast, the JCT and endothelial lining are supported by the compliant, sponge-like meshwork which can be compressed or expanded depending on the local pressure forces acting on it. This meshwork compliance allows the inner wall to distend radially against the rigid outer wall as the IOP changes, resulting in a variable height for the canal. Beam-like structures called septae [16] or endothelial tubules [18] originating from the endothelial lining will occasionally span across the canal lumen. Some of these structures completely bridge the lumen and temporarily divide the canal into two ducts for a limited circumferential distance [7]. The septae are especially numerous near the CC openings, suggesting that their role may be to prevent complete collapse of the canal and subsequent occlusion of the collector channels [16].

The aqueous humor exits the canal lumen into the collector channels, also referred to as aqueous veins. The collector channels run to the surface of the eye where they anastomose with the episcleral venous system. Casting studies have shown that the collector channels are 10-100μm in diameter [1] and approximately 1 mm in length. Calculations using Poiseiulle's law demonstrate that the apparent calibre of the veins cannot account for the outflow resistance as observed after a complete trabeculotomy [26]. Since the post-trabeculotomy resistances of normal and glaucomatous eyes do not differ significantly [13], the collector channels probably do not play a significant role in causing glaucoma.

1.2 Previous Models of the Outflow System

Past efforts to model the aqueous outflow system have focussed on the role of Schlemm's canal in tying together the three regions of the outflow network. In the following section, these models are reviewed to analyse their successes and limitations in modelling the observed behavior of the outflow system.

1.2.1 Model of Schlemm's Canal as a Porous, Rigid Duct

Moses [21] proposed a model consisting of the meshwork and Schlemm's canal regions of the outflow system. Schlemm's canal is modelled as a *rigid* duct with an elliptical cross-section of constant dimensions and the flow in the canal is assumed to be inertia-free. The meshwork is represented as a porous inner wall with a uniformly distributed conductance which leaks fluid into the canal from the anterior chamber. Since the model neither allows the height nor the width of the canal to vary as a function pressure across the inner wall, the flow resistance of the canal is constant per unit circumferential length. The collector channels are evenly spaced around the outer wall, and the resistance of each CC is negligible compared to the meshwork resistance; thus, the episcleral venous pressure is approximately equal to canal lumen pressure at the mouth of a CC. When all of the conductance parameters and the geometric arrangement of the elements are uniform, the model will be termed *homogeneous*. Under these conditions, the flow boundary conditions can be phrased as:

1. The flow along the canal at the midpoint between adjacent collector channels is zero due to the symmetry of the system.

2. All of the flow must enter the first collector channel reached during its transit in the canal. Thus the rate of flow entering a CC is the same from both sides of the canal.

It can be deduced from these boundary conditions that the pressure and flow distributions are symmetric with respect to a symmetry line located either at a collector channel or at the midpoint between two collector channels. Assuming that an average of 30 collector channels drain Schlemm's canal [21], there are a total of 60 segments in the outflow system with identical flow distributions. One of the major advantages of using a homogeneous model is that only a single segment of the outflow system (from midpoint to a CC opening) needs to be considered. Since the flow to each segment is identical, the correct flowrate for the entire system can be

calculated by multiplying the flowrate into a single segment by the total number of segments.

The governing differential equation for the fluid mechanical situation decribed above is linear and second order. This differential equation can be solved analytically to yield a solution which relates the pressure in the canal lumen to a hyperbolic function of the location in the canal [21].

$$p(x) = P_i + \frac{P - P_i}{cosh(\lambda X)} cosh(\lambda x) \tag{1}$$

where:

$\lambda = \sqrt{RG}$

R = canal resistance per unit circumferential length

G = meshwork conductance per unit circumferential length

x = circumferential coordinate along canal, with x=0 at midpoint

X = distance from midpoint to CC

P_i = intraocular pressure

P = episcleral venous pressure at mouth of CC = p(X)

Note that the collector channel resistance has been neglected, so that the episcleral venous pressure is equal to the pressure in the canal lumen at the CC opening.

This model correctly predicts that the pressure in the canal lumen decreases towards to CC'and is lowest at the mouth of a CC. However, the broad assumptions made to arrive at an analytical solution to the problem result in the following limitations on the phenomenological accuracy of the model:

1. Since the canal height is constant, the outflow resistance is also constant with respect to IOP, contrary to the findings of many studies of the pressure-resistance curve for enucleated human eyes [8,11,22].

2. The homogeneity conditions required to arrive at an analytical solution do not allow for any regional non-uniformities in the outflow system, which would violate the flow boundary conditions detailed above.

Despite these limitations, this model was useful in gaining a qualitative understanding of the fluid flow distribution posed by the geometry of the outflow system. The hyperbolic analytical solution demonstrates the non-linear decrease in pressure as the flow moves towards the collector channels.

1.2.2 Model of Schlemm's Canal as a Porous, Compliant Duct

The next logical step to increase the sophistication of the model introduced by Moses was to make the inner wall compliant, allowing it to distend towards the outer wall as the local pressure gradient between the anterior chamber and the canal lumen increased. Johnson [17] modelled the trabecular meshwork as a bed of linear springs with negligible flow resistance which supports an inner wall (JCT and endothelial lining) with significant resistance. The local canal height h(x) varies linearly with respect to the local pressure drop across the inner wall (IOP-P(x)) according to the relation:

$$\frac{h(x)}{h_0} = 1 - \frac{IOP - P(x)}{E} \tag{2}$$

where h_0 is the undeformed canal height and E is the elastic modulus (or stiffness) of the springs. The flow in the canal is modelled as inertia-free flow between two flat plates. Substantial mathematical complexity is introduced into the governing differential equation, and numerical integration is required to obtain a solution. The differential equation is second order and highly non-linear, with the pressure gradient along the canal inversely proportional to the third power of the local canal height ($dP(x)/dx \sim 1/h^3(x)$). A solutions was obtained for the case of a *homogeneous* outflow system; thus only a single segment from a midpoint between two CC's to the nearest CC was considered. The collector channels were again presumed to produce negligible flow resistance, so that only the meshwork and Schlemm's canal regions of the outflow system were incorporated into the model. Note that equation (2) is valid only in the pressure range where IOP-P(x)<E since the height of the canal cannot be negative. Therefore an additional support structure (septae) was

introduced to prevent the complete collapse of the canal. When the canal collapsed down to the septae support height h_s, the canal was either made more stiff by increasing E or it was made completely rigid by setting the height to be constant at h_s for all pressure drops greater than the value at which the septae become active.

This model simulated the effects of canal collapse on the outflow resistance, producing a moderate rate of resistance increase with increasing IOP. This result was in qualitative agreement with the existing experimental data, and lead to the conclusion that Schlemm's canal cannot be the primary cause of glaucoma because the resistance generated in the fully collapsed state is not glaucomatous.

1.3 Objectives

The Johnson and Moses models both require that the outflow system have a perfectly uniform geometry and conductance distribution. This places a limitation on the resistance which Schlemm's canal can contribute because the greatest possible distance traversed in the canal for the homogeneous case is from the midpoint between two CC's to the nearest CC opening. The Johnson model showed that the resistance generated by Schlemm's canal at 50 mmHg, which corresponds to a completely collapsed state of the canal, is not high enough to cause glaucoma. However, a model of the *entire* outflow system adds a new dimension to the role of Schlemm's canal because cases can be investigated where substantial flow between different regions of the outflow system is induced by significant inhomogeneity in the system. This can take the form of natural non-uniformities in the outflow structures or it can be induced in the system by interventions such as trabeculotomy. Regardless of the cause of the inhomogeneities, a model of the entire outflow system would give us the ability to study their relative importance in determining intraocular pressure in the eye.

The goal in developing a new model of the aqueous outflow system is to retain the complexity of the Johnson model of Schlemm's canal while expanding it to encompass the entire system. This results in the following model criteria:

1. Schlemm's canal is modelled with a porous, compliant inner wall which can deform to locally alter the height of the canal duct according to the mechanical loading on the support structures (i.e., trabecular meshwork and septae).

2. No symmetry or flow boundary conditions will be imposed within the outflow system, so that the flow is free to choose any path to go from the anterior chamber to the episcleral venous system.

3. The collector channel region will be included in the network. The resistance of this region will be based on experimental measurements which indicate that a significant fraction of the total outflow resistance resides in this region.

To accomplish criterion 1, a formulation of the canal height and resistance similar to that of the Johnson model will be used. Criterion 2 eliminates the possibility of an analytical solution and forces the model to encompass the entire outflow system rather than just a single symmetric segment. The approach taken to develop the network model is to accomplish both criteria 1 and 2 by allowing the complexity of the problem to increase to the level where numerical methods must by employed to obtain a solution. The model significantly raises the level of realism in simulating the outflow system at the cost of forgoing the advantages and insights gained by an analytical solution.

The Johnson model produces a pressure-resistance relation which is qualitatively consistent with the experimental data at lower pressures (IOP<40mmHg), where both show the resistance to increase with IOP. The agreement between the model and experimental data is less satisfactory at higher pressures (IOP>40mmHg). If the rigid septae model is chosen, the pressure-resistance curve levels off at high pressure when the inner wall is completely collapsed against the septae. On the other hand, septae which are stiffer than the meshwork but still linearly compliant result in a pressure-resistance relation which curves sharply upward as the canal closed off at high pressure. Thus one of the major tasks in developing the network model is to determine the resistance of the enucleated human eye at high pressure

and to find a relation for the septae which will result in good agreement with the experimental pressure-resistance curve.

2 The Outflow System Network Model

The conventional aqueous outflow pathway of the human eye consists of three distinct, structures: trabecular meshwork, Schlemm's canal and the collector channels. The goal in this chapter is to create a resistor network which simulates the flow system described in this section. A set of resistors will be defined for each of the three outflow regions; these three sets of resistors will then be assembled based upon the anatomical orientations of the outflow system components, thus creating the resistor model illustrated in figure 2.1.

2.1 Resistor Model of the Meshwork Region

Starting from the angle of the anterior chamber, the aqueous humor first encounters the trabecular meshwork (TM) region of the outflow network. Flow through the TM can be modeled as distributed flow through a porous medium. The primary sites of resistance in the meshwork, the JCT and the endothelial lining, are considered to be a single inner wall region due to the close proximity of the two layers. The TM and inner wall region are modelled together as a compliant spring bed which suppports the porous filter [17] and is tethered at Schwalbe's line and the scleral spur.

The inner wall can physically be modeled as a ring-shaped filter with thickness 't' equivalent to the radial distance the aqueous humor must flow to pass through the inner wall. The effective width 'W' of the ring participating in the transport of aqueous humor is equal to the canal width because the inner wall must be directly underlying Schlemm's canal to have access to it. The radius 'R' of the ring is equal to the radius of the iris at the angle of the anterior chamber. Flow through the ring is assumed to be purely radial, driven by a pressure gradient between the inside and outside of the ring. Assuming that the flow through the meshwork can be characterised as flow though an isentropic, porous medium which obeys D'Arcy's law [28],

$$\vec{V} = -\frac{k}{\mu}\nabla P \tag{3}$$

where:

$\vec{V}$ = flow velocity vector in the meshwork

k = permeability of the meshwork

A = cross-sectional area

μ = viscosity of aqueous humor

∇P = pressure gradient

then the ratio of the circumferential velocity divided by the radial velocity can be approximated as,

$$\frac{V_\theta}{V_r} = \frac{\frac{1}{R}\frac{\partial P}{\partial \theta}}{\frac{\partial P}{\partial r}} \tag{4}$$

The radial pressure gradient can be approximated as $\frac{\partial P}{\partial r} \sim \frac{IOP}{t}$, and in the circumferential direction, the pressure gradient is on the order of $\frac{1}{R}\frac{\partial P}{\partial \theta} \sim \frac{IOP}{X_{cc}}$. Substituting the pressure gradients into equation (4), the velocity ratio becomes,

$$\frac{V_\theta}{V_r} = \frac{t}{X_{cc}} \tag{5}$$

The thickness of the JCT and endothelial lining is t$\simeq$10μm [5] and $X_{cc} = 1200\mu m$ is the average distance between collector channels [21]. Thus the ratio of the circumferential flowrate to the radial flowrate is $O(10^{-2})$, which justifies neglecting circumferential flow in the meshwork itself.

It is further assumed that the pressure outside of the ring (in Schlemm's canal) is dependent upon θ (the circumferential direction coordinate) but induces no circumferential flow in the inner wall itself. This conceptualization of the flow through the meshwork region is consistent with the earlier models of Moses [21] and Johnson & Kamm [17].

The inner wall ring described above is modeled as a homogeneous, porous filter. Although one can intuitively sense that the outflow system is not a perfectly uniform structure, this assumption will nevertheless be made since the statistical variation of the properties of the outflow system is not known. The model can accomodate such non-homogeneities, but these will be considered individually as special cases of the more general, homogeneous model. A total inner wall conductance G_{tm} can be

defined for the entire ring as the total flow through the ring divided by a constant pressure drop across the inner wall which is independent of θ. The local flowrate through the inner wall depends upon the local pressure drop across the inner wall, $\Delta P = IOP - P(\theta)$. If we define the inner wall conductance per unit circumferential distance to be $G^*_{tm} = G_{tm}/2\pi R$, the inner wall could then be sectioned off and replaced by $N \times M$ (or simply NM) resistors in parallel. N is equal to the number of collector channels and M is equal to the number of nodes assigned from one CC to the next, making NM the total number of nodes in the canal. Each resistor has a flow conductance of $\Delta G_{tm} = G^*_{tm}\Delta x$, where $\Delta x = R\Delta\theta$ is the circumferential width of each section.

2.2 Resistor Model of Schlemm's Canal

Immediately upon passing through the inner wall, the aqueous humor enters Schlemm's canal, the second region of the outflow network model. Schlemm's canal is modeled as a compliant, porous duct roughly elliptical in cross-section (see section 1.1). The height of the canal 'h' (ie. the inner to outer wall distance) is defined to be twice the semi-minor axis of the elliptical cross-section. The canal height is variable because the spring bed (TM) allows the inner wall to move relative to a fixed outer wall (comprised of the scleral tissue). The width 'W' (in the limbus to scleral spur direction) is equal to twice the semi-major axis of the same cross-section. Note that the trabecular meshwork underlying the canal is also of width W, exactly matching the width of the canal. The width of the canal can be considered constant because the outer wall sclera is relatively rigid compared to the inner wall meshwork and does not strain appreciably when stressed by intraocular pressure. In the human eye, the meshwork actually extends well beyond the width of the canal on both sides towards the scleral spur and the limbus. However, only the meshwork directly underlying the canal is assumed to participate in the outflow of aqueous humor, this being consistent with the earlier assumption that the flow cannot move circumferentially in the TM and inner wall region.

Upon entering the canal, the aqueous humor flows circumferentially in the θ direction. The curvature of the canal in the θ-direction can be neglected if h$\ll$R, which is the case for the human eye. Thus circumferential flow in the direction parallel to the axis of the duct can be denoted in Cartesian coordinates as the x-direction (with x=Rθ), replacing the θ notation in cylindrical coordinates used earlier. The flow conditions in the canal can be determined by calculating the Reynold's number:

$$Re_h = \frac{\rho Q(x) h(x)}{A(x)\mu} < \frac{4Q_{max}}{W\pi\nu} \simeq 3 \times 10^{-3} \tag{6}$$

where:

W = canal width = 300 μm

Q(x) = volumetric flowrate at point x in canal

$Q_{max} = Q_T/2N = 2/60 = 0.033$ μl/min

h(x) = local canal height

A(x) = πWh(x)/4

ν = kinematic viscosity of aqueous humor = $7 \times 10^{-7} m^2/s$ (T=37^{0}C)

Note that the flow Reynold's number is based on the height of the canal (h) rather than the width (W) because h$\ll$W in Schlemm's canal. The quantity Q(x)/A(x) represents the average flow velocity in the duct. The maximum canal flowrate Q_{max} can be calculated for the case where the aqueous humor exits via N=30 evenly spaced, uniform collector channels. For such a case, the maximum canal flowrate will occur right at the entrance to any of the CC openings and is equal to $Q_T/2N$, where Q_T equals the total outflow rate of 2μl/min. Since Re$_h$=3$\times$10$^{-3}\ll$1 based on Q_{max} represents the maximum Re_h in the canal, the canal flow must clearly be inertia-free. It can be further assumed that the flow along the canal is fully-developed and one-dimensional if the change in canal height is much less than the section length for each section ($\Delta h \ll \Delta x$). Assuming that the canal height varies linearly according to equation (11), this condition can be written as:

$$\frac{\Delta h}{\Delta x} = \left(\frac{h_o}{E_{tm}}\right)\frac{\partial P}{\partial x} \ll 1 \tag{7}$$

If the above condition is satisfied, the governing equation for fully-developed, inertia-free flow in an elliptical duct can be applied to flow in Schlemm's canal [33]:

$$\frac{\partial P}{\partial x} = \frac{64\mu Q(x)(h^2(x) + W^2)}{\pi W^3 h^3(x)} \tag{8}$$

Since h(x)$\ll$W, the above expression can be simplified to

$$\frac{\partial P}{\partial x} = \frac{64\mu Q(x)}{\pi W h^3(x)} \tag{9}$$

This equation is identical in form to the equation used by Johnson & Kamm [17], the only difference being that the constant factor multiplying the pressure gradient is $64/\pi$ rather that 12 for the Johnson & Kamm model. This difference arises from the modelling of the canal as an elliptical duct as opposed to two infinite flat plates. The elliptical shape genererates more flow resistance for a give cross-sectional area because of end-effects from the two-dimensionality.

By discretizing the above differential equation using finite differences, Schlemm's canal can now be modelled as a set of resistors arranged in series (see figure 2.1). The pressure, flowrate and height are determined at the nodal points between each of the canal sections of length Δx. The conductance of each resistor between nodal points numbered i and i+1 is calculated by assuming the height and pressure vary linearly between any two adjacent nodes. The conductance in each Schlemm's canal resistor can be determined by integrating equation (9) from i to i+1:

$$G_{sc_{i+1}} = \frac{Q(x)}{P_{i+1} - P_i} = \frac{\pi W h_i^2 h_{i+1}^2 \Delta x}{32\mu(h_i + h_{i+1})} \tag{10}$$

From equation (10), it is apparent that the dominant controlling parameter determining the flow resistance of Schlemm's canal is the canal height. This is due to the cubic dependence of the canal conductance on the local height h(x). Thus it is important to accurately model the local canal height as a function of the other known parameters to arrive at the correct flow characteristics for the overall model.

•Determination of the Canal Height

The height of Schlemm's canal is controlled by the movement of the meshwork and inner wall relative to a fixed outer wall (sclera). The movement of the inner

wall is governed by the material properties of the trabecular meshwork, which acts as the support structure for the inner wall. The zero-flow, zero-load condition must first be determined; this was defined by Johnson & Kamm[17] to be the uncollapsed height h_o of the canal when the anterior chamber pressure is equal to the (local) pressure in the canal lumen. Assuming the meshwork to be linearly elastic with a constant modulus of elasticity E_{tm}, the canal height h(x) can be decribed by the equation,

$$h(x) = h_o(1 - \frac{\Delta P}{E_{tm}}) \tag{11}$$

It is evident that when $\Delta P=0$, the zero loading condition of $h(x)=h_o$ is recovered. Conversely, when $\Delta P=E_{tm}$, the canal is completely collapsed with $h(x)=0$; thus E_{tm} is actually a measure of the minimum pressure drop across the meshwork required to completely obliterate Schlemm's canal in the absence of any other support mechanism to affect the height of the canal. Note that when the inner wall distends towards the outer wall, the meshwork is under a tensile loading stress.

In reality, it is unlikely that Schlemm's canal can collapse down to a state which completely seals off the duct because of two intervening physical effects:

1. The inner and outer walls of Schlemm's canal are not smooth surfaces which can perfectly intermesh. A complete apposition of the two walls would still leave many gaps due to irregularities in both walls surfaces.

2. Between the inner and outer wall, there exist support structures in the canal commonly known as septae [16]. The septae can be thought of as beams or posts which separate the walls and prevent complete canal collapse [17]. Note that the septae balance the force caused by the pressure differential between the anterior chamber and the lumen of the canal by undergoing compressive stress, unlike the meshwork which is under tensile stress.

The mechanical characteristics of the canal structures can be modelled as two different regimes of inner wall support. The first is the linear, elastic deformation regime during which the tensile loading of the trabecular meshwork determines the

canal height; the governing relation for the canal height in this regime is given by equation (11). In this regime, the septae do not contribute significantly in opposing the collapse of the canal; the septae act like distended springs which must fully contract before they can produce any compressive stresses to balance the forces collapsing the canal. When the septae have reached this fully contracted state, the deformation of the canal enters the second regime where the canal height is controlled by the compression of the septae as well as the stretching of the meshwork. The degree of control exerted by the septae will depend on their relative stiffness compared to that of the trabecular meshwork. If the septae are the stiffer of the two structures, the compressive stresses opposing canal collapse will dominate over the tensile stresses which are acting cumulatively in the same direction.

The form chosen for the relation governing the canal height when supported by the septae is as follows:

$$h(x) = \frac{K_{sc}}{\Delta P^{\frac{1}{3}}} \tag{12}$$

where K_{sc} is the septae stiffness parameter to be determined later.

The characteristics of the septae are determined empirically by matching the septae height to the pressure drop across the meshwork such that the overall outflow resistance calculated by the model agrees with the experimental data, which shows the resistance to increase linearly with pressure (see chapter 4). The exact mathematical form of the empirical relationship between canal height h(x) when held up by septae and the pressure drop $\Delta P = IOP - P(x)$ is based on an order of magnitude analysis of Schlemm's canal resistance as a function of pressure. The resistance of Schlemm's canal varies as the inverse third power of the height (see equation 9).

$$R_{sc} \sim \frac{1}{h^3} \tag{13}$$

Given that the total resistance increases linearly with intraocular pressure, we can write

$$\frac{\partial R_{sc}}{\partial IOP} \propto constant \propto \frac{1}{h^4}\frac{\partial h}{\partial IOP} \tag{14}$$

Intraocular pressure can be approximated by ΔP and substituting $\frac{\partial h}{\partial IOP} \sim \frac{h}{\Delta P}$ into equation (14) results in

$$\Delta P \sim \frac{1}{h^3} \tag{15}$$

which can be rewritten in the form given in equation 12 by taking the cube root of both sides and introducing the septae stiffness parameter K_{sc}.

The $\frac{1}{3}$-power law can be further motivated by the tube law depicting the behaviour of a collapsible tube [27],

$$\Delta P^{-\frac{2}{3}} \sim A(x) \sim h^2(x) \tag{16}$$

where $A(x)=\frac{\pi}{4}Wh$ is the cross-sectional area of an elliptical duct. In the highly collapsed state, Schlemm's canal is assumed to be supported by septae which act as posts which keep the canal locally open. If the inner wall conforms around the septae, apposition of the inner and outer wall would occur between adjacent septae, and the width of the canal is no longer a characteristic length scale of the cross-sectional area. Approximating the width of the local section of open canal by the septum height itself, the area of the canal in the collapsed state is proportional to the septum height squared, and the tube law for a collapsible tube results in an identical functional relation between the local canal height and the local pressure drop across the inner wall.

Since the meshwork supports the canal for relatively small strains, the linear relation (eqn. 11) should initially be used for ΔP less than some ΔP_s. For large strains with $\Delta P > \Delta P_s$, the septae support the canal and thus equation 12 should be used. ΔP_s is the pressure drop at which the two height relations give the same canal height; this height at which the septae start acting will be denoted by h_s, and can be calculated using the relation

$$h_s = h_o(1 - \frac{\Delta P_s}{E_{tm}}) = \frac{K_{sc}}{\Delta P_s^{\frac{1}{3}}} \tag{17}$$

Using the appropriate values for the parameters (see section 3.1), the canal height can be plotted as a function of the local pressure drop across the meshwork (see

figure 2.2). Note that the septae begin to support the canal at a height of 2.4 μm. This value corresponds with the dimension reported by Van Buskirk [31], who found the canal lumen area to be 1000±700 μm^2 at IOP=40 mmHg, or h=3.3±2.7 μm assuming the canal width is 300 μm. For the linear height relation, the stiffness of the meshwork

$$-\frac{\partial \Delta P}{\partial h} = \frac{E_{tm}}{h_o} \tag{18}$$

is constant and independent of the force acting upon it. But for the $\frac{1}{3}$-power law, the stiffness of the septae holding up the inner wall is variable and increases with increasing ΔP as given by

$$-\frac{\partial \Delta P}{\partial h} = \frac{3\Delta P^{\frac{4}{3}}}{K_{sc}} \tag{19}$$

It is intuitively plausible that it should become increasingly difficult to decrease the size of the canal lumen as the septae become compressed and the inner wall conforms around the septae structures.

The model developed for Schlemm's canal is quite rigorous in its derivation of the flow resistance from fundamental fluid mechanics. In comparison, the resistances of the meshwork and collector channel regions are empirically derived with a 'black box' approach. It is not necessary to know in detail how and where the flow resistances are generated in these two regions because they do not play the critical interconnective role as Schlemm's canal does. Since one of the objectives of this study is to investigate the role of Schlemm's canal as a communications pathway between various regions of the entire outflow system, it is the canal which must be carefully modeled in a rigorous manner.

2.3 The Collector Channel Resistance Component

The collector channnels (CC's) are vessels which connect the canal (from openings in the outer wall) to the episcleral venous system. The collector channels constitute the third and final flow region through which the aqueous humor pass through to complete the passage from the anterior chamber to the episcleral venous

system. There exists some ambiguity as to the distinction between collector channels and aqueous veins in the outflow system. For the purpose of clarity, all ducts which allow fluid to flow from Schlemm's canal to episcleral veins will be singly referred to as collector channels.

In the human eye, there are typically 30 collector channels distributed throughout the canal [21]. The collector channels are exit points located on the outer wall of Schlemm's canal which allow the aqueous humor to flow out of the canal and into the episcleral venous system. The episcleral venous pressure is approximately 9 mmHg in the live human eye, and effectively zero in the enucleated eye. The collector channels are modeled as 30 flow resistors arranged in parallel which connect 30 separate points in Schlemm's canal to a common venous pressure. These collector channel resistors are functionally independent of the Schlemm's canal and trabecular meshwork resistors. As will be detailed in section 3.1, the collector channel resistors are assumed to be dependent only upon the intraocular pressure. If the CC resistance decreases with increasing IOP as suggested by recent experiments [26], the CC's that control the resistance (by carrying most of the flow) are likely to be radially oriented so that the vessels will expand (and decrease in resistance) as the sclera stretches with increasing IOP [4]. The resistance of a collector channel under these conditions has been shown by Battaglioli [4] to be weakly dependent on the internal vessel pressure. The appropriate total conductance for the collector channels can be determined experimentally by measuring the outflow resistance of the human eye at various IOP's after a complete trabeculotomy has been performed. This data can then be curve-fitted to obtain a working relationship between CC resistance and IOP (see section 3.1).

3 Numerical Implementation of the Network Model

In chapter 2, an electrical network equivalent to the aqueous outflow system was formulated. In order to solve this network, the parameters which determine the values of the resistors must be specified, and an algorithm is developed to numerically solve the non-linear matrix representation of the network.

3.1 Parameters of the Network Model

In this section, numerical values are assigned to the parameters used to calculate the conductances of the elements in the network. The motivations for the particular choices of parameter values come from direct morphological observations of the outflow system and inferred characteristics based upon experimental measurements of flow resistance in enucleated eyes.

Number of Collector Channels–N

The generally accepted average value for the number of collector channel openings observed in the outer wall of Schlemm's canal is 30. This value has been used in previous models of the outflow system by Moses [21] and Johnson & Kamm [17].

Width of the Canal–W

Using electron microscopy, Hoffmann & Dumitrescu [16] found the width of the canal to range from 190μm to 350μm, while Duke-Elder reported an average width of 280μm [10]. A width of W=300 μm was chosen for the model, which is the same value used by Moses [21].

Trabecular Meshwork Stiffness–E_{tm}

The meshwork is assumed to behave like a perfectly elastic material, with the local canal height h(x) directly proportional to the local pressure drop ΔP=IOP-P(x) across the meshwork as described in section 2.2. By correlating the morphological data for canal height at a given IOP to equation (11), an approximate value for the the meshwork stiffness E_{tm} can be calculated. From the study of Johnstone &

Grant [19], the canal first appeared to be collapsed when fixed at a pressure of 20 mmHg. If it is assumed that roughly one half of 20 mmHg pressure drop is across the meshwork [26], E_{tm} would then be equal to 10 mmHg.

Undeformed Canal Height–h_o

The undeformed canal height is defined to be the height corresponding to a zero pressure differential between the canal lumen and the anterior chamber. The morphological findings of various investigators [21,23,24,31] report this height to be in the 20-30 μm range. An undeformed canal height of h_o=20 μm was chosen for the model so that the predictions would be in agreement with data from Rosenquist et al. [26] for a one-hour trabeculomy done at IOP=7 mmHg (see section 5.2).

Viscosity of Aqueous Humor–μ

The viscosity of aqueous humor was assumed to be that of water at normal body temperature (37^oC), which is $\mu = 7 \times 10^{-4}$ kg/m·s.

Distance Between Adjacent Collector Channels–X_{cc}

The total circumferential length of Schlemm's canal is approximately 2πR, where R$\simeq$6000 μm is the radius of the eye (see section 2.1). Assuming that the 30 collector channels are evenly spaced, the average distance between adjacent collector channels would then be

$$X_{cc} \simeq \frac{2\pi(6000\mu m)}{30} \simeq 1200\mu m \tag{20}$$

Septae Stiffness Parameter–K_{se}

As will be shown in section 4.3, the septae stiffness parameter is chosen to be 5μm/mmHg$^{\frac{1}{2}}$ to match the pressure-resistance data presented in chapter 4.

Collector Channel Resistance–R_{cc}

After eliminating the inner wall resistance by complete trabeculotomy, the only remaining component of the outflow system which could exhibit flow resistance is the collector channel region. Rosenquist et al. [26] measured the collector channel resistance to be R_{cc} = 1.8 mmHg/μl/min at IOP=7 mmHg, and R_{cc}=1.2 mmHg/μl/min

at IOP=25 mmHg. An empirical correlation between R_{cc} and IOP is obtained by linear interpolation of these two data points, resulting in

$$R_{cc} = 2.033 - 0.033 \cdot IOP \tag{21}$$

It can be assumed with a fair degree of confidence that equation 21 is valid in the 7-25 mmHg pressure range. However, there is no justification to assume that R_{cc} would continue to rise as IOP decreases below 7 mmHg. Likewise, it cannot be not be assumed that R_{cc} would continue to linearly fall as IOP increases above 25 mmHg. Thus the assumption is made that R_{cc} is constant outside of the specified IOP range between 7 mmHg and 25 mmHg; in other words R_{cc} remains at the value measured at 25 mmHg for all IOP>25 mmHg, and R_{cc} remains at the value measured at 7 mmHg for all IOP<7 mmHg.

Trabecular Meshwork Resistance–R_{tm}

To isolate the contribution of the meshwork to the total outflow resistance, it is assumed that Schlemm's canal is wide open at low intraocular pressure and contributes negligible outflow resistance. This is justified by comparing the low pressure outflow resistance of a single segment of the outflow system (from midpoint to CC) to the resistance of a corresponding segment of Schlemm's canal in the uncollapsed state. Similar to Johnson & Kamm [17], we introduce the term β^2 to be the ratio between the resistance in the undeformed canal and the resistance of the outflow system in a segment spanning one half of the distance between adjacent collector channels ($0.5X_{cc}$):

$$\beta^2 = \frac{\frac{0.5X_{cc} \cdot 64\mu}{\pi W h_o^3}}{\frac{R_{total} 2\pi R}{0.5X_{cc}}} \tag{22}$$

Using values for the parameters previously defined in this section and a typical total outflow resistance of R_{total}=4 mmHg/μl/min, we find that β^2=1.8$\times 10^{-3}$, which means that the resistance of the undeformed canal is 3 orders of magnitude smaller that the total resistance of the entire system.

The inner wall resistance can be isolated by experimentally measuring the resistance before and after a complete trabeculotomy and assuming the difference

between these two measurements represents the isolated meshwork resistance Such a method requires the further assumption that the collector channel resistance measured after a complete trabeculotomy is the same if the trabecular meshwork overlying the collector channels is intact. From the study of Rosenquist et al. [26], the outflow resistance at IOP=7 mmHg, was found to be 3.8 mmHg/μl/min before trabeculotomy, and 1.8 mmHg/μl/min after a complete trabeculotomy. R_{tm} is thus calculated to be 2.0 mmHg/μl/min, and the conductance of each meshwork element is determined using the formula

$$G_{tm_i} = \frac{\Delta x_i}{R_{tm}\pi D} \tag{23}$$

where D is the diameter of the eye at the plane of the limbus.

An important assumption which has been implicitly made in this analysis is that the inner wall resistance is constant with respect to the local pressure drop across the meshwork. Thus, the inner wall is assumed to play a negligible role in raising the outflow resistance with increasing intraocular pressure. The validity of this modeling assumption can be evaluated by comparing the behavior of the network model to experimental findings (see chapter 5).

3.2 Numerical Algorithm for Solving the Network

3.2.1 The Nodal Equations and Kirchoff's Laws

For a network with N collector channels (CC's) and M nodes between adjacent CC's, the total number of nodes in the canal is N$\times$ M, (denoted by NM). The anterior chamber is represented by a single node at intraocular pressure, bringing the total number of nodes to NM+1 in the network with unknown pressures. The pressure of the episcleral venous system is defined to be zero (for the case of an enucleated eye), giving us a common ground potential which all of the collector channels exit to. The total number of resistor elements in the network is 2NM+N, consisting of NM elements in parallel representing the meshwork, NM elements in series representing the canal, and N elements connecting each collector channel

entrance at the outer wall of the canal to the episcleral veins (see figure 2.1). The flowrate through each of these resistor elements is also unknown. Note that pressure in the network is equivalent to voltage in an electric circuit, and flow is equivalent to current.

The total number of variables in the outflow network is 3NM+N+1, obtained by adding together the flow and pressure variables. The object now is to formulate a matching number of equations which will give a unique solution to the network problem which has been formulated.

Kirchoff's Voltage Law is applied to each resistor in the network, resulting in 2NM+N equations. For the meshwork resistors, one end of each element is connected to the node in the anterior chamber (at IOP). The other end of each meshwork element is connected to the node in the canal which is directly underlying the element of meshwork. Using Ohm's Law, the flow (or current) going through the i^{th} meshwork element (or resistor) can be expressed as a function of the pressure drop (or voltage) across this element.

$$Q_{tm_i} = G_{tm_i}(IOP - P_i) \tag{24}$$

The flowrate is defined to be positive for flow going from the anterior chamber to the canal. The canal elements are connected in series at both ends to nodes in the canal, and the flow along the canal can be expressed as a function of the discretized pressure change between two adjacent nodes.

$$Q_{sc_i} = G_{sc_i}(P_i - P_{i+1}) \tag{25}$$

The flowrate is defined to be positive for flow going from the i^{th} node to the $i+1^{th}$ node. Each collector channel element is connected at one end to the node in the canal located at the entrance of a channel opening, and at the other end, to the episcleral venous pressure (which is 0 by definition). Flow through the K^{th} collector channel is denoted by Q_{cc_K}, and can be expressed as

$$Q_{cc_K} = P_{tm} \cdot G_{cc_K} \tag{26}$$

where P_{km} is the pressure in the canal at the $(K \times M)^{th}$ node.

By applying Kirchoff's Current Law (KCL) to each node in the canal, a further NM equations are obtained. As applied to the network, KCL states that the sum of the flows entering a node must equal the sum of the flows leaving a node. For nodes not located at a collector channel opening, the circuit is illustrated in figure 3.1 with the appropriate nomenclature assigned to the nodes, pressures, flows and conductances; application of KCL to this circuit results in the equation

$$Q_{tm_i} + Q_{sc_i} + Q_{sc_{i+1}} = 0 \tag{27}$$

All of the flows have been arbitrarily assigned directions, with the sign convention that all flows entering a node are defined to be positive. For nodes at collector channel openings, the circuit given in figure 3.1 is slightly modified to produce the circuit of figure 3.2, and the current law equation for this circuit is

$$Q_{tm_i} + Q_{sc_i} + Q_{sc_{i+1}} - Q_{cc_K} = 0 \tag{28}$$

If intraocular pressure is specified, (ie. in the constant pressure mode), the number of unknowns is reduced by 1 to 3NM+N, and equations (24) to (28) form a closed problem with an equal number of equations and unknowns. However, if the total system flowrate (Q_T) is specified in the constant flow mode, one more equation is required. Applying KCL globally from the anterior chamber to the canal lumen, we find that the total outflow rate (Q_T) must equal the sum of the flow going through all of the meshwork elements, which results in the equation

$$Q_T - \sum_{i=1}^{NM} Q_{tm_i} = 0 \tag{29}$$

where Q_{tm_i} is positive flowing from the anterior chamber to the canal. The number of equations and unknowns can be reduced from 3NM+N+1 to NM+1 by substituting equations (24) to (26) for each element into equations (27) to (29) for each node. The KCL equations can then be rewritten as

$$G_{tm_i}(IOP - P_i) + G_{sc_i}(P_{i-1} - P_i) + G_{sc_{i+1}}(P_{i+1} - P_i) = 0 \tag{30}$$

$$G_{tm_i}(IOP - P_i) + G_{sc_i}(P_{i-1} - P_i) + G_{sc_{i+1}}(P_{i+1} - P_i) - G_{cc_K}P_i = 0 \qquad (31)$$

$$\sum_{i=1}^{NM} G_{tm_i}(IOP - P_i) - Q_T = 0 \qquad (32)$$

A sample matrix is presented in figure 3.3 for a network with 2 collector channels (N=2) and 2 nodes per CC (M=2). Note that if the constant pressure mode is specified, the last row and last column of the system matrix are eliminated, reducing the matrix to NM by NM in size. In such a case, the canal node pressures are solved for first before the outflow rate Q_T is calculated using the global KCL equation.

3.2.2 Numerical Methods and Costs

To begin solving the system of equations derived in the previous section, an initial guess of the pressure in the canal is obtained by neglecting the canal resistance and lumping R_{tm} and R_{cc} into two global resistance values, resulting in a single pressure guess for the all the canal nodes. In the constant pressure mode (with IOP specified), the initial estimate of the canal pressure would be

$$P_{guess} = IOP\left(\frac{R_{tm}}{R_{tm} + R_{cc}}\right) \qquad (33)$$

In the constant flow mode, an initial guess would be required for IOP as well as the pressure in the canal.

$$IOP_{guess} = Q_T(R_{tm} + R_{cc}) \qquad (34)$$

$$P_{guess} = Q_T R_{cc} \qquad (35)$$

The number of nodes from CC to CC (M) required to obtain an acceptable level of numerical accuracy ($error < 1\%$) under all conditions was determined by trial and error to be 40. The error is defined to be:

$$\%error = \frac{|R(M) - R_\infty|}{R_\infty} \qquad (36)$$

where R(M) is the outflow resistance for a given M and R_∞ is the asymptotic outflow resistance as $M \rightarrow \infty$. A typical percentage error curve as a function of M for an

intraocular pressure of 50 mmHg (see figure 3.4) shows the error to be less than the set criterion at around M=20.

Solving the system matrix (see figure 3.3 for an example) by numerical iteration involves two separate processes. The inner-loop process solves the linear system

$$G(\underline{p}^{(k)})\underline{p}^{(k+1)} = \underline{q} \tag{37}$$

where $G(\underline{p})$ is the conductance matrix, $\underline{p}$ is the pressure vector $[p_1, p_2, ..., p_{NM}, IOP]$, and $\underline{q}$ is the flowrate vector $[0, 0, ..., 0, Q_T]$. Each time this linear system is solved, the updated pressure vector is used to recalculate the conductance matrix, which forms the outer-loop (non-linear) iteration process. The conductance matrix is recalculated using the updated values of the pressure vector, and usually must be performed $O(10^2)$ times before convergence is achieved. The linear system is solved using two methods: Gauss-Seidel iteration with over-relaxation and direct Gaussian elimination. The Gaussian elimination method uses a special algorithm to take advantage of the sparseness of the G-matrix, and vectorizes the G-matrix to minimize memory storage requirements. Standard LU decomposition method requires $n^3/3 + O(n^2)$ floating point operations (flops) to decompose the matrix and backsolve, where 'n' is the rank or size of the matrix. The specialized Gaussian elimination solver written to solve the specific system matrix generated by the network model maintains the sparseness of the matrix, dramatically lowering cost to approximately $16n$. With N=30 and M=40 for the network model, the numerical cost incurred in solving the 1200×1200 matrix is $\sim 6 \times 10^8$ flops by standard Gaussian elimination, while the vectorized Gaussian solver costs only $\sim 2 \times 10^4$ flops. The vectorized Gaussian solver is very efficient but the residual of the non-linear iteration process, which is defined to be

$$Res = \sqrt{\frac{\sum_{i=1}^{n}(p_i^{(j+1)} - p_i^{(j)})^2}{n}} \tag{38}$$

can only be brought down to $O(10^{-2})$ before numerical fluctuations prevent further gains in accuracy. For this reason, the Gauss-Seidel method is used after an initial

stage of vectorized Gaussian elimination to bring the residual down to $O(10^{-4})$ mmHg or less. The Gauss-Seidel method iteratively arrives at $\underline{p}^{(j+1)}$ according to the algorithm

$$\underline{p}^{(j+1)} = \omega_{sor}(-(D+U)^{-1}(L\underline{p}^{(j)} + \underline{q})) + (1-\omega_{sor})\underline{p}^{(j)} \tag{39}$$

where ω_{sor} is the successive over-relaxation factor, and the conductance matrix has been subdivided into the diagonal (D), strictly upper triangular (U), and strictly lower triangular (L) such that G=D+L+U. By trial and error, the optimum ω_{sor} factor was found to be around 1.5. Since D+U is an upper triangular matrix, the above expression can be backsolved directly. The numerical cost of a single iteration of the Gauss-Seidel algorithm is roughly $8n$, or about one-half of the cost of a single call of the vectorized Gaussian routine. However, the number of iterations with Gauss-Seidel required to obtain reasonably accurate solution to the linear system is $O(10^2)$, making the total cost incurred ~50 times greater than an equivalent single call of the vectorized Gaussian routine. Gauss-Seidel does offer one major advantage in that a (non-linear) update of the conductance matrix can be performed before an accurate solution to the linear system (equation 37) is obtained. Indeed, it seems logical to avoid unneccessary numerical expense incurred in solving accurately the linear system when the conductance matrix itself is incorrect because the pressure vector used to calculate it is far from the final answer. The optimum combination of linear Gauss-Seidel iterations and non-linear system matrix updates was found to be approximately 10 Gauss-Seidel iterations between each update of $G(\underline{p})$.

The final algorithm chosen to numerically solve the system matrix, a combination of vectorized Gaussian elimination and Gauss-Seidel with over-relaxation, is outlined below:

1. Vectorized Gaussian elimination is used for the first 10-20 iterations, which typically will bring down the residual to $O(10^{-2})$ from an initial value of $O(1)$ after the first iteration.

2. Gauss-Seidel is used for 400-800 iterations with a non-linear update every 10

iterations, for a total of 40-80 updates of the system matrix which will lower the residual to $O(10^{-4})$.

The computational time required to achieve numerical convergence is typically on the order of one minute of CPU time on a VAX 11/755 machine.

4 Experimental Perfusion of Human Eyes

4.1 Purpose of the Experiment

A number of investigators have measured the resistance of enucleated human eyes as a function of IOP [8,11,22]. All of these studies measured the resistance only up to a maximum pressure of 50 mmHg or less. The IOP of a normal living eye is ~15 mmHg, (or ~7 mmHg pressure drop across the outflow system), and an IOP of ~25 mmHg or greater is generally considered glaucomatous. The question then arises: what is the usefulness of studying the human eye under high pressure conditions that are never clinically manifested? Intraocular pressure induces a number of changes to the outflow system, and septae which normally do not play a significant role in determining the outflow resistance can be studied under such conditions.

Consider the morphologically observed appearance of the canal lumen when fixed at an IOP of 50 mmHg. By all accounts, the lumen is only a small fraction of its original cross-sectional area, and in some places it may appear to be completely obliterated [19,23,29]. The inner wall cannot be modelled as a linear elastic material when subject to such a high degree of deformation. In this state, the inner wall mechanically counters the pressure force causing collapse by compressing and deforming around the septae. Johnson & Kamm [17] modelled the septae in two ways: perfectly rigid (with $E_{septae} \to \infty$) or linearly compliant (eg. $E_{septae} = 8E_{tm}$). The behavior of the outflow system is markedly different for the two different septae models. For the case of the rigid septae, the resistance increases with increasing IOP in the low pressure range but gradually reaches an asymptotic limit in the mid to high pressure range, (say 30-70 mmHg, depending on the model parameters chosen). With the linearly compliant septae, the slope of the P-R curve increases in the mid to high pressure range. The model eventually becomes numerically unstable at high IOP when the P-R curve turns up sharply. Note though that the characteristics of the P-R curves for rigid and compliant septae differ significantly

only in the high pressure range when the canal is collapsed against the septae.

The method chosen to model the septae should result in a P-R curve which correctly reproduces the behavior of the eye at high pressure, since it is assumed that canal collapse accounts for all of the change in outflow resistance with increased intraocular pressure and septae are the dominant factor in determining canal resistance in the highly collapsed state. However, the P-R characteristics of the eye at high IOP have not been established by previous investigators. Studies on enucleated eyes have shown the resistance to increase linearly with IOP, but the highest pressure measured previously is only 50 mmHg [1][8]. Thus, the P-R curve must be established in the high pressure range above 50 mmHg to determine what the best model of the septae should be to correctly reflect the highly collapsed state of Schlemm's canal.

A secondary objective of this experimental study is to investigate the role of canal collapse as a possible mechanism causing glaucoma. By finding the maximum increase in outflow resistance which can be realized by raising the intraocular pressure to very high levels, one could determine whether canal collapse as might be caused by a loss of elasticity in the trabecular meshwork could generate glaucomatous flow resistance.

4.2 Methods

Human eyes provided by National Disease Research Institute were perfused within 24 hours of enucleation using a constant pressure technique with feedback control of the flowrate. Between the time of enucleation and the start of the perfusion experiment, the eyes were stored in a sealed container packed in ice. Thirty minutes prior to initiating the perfusion, the eyes were placed in a 0.9% saline bath, where they remained for the duration of the experiment.

The eyes were perfused using Dulbecco's buffered phosphate solution, with 99 mg

[1] Levene & Hyman [20] measured the resistance up to a pressure of 70 mmHg with tonography on live eyes, and found the resistance reached a maximum at high IOP.

of glucose added per 100 ml of fluid. A 23G needle is passed through the cornea near the limbus and then inserted under the iris to allow free communication between the posterior and anterior chambers. All equipment which comes in contact with the perfusion fluid was pre-washed with water cleaned by passing it through a 0.08μm Millipore filter. The perfusion fluid was also cleared of contaminants in the same way after glucose had been added to it. The eyes were suspended in 0.9% saline solution up to the level of the limbal area. A Kimwipe tissue was placed over the cornea to keep it moist during the experiment. A cover was closed over the saline bath of each eye and the bath was heated to maintain an isothermal 30^{o}C environment.

A schematic diagram of the experimental apparatus is given in figure 4.1. The set-up perfuses two eyes simultaneously, but measures the flow resistance of only one eye at a time. Two methods were used to perfuse the eyes under pressure. The first uses a reservoir placed at a variable height relative to the eye. The pressure is monitored with the pressure transducer (Microswitch Honeywell piezoelectric pressure transducer, model 130PC, Marshall Industries, Burlington, MA), but the inflow rate cannot be determined. This first method is used during the equilibration period following the alteration of the perfusion pressure to a new level. The second perfusion method uses the Harvard pump (Model 944, Harvard Apparatus Co., South Natick, MA) with computer control (Minc 11-23 digital computer) of the inflow rate via pressure signal feedback. This method is used when it is desired to measure the instantaneous flow resistance. The pump pushes forward the plunger of a 2.5 ml glass syringe (Hamilton Syringe Co., Reno, Nevada) to provide a known flowrate which is input controllable. Assuming that the flow resistance of the connecting lines is negligible, the pressure monitored by the transducer should be equal to the pressure in the anterior chamber of the eye. In constant flow mode, the desired inflow rate is entered into the computer control unit, and the pressure in the eye would then be an open-loop output signal. In constant pressure mode, the inflow rate is continuously varied by the computer to maintain pressure at the

desired level. The pressure signal P(t) is compared to a desired set-point P_d, and the inflow rate Q(t) is varied according to the control law

$$\frac{dQ(t)}{dt} = \alpha(P(t) - P_d) - \beta\frac{dP(t)}{dt} \tag{40}$$

If the pressure is given in mmHg and the flowrate in μl/min, typical values for the control parameters are $\alpha = 5$ and $\beta = 3$ in the appropriate units.

The eyes were perfused at 10 mmHg, 50 mmHg and 100 mmHg;, the pressure sequence was randomly chosen between pairs of eyes. The perfusion pressure was maintained for 60 minutes before it was changed, and every eye was perfused for two separate 60 minute periods at each pressure level, which resulted in a total perfusion time of 6 hours. The pressure sequence for any given pair of eyes was staggered by a 30 minute time lag between the two eyes. The first 30 minutes of a 60 minute period was spent perfusing with the reservior, since resistance measurements are not required during the equilibration period after a pressure change. During the last 30 minutes, the Harvard pump was used to obtain measurements of the flow resistance at steady state.

4.3 Results and Discussion

The resistance measurements for 5 eyes are presented in table 1, as are the average resistances for the group of 5 eyes at each pressure ($\overline{R}$) and the average resistances when normalized with respect to the resistance of each eye at IOP=10 mmHg ($\overline{R/R_{10}}$). The average resistances and normalized average resistances are plotted in figures 4.2 and 4.3 respectively (see section 5.1 for an explanation of the normalization method used to present the P-R data). The results indicate that the resistance increases linearly as a function of intraocular pressure in the 10-100 mmHg range covered in this study. This is consistent with the earlier study by Brubaker [8] that found the outflow resistance to increase linearly with respect to IOP in the 5-50 mmHg range.

The normalized rate of resistance increase was calculated to be 0.9% per mmHg

rise in IOP, which agrees fairly well with the 1.2% figure found in the Brubaker study [8]. The slopes from both of these studies are substantially lower than the 2.0% per mmHg slope found by Ellingsen and Grant [11] in the smaller 10-30mmHg IOP range.

Assuming that the average rate of resistance increase as a function of IOP for a normal human eye is 1.0% per mmHg, this would limit the pressure increase which could be caused solely by meshwork weakening and a concomitant collapse of Schlemm's canal. At pressures which can be considered glaucomatous (ie. a pressure drop of 20 mmHg or more), the outflow resistance increases by only ~20% from the baseline value at zero pressure, which correlates to only a small increase in pressure (~2mmHg) under constant flow conditions.

K_{sc} was determined by numerical trial and error so that the model produces a normalized resistance vs. pressure slope of ~1% per mmHg in the 50-100mmHg pressure range to match the experimental data presented in this chapter. If the pressure drop is given in units of mmHg, and h(x) in μm, K_{sc} would be equal to 5.0 $\mu m/mmHg^{\frac{1}{2}}$.

5 Comparison of the Model to Experimental Data

5.1 The Relationship Between IOP and Outflow Resistance

•Experimental Pressure-Resistance Data

One of the major difficulties with modelling the P-R characteristics of the enucleated human eye is the enormous scatter in the data between different researchers (see figure 5.1). A number of factors can cause this variability, amongst which are the average age of the eyes and the time allowed for steady state conditions to be achieved. It is desirable to collapse the data of the various researchers into a single curve which would represent the P-R characteristics of the 'typical' human eye. Normalizing the experimental data by the resistance measured at IOP=10 mmHg for each data set produces the desired effect, reducing the data scatter to an acceptable level. The resistance at 10 mmHg (R_{10}) was selected as the normalization parameter because it is the lowest pressure common to all the data sets. A similar method of analysis was used by Brubaker [8] to compare the P-R curves of different investigators. Noting that all of the P-R curves were roughly linear, Brubaker introduced an 'outflow obstruction coefficient' Q which is the slope of the normalized P-R curve. These two methods of analysis are equivalent because scatter reduction after normalization would only occur if the Q's of the various data sets are similar. One can show that the normalization procedure is at least consistent within itself for a given set of data. By separating the data of Brubaker (courtesy of Dr. R. Brubaker, via letter to Dr. M. Johnson) into two groups consisting of the eyes with the five highest and five lowest resistances, one can replot the data set as two separate P-R curves (figure 5.2). At first glance, the correlation between these two data sets seems to be quite minimal, but normalizing with respect to (R_{10}) again results in the collapse of the two curves into a single line (figure 5.3).

The success of the normalization suggests that the change in resistance as a function of IOP is dependent upon the characteristics of the outflow system in the

uncollapsed state (at low pressure). The network model assumes that the change in resistance as a function of IOP is solely caused by canal collapse. If such an assumption is indeed valid, the normalized P-R curve of the model would also have to be indepedent of the resistance at low pressure, a hypothesis which is tested in section 6.1.

•Pressure-Dependent Characteristics of the Network Model

To model the P-R curve, all the network parameters are taken to be uniform throughout the system; in other words, the homogeneous case (see section 1.2) is studied as the basis for comparison. The absolute and normalized resistance curves of the network model are plotted in figures 5.4 and 5.5 respectively, with the experimental data also included for figure 5.5. The slight decrease in resistance in the 5-10 mmHg range is caused by the decrease in collector channel resistance. Such fine details in the P-R curve would not expected to be rendered in the human eye because of natural variability in the outflow system. Parameter variability tends to "smooth out" the model P-R curve because canal collapse would then occur at different pressures in various regions of the system.

The experimental results presented in chapter 4 show that the resistance increases linearly with respect to IOP in the 10-100 mmHg pressure range. The $\frac{1}{3}$-power law chosen to model the septae height (see section 2.2), produces a fairly linear P-R curve in the range covered by the experiment. Agreement with the previous experimental data in the 10-50 mmHg pressure range is quite good, the closest correlation being with the Brubaker data.

The pressure distribution in Schlemm's canal as predicted by the model is presented in figure 5.6 normalized with respect to IOP. At IOP=10 mmHg, canal resistance is negligible, and thus the pressure in the canal is independent of location in the canal. As IOP increases, the pressure in the canal increases everywhere but the normalized pressure (P(x)/IOP) decreases in the region surrounding a collector channel, while incressing in the midsection between adjacent CC's. Canal resistance increases as IOP is elevated, resulting in a greater fraction of the total

pressure drop across the outflow network occurring before the collector channels.

The canal height distribution in Schlemm's canal as predicted by the model is presented in figure 5.7. Canal collapse begins to occur at IOP~15 mmHg, when the canal starts to pinch down near the CC's. Quantitatively, the average height of the canal predicted by the model as a function of IOP agrees well with the findings of Johnstone & Grant [19], which is to be expected since the meshwork stiffness (E_{tm}) is based on data from the same study. At IOP=5 mmHg, Johnstone & Grant observed the canal to be wide open, which is consistent with the model prediction that the canal retains 75% of its maximum (uncollapsed) height at that particular IOP. At IOP=15 mmHg, Johnstone & Grant found the canal lumen to be in a transition state, being partially collapsed in some areas. Again, this is consistent with the model results which show the canal to be partially collapsed only near the CC's when IOP=15 mmHg. Finally, Johnstone & Grant observed the canal to be fully collapsed at IOP=30 mmHg, which agrees with the model prediction that ~70% of the canal lumen is compressed down to the level of the septae support structures.

One interesting finding which can be inferred from the height distribution plot (figure 5.7) is that the canal height remains almost constant in the 40-100 mmHg IOP range, with the average height decreasing by less than 0.5 μm. In morphological studies, the canal is generally considered to be obliterated when fixed at an intraocular pressure of 40mmHg or higher. No attempt is made to identify any changes in the canal height at these higher pressures; it is simply considered to be completely collapsed at some sort of end state. Indeed, the characteristic height of the canal is predicted by the model to be in the 1-2 μm range when IOP$\geq$40 mmHg, which would make any changes in height within that range too small to be reliably resolved by morphology. Artifacts such as tissue shrinkage during fixation would overwhelm such detailed distinctions in structure. However, in that same IOP range of 40-100 mmHg, the model produces (in agreement with experimental data) a normalized resistance increase of nearly 60%, although the canal height decreases by

less than 0.5 μm. One can conclude from these observations that when the canal is traditionally thought of as collapsing from an initial state ($h/h_o = 100\%$) to a fully collapsed state ($h/h_o \approx 10\%$), the canal resistance increases only marginally. Most of the canal resistance is generated in a very narrow height range (h$\approx$1-2 μm). In other words, Schlemm's canal only begins to play a significant role in generating outflow resistance when the canal height is at least one order of magnitude smaller than the dimensions generally associated with an open canal, a conclusion also reached by Moses [21].

The septae are modeled as being uniformly distributed throughout the canal lumen. Since the canal resistance is a non-linear function of the local height, the canal height as determined by the model in the highly collapsed state represents an *effective* septae height (which produces the correct outflow resistance) and not the *average* septae height. In a more realistic scenario, the septae could be non-uniformly distributed in the canal lumen as occasional 'posts' holding up the inner wall. The canal is likely to be completely collapsed away from the septae and the flow in the open regions near the septae may not be truly one-dimensional as has been assumed in the model. However, such effects have been neglected for the purposes of the model by assuming that they do not significantly affect the overall behavior of the canal resistance component.

5.2 Modelling of Partial Trabeculotomies

5.2.1 Simulation of the Trabeculotomy Procedure

In the trabeculotomy procedure, trabecular meshwork is incised with a cystotome to create a patency between the anterior chamber and Schlemm's canal. This procedure presumably eliminates the flow resistance of the canal and meshwork underlying the incised section. The effects of such an alteration to the outflow network are illustrated in figure 5.8; for clarity, only a single meshwork resistor of the simplified system has been removed. Note that the pressure in the canal at the edge of

the incised section is expected to be equal to the anterior chamber pressure, as are the pressures at the entrances of the collector channels exposed by the incision to the anterior chamber.

The alterations introduced to the simulate the effects of a partial trabeculotomy on the outflow network model clearly violate the flow boundary conditions specified in chapter 1. The flow enters directly into the canal via the trabecular incision without encountering any significant flow resistance, and then proceeds along the canal in a unidirectional manner away from the incision opening. The flowrate along the canal decreases as it passes each collector channel, with part of the flow entering the channel opening and the rest of the flow proceeding on towards the next collector channel. As the flow moves along the canal, the pressure gradually decreases due to the flow resistance of the canal itself, and the flowrate driven through the meshwork gradually increases as the pressure drop between the anterior chamber and the canal lumen increases.

In this section, the data from a study of partial trabecumotomies performed by Rosenquist et al [26] are analysed and compared to model predictions of the effects of such alterations to the outflow system. The Rosenquist study focussed on the effects of partial trabeculotomies under physiologic conditions (IOP=7 mmHg) and at elevated pressure (IOP=25 mmHg). The partial trabeculotomies performed on enucleated eyes were designed to study the effects of improved access to the collector channels via Schlemm's canal (in a limited trabeculotomy) compared to the complete removal of the meshwork itself. The modelling of partial trabeculotomies help evaluate the role of Schlemm's canal in the normal eye by placing it in a scenario where it is the primary factor determining observed changes in outflow resistance.

5.2.2 Experimental Trabeculotomy Data

Experimental data from Rosenquist et al. [26] are reviewed in this section for the purpose of comparing this data to the predictions by the model presented in section 5.2.3. Facility was measured at four stages of the experiment:

1. F_0: a baseline measurement before any incisions were made,

2. F_1: after a one hour incision had been performed,

3. F_4: after a further 3 one-hour incisions were made, for a total of four one-hour cuts placed in a symmetric pattern 90° apart from each other, and

4. F_{12}: after a complete 12-hour trabeculotomy was performed to remove all the remaining meshwork.

When plotting the trabeculotomy data, one has the choice of presenting the data in terms of facility or resistance. The changes in outflow facility (resistance) are usually presented in a normalized form where the changes in facility (resistance) are divided by the maximal changes in facility (resistance) observed for a complete trabeculotomy. In terms of facility, this normalized parameter $\Delta\overline{F_i}$ is calculated using the formula

$$\Delta\overline{F_i} = \frac{F_i - F_0}{F_{12} - F_0} \tag{41}$$

where i=0,1,4,12 is the number of clock hours incised. The analogous formula for calculating normalized resistance change $\Delta\overline{R_i}$ is obtained by substituting in $R_i = \frac{1}{F_i}$, and multiplying both the numerator and denominator by -1.

$$\Delta\overline{R_i} = \frac{R_0 - R_i}{R_0 - R_{12}} \tag{42}$$

Data from Rosenquist's trabeculotomy study for IOP=25 mmHg are presented in table 2 and plotted in figures 5.9 and 5.10 in terms of normalized facility and resistance changes, respectively. In both figures, curves of zero circumferential flow are plotted. These curves represent the theoretical change one would observe if the ends of the incisions were sealed off to eliminate direct access to the canal and Schlemm's canal resistance was negligible in the *intact* sections of the outflow system. We can express the theoretical change in normalized facility in terms of the fractional degree of trabeculotomy α, the total trabecular facility F_{tm}, and the total aqueous vein facility F_{av}.

$$\Delta\overline{F}_{theory} = \frac{F_{total}(1-\alpha) + \alpha F_{av} - F_{total}}{F_{av} - F_{total}} = \alpha \tag{43}$$

where:

$$F_{total} = \frac{1}{\frac{1}{F_{tm}} + \frac{1}{F_{av}}} \tag{44}$$

Note that $\Delta\overline{F}_{theory}$ varies linearly with respect to α and is independent of F_{tm} and F_{av} [13]. However, when we express the theoretical change in normalized resistance in terms of the total trabecular resistance R_{tm}, total aqueous vein resistance R_{av} and α,

$$\Delta\overline{R}_{theory} = \frac{R_{tm} + R_{av} - \frac{1}{\frac{1-\alpha}{R_{tm}+R_{av}} + \frac{\alpha}{R_{av}}}}{R_{tm}} \tag{45}$$

$\Delta\overline{R}_{theory}$ turns out to vary non-linearly as a function of α, and also depends on the particular values of R_{av} and R_{tm}. Thus, the trabeculotomy data is analysed and compared to numerical results in terms of normalized facility changes.

5.2.3 Results of the Numerical Simulations

The Rosenquist data thus provides us with a total of four partial trabeculotomy scenarios to consider:

1. one-hour trabeculotomy at IOP=7 mmHg
2. one-hour trabeculotomy at IOP=25 mmHg
3. 4 one-hour trabeculotomies at IOP=7 mmHg
4. 4 one-hour trabeculotomies at IOP=25 mmHg

The model predictions are presented and compared to the experimental results of Rosenquist et al. in table 2 and figures 5.11-5.12.

The numerical prediction of $\Delta\overline{F}_1$=41% for case 1 is within the standard error of the experimental result ($54 \pm 16\%$), and the difference is statistically insignificant ($p > 0.25$). Examining the canal height (figure 5.13) distribution for case 1, we see that the canal remains relatively open throughout the outflow system. The pressure starts at IOP at the edge of the trabecular incision, and decreases monotonically moving away from the cut.

For case 2, the model predicts a facility increase of 27% compared to the experimental result of $19 \pm 5\%$, which again is a statistically insignificant difference

(p>0.1). The canal height distribution (fig 5.14) indicates that circumferential flow reaches only 3 collector channels away from the edge of the incision before the outflow system is essentially unaware of the existence of the trabecular incision. This is because the experiment is run at a constant pressure of 25 mmHg, which is sufficiently high to collapse the canal, thus limiting the effect of the trabecular incision as a bypass mechanism. This observation supports the qualitative hypothesis by Rosenquist et al. [26] that a higher IOP reduces the degree of circumferential flow by collapsing Schlemm's canal.

The model predicts that 4×1-hour trabeculotomies at both 7 mmHg and 25 mmHg (cases 3 and 4) produce nearly as much facility increase as that realized after removing all the trabecular meshwork. Roughly 95% of the meshwork resistance is eliminated by removing 33% of the trabecular meshwork. This result is virtually independent of IOP, with $\Delta\overline{F}_4$ decreasing by less than 1% as IOP increases from 7 mmHg to 25 mmHg. At 25 mmHg, $\Delta\overline{F}_4 = 55 \pm 7\%$ for the experiment, which is a highly significant difference from the numerical prediction ($p < 0.001$). The agreement at 7 mmHg seems to be quite good if $\Delta\overline{F}_4 = 99 \pm 32\%$ for the experiment, but the exclusion of a single data point (350%) changes the result to $\Delta\overline{F}_4 = 68 \pm 10\%$. The exclusion of this data point cannot be statistically justified despite the fact that it exerts undue influence on the average result for the data set. No conclusions will be made based on comparisons to numerical predictions for case 3 because of the high degree of uncertainty in the experimental data.

The canal height distribution for case 3 (figure 5.15) shows the canal to be almost fully uncollapsed everywhere, resulting in the nearly maximal facility increase. The corresponding plot for case 4 (figure 5.16) is very similar to that of case 3; the canal is slightly smaller, but not significantly so. The magnitude of the discrepancy between model and experiment for case 4 suggests that the canal is actually in a collapsed state, and not in the open regime as predicted by the model. If we consider the loss in effectiveness caused by circumferential flow resistance, $1 - \Delta\overline{F}_4$, the loss predicted by the model (5%) is an order of magnitude smaller than the

loss observed experimentally (45%). This result suggests that the behavior of the outflow system after a 4×1-hour trabeculotomy is different in some fundamental aspect which has not been accounted for in the modelling process.

•Conclusions from Comparing of Experimental and Numerical Results

1) Agreement between experiment and theory could be achieved for case 1 by choosing an uncollapsed canal height of h_o=20 μm, which is within the limits reported from morphological studies [19,24,31]. Since h_o is the dominant controlling parameter for $\Delta\overline{F}_1$ at low intraocular pressures, this result indicates that the model assumptions and parameters chosen to determine the conductance of Schlemm's canal in the uncollapsed state produce reasonable values for the overall flow resistance exhibited by the canal.

2) The large discrepancy between numerical and experimental results for the 4×1-hour case at IOP=25 mmHg suggests that the effects of the four incisions on the outflow system are not fully accounted for simply by removing the corresponding network resistances over the incised area. The trabecular incisions must produce some other alteration(s) in the system which are as yet unmodeled, and these alteration(s) are of lesser significance when the outflow system is traumatized to a lesser degree by a single one-hour incision.

In the next section, a possible explanation is proposed to account for the apparent degree of canal resistance suggested by the experimental data for case 4, which is significantly greater than predicted by the model.

5.2.4 Effects of Meshwork Weakening Caused by Trabeculotomy

The hypothesis is proposed that the resistance of the canal to circumferential flow appears to be greater than expected because the trabeculotomy procedure produces damaging physical stresses to the surrounding tissue, thus weakening it mechanically. The model is thus altered appropriately to incorporate this effect. The criterion followed in modifying the model was that the alteration must lower

the circumferential flow for cases 3 and 4, and must at the same time produce a negligible effect on the result for case 1, which is already in good agreement. For case 2, the model predicts a facility increase which is greater than the experimental result, but the difference is not statistically significant. A small decrease in facility due to local meshwork weakening would improve the agreement, but the decrease must not be so great as to cause the model prediction to significantly underpredict the experimental result. A local weakening of the meshwork could produce the desired effects for the 4×1-hour cases and leave case 1 unaffected if the meshwork is sufficiently stiff to hold open the canal under the conditions for case 1 but not for the other cases.

Since the only important discrepancy which must be considered is for case 4 (see section 5.2.3), we propose that meshwork weakening becomes significant only when four incisions are made in the trabecular meshwork of the outflow system. For the purpose of simplicity, the meshwork stiffness is reduced uniformly by an order of magnitude from E_{tm}=10 mmHg to E_{tm}=1 mmHg. $\Delta\overline{F}_4$ predicted by the model decreases from 95% for E_{tm}=10 mmHg to 57% for E_{tm}=1 mmHg, which is in good agreement with experiment ($\Delta\overline{F}_4$ = 55%). Note that the canal height distribution predicted by the model with the lower meshwork stiffness (figure 5.17) is radically different from that predicted with the normal meshwork stiffness (figure 5.16). The canal collapses to such a high degree with the lower stiffness that the sections of the outflow system right in the middle of the intact meshwork segments are essentially unaffected by the 4×1-hour trabeculotomy.

Meshwork weakening is only one of a number of different alterations to the outflow system which could account for the high degree of circumferential resistance observed experimentally. However, the conclusion remains the same that Schlemm's canal must be highly collapsed if experimental artifacts such as the clogging of collector channels by meshwork debris are ruled out. In the next chapter, the effects of other such hypothetical alterations to the outflow system are studied to evaluate their potential for decreasing the overall resistance of the network.

6 Model Predictions

In this chapter, the network model is used to predict the effect of various outflow system alterations which have not been studied experimentally. The goal in modelling hypothetical cases is to theoretically investigate the effectiveness of different changes in reducing the resistance to relieve high intraocular pressure which results in glaucoma. The model gives the investigator the capability to consider a variety of interventions to the outflow system, and hopefully identify effective procedures which could be further studied by experiments.

6.1 The P-R Curve for a Glaucoma Model

Having concluded previously with experiments and with the model that a glaucomatous level of flow resistance cannot be achieved by meshwork weakening and a concomitant collapse of the canal, we now consider the case where an increase in meshwork resistance is the primary cause of glaucoma. A typical glaucomatous eye has a pressure drop of 20 mmHg across the outflow system and a normal aqueous outflow rate of 2 μl/min [5]; measured in the above units given for IOP and Q, the outflow resistance is 10 units, where a unit of resistance is equal to 1 mmHg/μm/min. To model the glaucoma flow conditions, it will be assumed that the meshwork resistance R_{tm} is the only component which changes by increasing from 2 units to 7 units, with all other parameters remaining at their normal values as given in section 3.1. Since the outflow rate remains normal, this yields a pressure drop of 20.6mmHg and a resistance of 10.3 units which are satisfactory values for a glaucoma model. Note that an increase in R_{tm} of 5 units results in a total resistance increase of 6.5 units; the secondary effect is canal collapse, which accounts for 23% of the total increase in resistance from normal to glaucomatous levels.

The glaucoma model P-R curve is plotted along with the normal model P-R curve (from section 5.1) in terms of the absolute resistances (figure 6.1) and normalized resistances (figure 6.2). Although the normal and glaucoma model resistances differ by 100-150%, the normalized resistances differ by only 25% or less. In terms

of the slope of the normalized P-R curve, (ie. the outflow obstruction coefficient 'Q' as given in section 5.1), the slope is ~1.0% for the normal curve and ~0.7% for the glaucoma model curve. This shows that the normalized resistance curve is fairly insensitive to changes in R_{tm}, since a 130% change in the resistance at 10 mmHg induces only a 30% change in normalized P-R slope. The increase in meshwork resistance enhances the pressure drop across the meshwork for a given flowrate, and thus increases both the degree of canal collapse and the resistance generated by Schlemm's canal.

The results also suggest that substantially stiffening the meshwork ($E_{tm} \uparrow$) to open up the canal would reduce the outflow resistance by only 15%, which is equivalent to a 3 mmHg drop in IOP at physiologic constant flow conditions. Note though that pilocarpine, which is thought to act on the outflow system by increasing the tension on the ciliary muscle and scleral spur [14], can clinically decrease IOP in glaucomatous eyes from an untreated level of 30 mmHg or more down to acceptable levels 20 mmHg or lower [9]. Such an effect could not be explained by meshwork stiffening and uncollapsing of the canal alone. Schlemm's canal collapse could account for a much larger resistance increase in the glaucomatous eye if the septae support deteriorated after a long-term collapse of the canal [23]. Alternatively, tension induced by pilocarpine could have an effect on the primary site of flow resistance in the JCT and endothelial lining.

6.2 YAG Laser Holes in the Meshwork

The clinical purpose of creating holes in the trabecular meshwork with localized laser blasts is to reduce the outflow resistance by attempting to bypass the meshwork with an alternate pathway.

The YAG laser transfers energy to the trabecular meshwork via the mechanism of photodisruption. This mechanism exploits the non-thermal effects of laser radiation and thus is often referred to as 'cold lasing'. On the other hand, ophthalmic operations such as laser trabeculoplasty rely on the thermal effects of photocoag-

ulation to achieve the desired effects. A YAG laser used in the Q-switched photodisruption model three-dimensionally aims the beam to a target point within the meshwork region. In such an ophthalmic application, the typical pulse duration will be less than 1 μsec, the irradiance is on the order of 1 MW/cm^2 and target point can be focussed down to microns in diameter [30]. The physical mechanism of photodisruption requires optical breakdown, the formation of a plasma and the subsequent propogation of pressure waves from the target point. It is the pressure waves which transmit mechanical energy to the surrounding tissue to create a hole in the meshwork.

The effects of YAG holes are theoretically similar to those produced by trabeculotomy. The intact meshwork adjacent to a hole or incision is locally bypassed to provide direct communication between the anterior chamber and the canal lumen. The canal acts as a communications channel through which a local opening in the meshwork can affect a large circumferential section of the meshwork many times greater than the extent of the section of meshwork which is actually removed. The difference between a trabecular incision and a YAG hole is primarily in the extent of the meshwork opening.

The effective diameter of holes produced by a YAG laser focussed on the meshwork is typically about 50μm (personal communication, Dr. Mark Latina). For holes of this size, it can be demonstrated with the network model that the effectiveness of the holes is practically independent of their size. The holes are too large to create a significant pressure drop in the flow entering the canal through them. The largest possible pressure drop across the YAG hole can be calculated by assuming the entire aqueous outflow is diverted through the hole and using Sampson's law [15] for flow through an aperture:

$$\Delta P = \frac{3\mu Q_{total}}{r^3} \simeq 3 \times 10^{-2} mmHg \tag{46}$$

where:

Q_{total} = total outflow rate = 2 μl/min (physiologic conditions)

r = radius of YAG hole $\simeq$ 25 μm

The pressure drop across the YAG hole can thus be neglected because it is 3 orders of magnitude smaller than the pressure drop across the outflow network. At the same time, the holes are too small (and generally too few in number) to remove a substantial fraction of the meshwork.

•Effect of YAG Holes on Normal and Glaucomatous Eyes

The effects of a variable number of YAG holes placed equidistantly in the meshwork are modeled under constant flow conditions where Q=2μl/min (see figure 6.3). The normal eye results were produced with R_{tm}=2 units, and the glaucoma model results were run with R_{tm}=7 units (see section 6.1). The initial IOP of the glaucomatous eye is nearly 3 times higher than normal IOP. The first hole produces the most dramatic effect on the glaucoma model, decreasing the IOP by over 12 mmHg so that it is now only 32% higher than the IOP of the normal eye under the same conditions. With two holes placed 180° apart, the difference in IOP between the normal and glaucoma models now becomes nearly indiscernable. If such a conclusion could be verified experimentally, this would support the hypothesis that glaucoma is primarily caused by a pathological change in the meshwork because a direct alteration of the meshwork itself could account for nearly all of the abnormal pressure drop across the outflow system.

6.3 Trabeculotomy Under Constant IOP vs. Constant Flow

Experiments on enucleated human eyes have historically been performed under constant pressure. This is partially out of neccessity, since constant pressure is much easier to achieve under experimental conditions than constant flowrate on the order of microlitres per minute. However, flow is considered to be constant in the live human eye because the aqueous production rate in the posterior chamber is constant and largely independent of intraocular pressure [5]. The effects of biochemical agents or mechanial alterations could be altered if the basis for comparison is constant pressure rather than constant flow. This could lead to the situation where the

beneficial effects of a particular modality of treatment are erroneously evaluated; the effects observed experimentally under constant pressure may or may not be manifested under clinical conditions at constant flow.

In section 5.2.3, the data from the Rosenquist study [26] of partial trabeculotomies at IOP=25 mmHg was presented. The normalized facility increase after a 4×1-hour trabeculotomy was calculated to be $(\Delta\overline{F}_4)$=55% using equation 41. It was found in section 5.2.4 that reducing the meshwork stiffness E_{tm} from 10 mmHg to 1 mmHg could give us good agreement between the model and experiment. We now consider the scenario where meshwork weakening is *assumed* to be the correct mechanism which accounts for the limited effectiveness of the 4×1-hour trabeculotomy and investigate what the effect would have been if the trabeculotomy had been studied at constant flow.

At IOP=25 mmHg, the model predicts an initial facility of 0.21 μl/min/mmHg, or a flow of Q=5.4 μl/min. With IOP constant and the meshwork weakened, the facility increases to 0.57 μl/min/mmHg after a 4×1-hour trabeculotomy and reaches 0.83 μl/min/mmHg after a total trabeculotomy; $(\Delta\overline{F}_4)$ for the partial trabeculotomy is 57%. If Q is now held constant at 5.4 μl/min and the meshwork is identically weakened, we find the facility increases to 0.51 μl/min/mmHg and IOP decreases to 10.5 mmHg after a 4×1-hour trabeculotomy. The facility reaches a maximum value of 0.58 μl/min/mmHg and IOP drops to a minimum value of 9.3 mmHg after a total trabeculotomy; thus, $(\Delta\overline{F}_4)$ under constant flow is 82%. The effectiveness at constant flow is significantly higher than at constant pressure; in this example, a procedure which is nearly completely effective under physiologic conditions is only partially effective under the experimental conditions of the Rosenquist study.

6.4 Canalicular Blockade as the Cause of Glaucoma

It has been proposed that glaucoma may be caused be a collapse of Schlemm's canal. This hypothesis is based on the morphologic findings of many investigators which have demonstrated that the canal lumen narrows as intraocular pressure is

increased [19,23]. This theory is attractive because the correlation between canal collapse and an increase in outflow pressure (and resistance) can easily be substantiated by morphology. However, one cannot naively conclude that, based upon the above information, canal collapse is the mechanism which causes primary open angle glaucoma. The effects of canal collapse must be closely scrutinized and modeled to determine whether this mechanism by itself can generate sufficient levels of flow resistance which can be considered glaucomatous.

One mechanism which could cause canal collapse is the mechanical deterioration of the collagenous beams in the corneo-scleral meshwork, i.e., a weakening of the trabecular meshwork. These structures presumably provide mechanical support to hold the inner wall away from the outer wall when a pressure gradient across the inner wall maintains a force tending to collapse the canal.

Reducing the meshwork stiffness E_{tm} from 10 mmHg to 3 mmHg under a constant flow of 2 μl/min collapses all of the inner wall down to the level where it is now being supported by the septae (under compression) rather than the meshwork (under tension). This weakening only raises the intraocular pressure by less than 1 mmHg (see figure 6.4); the septae are able to maintain the canal open to a sufficient degree such that the resistance generated by the apparent collapse of the canal is negligible.

Another scenario that can be considered is the simultaneous weakening of meshwork and the septae to seal off the canal to a much greater degree. This hypothesis is less likely because it requires that two entirely independent pathological changes occur. The meshwork is under tensile stress, and counters this stress with the mechanical behaviour of collagenous structures. On the other hand, the septae must undergo compressive stress, countering this stress simply by maintaining the volume of its cells and other structures which rely on a cell wall for integrity. While this hypothesis cannot be ruled out entirely, it should be relegated to a secondary status while more likely scenarios are investigated first.

Regarding the controversy concerning the location of the bulk of the outflow re-

sistance in glaucomatous eyes, Nesterov is a strong supporter of canalicular blockade as the primary cause of open angle glaucoma, and puts forth the following evidence in favor of this theory [23]:

1. Trabeculotomy has been shown by Grant [12] to decrease both the outflow resistance and IOP to normal levels in eyes with early POAG. The canalicular blockade theory would explain the trabeculotomy result by assuming that the removal of the meshwork also uncollapses the canal, a theory which is supported by the model results from section 5.2.

2. Nesterov argues that since both trabeculotomy and sinusotomy in POAG produce roughly the same effects, the main fraction of the outflow resistance must be in the canal because the canal lumen is opened up in both operations. However, the effects of sinusotomy on the outflow system are even less known than trabeculotomy and is unlikely to leave the meshwork region unaffected. It is probable that the delicate inner wall could be artifactually damaged while the stronger outer wall is being removed. Natural attachments such as septae would unavoidably cause tears in the inner wall as the outer wall is pulled away. In addition, the removal of the outer wall allows the inner wall to freely distend as the pressure drop across the meshwork increases. Compaction of the JCT and endothelial lining against the septae and the outer wall no longer can occur, resulting in loss of a mechanism which could possibly account for a large fraction of the resistance change in POAG.

3. Laser trabeculoplasty is also cited as supporting evidence for the canalicular blockade theory. Nesterov proposes that laser trabeculoplasty relieves the pressure elevation in POAG by stiffening the meshwork and uncollapsing the canal. It would seem that, as was the case for sinusotomy, this does not support canalicular blockade as opposed to meshwork blockade because it is unlikely that the meshwork would remain largely unaffected after being photocoagulated. Van Buskirk et al. [32] found facility at IOP=40 mmHg to be

statistically invariant after laser trabeculoplasty was performed on enucleated human eyes despite a significant increase in canal cross-sectional area. This again suggests that the primary site affected by the laser is not Schlemm's canal.

4. In correlating morphological findings for glaucomatous eyes to the pathogenesis of the disease, Nesterov cites the morphologically observed narrowing and partial collapse of the canal in eyes with POAG [24]. However, the network model and the work of Johnson & Kamm [17] both indicate that a partial collapse of the canal generates a negligible amount of flow resistance.

The findings of network model generally do not support the canalicular blockade theory. IOP can be significantly elevated by canal collapse only if both the meshwork and the septae are simulataneously altered from conditions present in the normal eye. An increase in the meshwork resistance will, on the other hand, have the dual effect of raising the pressure drop across the inner wall and collapsing the canal (see section 6.1). However, the body of evidence which has been presented cannot rule out canalicular blockade as a possible cause of POAG because many implicit assumptions have been made regarding the role of Schlemm's canal in the normal eye. Homogeneity of the aqueous outflow system as defined in chapter 1 minimizes this role. It is plausible that regional non-uniformities which enhance the role of the canal could occur in the the normal eye without noticeably affecting the P-R curve observed experimentally. Under such conditions, canal collapse could significantly increase intraocular pressure by magnifying the effects of the regional non-uniformities. In an attempt to confirm this hypothesis, a scenario which satisfies the conditions of 'normal non-uniformity' will be considered in the following section.

•Meshwork Weakening and Non-Uniform Collector Channels

In all the models examined thus far, all of the collector channels are evenly spaced and equal in flow resistance. This perfect symmetry clearly is not an accurate representation of the behavior of an actual eye behaviour. A large collector channel

(with low resistance) could dominate a large region of meshwork, attracting all the flow coming through the meshwork and causing the flow to bypass the nearest collector channels which may be much smaller (with high resistance). In what follows, the hypothesis that a non-uniform collector channel distribution exists in the *normal* eye is combined with an abnormal state of meshwork weakening to see if glaucoma could result under such conditions. The objective is to examine scenarios where meshwork weakening could possibly be significant if the model of the normal eye is altered to account for factors such as non-uniformity of the network parameters. The modified outflow system model must still exhibit all of the known characteristics of the average normal human eye to be considered a possible 'normal' state of the eye.

An important stipulation of the above hypothesis is that the non-uniform CC distribution must not significantly alter the P-R curve so that the distribution could be considered a common characteristic of a normal eye. This requires that the septae stiffness parameter (K_{sc}) be appropriately adjusted to compensate for any changes in the P-R curve caused by the CC distributions. In general, non-uniformity in the CC's will cause K_{sc} to increase, decreasing the degree to which the canal can collapse to compensate for greater distances which must be traversed in the canal. Based on observations of aqueous veins by casting or India ink injection [25], one can propose a model with 5 large CC's in the system which carry most of the flow. The first distribution (A) to be studied is 5 large CC's and 25 small CC's, with the large CC's equidistantly spaced. Each large CC has 10 times the conductance of a small CC. Investigators have also observed the large CC's to be concentrated in a limited sector of the limbal region [1,2,3]. To account for this, the second distribution (B) to be studied will have the 5 large CC's concentrated in a group separated by $3X_{cc}$, $2X_{cc}$, $2X_{cc}$, and $3X_{cc}$ circumferentially in the canal, where X_{cc}=1200 μm (see section 3.1).

The P-R curve previously presented for a normal eye (see section 5.1) is plotted along with the P-R curves for the two distributions to show that the compensated

changes due to the non-uniform distributions are not significant (see figure 6.5). The K_{sc} values used in figure 6.5 are (in units of $\mu m/mmHg^{\frac{1}{3}}$) 5.0 for the uniform CC distribution, 5.37 for distribution A, and 5.22 for distribution B.

The trabecular meshwork can now be weakened at constant flow (Q=2 μl/min) to see if the non-uniform distributions could cause the intraocular pressure to increase to glaucomatous levels. The results plotted in figure 6.4 show that IOP increases by about 3 mmHg with either distributions A or B, as opposed to an increase of about 1 mmHg with the uniform CC distribution. The change is not negligible, but the maximum IOP which can be generated is still far below what is typically observed in glaucoma cases. Note also that there are almost no differences observed when the 5 large CC's are placed in a skewed formation (B) rather than equidistantly (A).

The model shows that a non-uniform distribution of the CC's as chosen will not cause a significant increase in outflow resistance when Schlemm's canal is collapsed. This does not rule out non-uniform CC's as being important in other scenarios where there are fewer large CC's with a higher large:small conductance ratio, but the relative degree of non-uniformity of the studied cases is insufficient to cause significant resistance due to regional flow redistribution.

7 Conclusions

The following conclusions are reached based upon the results of the network model and the comparison of the results to experimental data:

1. A network model of the entire aqueous outflow system was constructed and numerically solved.

2. The experimental pressure-resistance curve for enucleated eyes was extended to the 50-100 mmHg range. Results indicate that resistance continues to increase linearly with pressure in this range.

3. A one-third power law governing septae compression was proposed and tested. This model successfully produces a linear relationship between pressure and resistance in agreement with the experimental data.

4. The observed resistance increase associated with elevating IOP in normal enucleated eyes can be reproduced by the model with a collapse of Schlemm's canal alone. Attributing the increase in resistance to canal collapse is consistent with experimental results considered in this study.

5. By calculating the resistance of Schlemm's canal based upon its morphologically observed dimensions, the model correctly predicts the circumferential flow resistance of the canal in the uncollapsed state following a one-hour trabeculotomy.

6. According to the model, it appears that a weakening of the compliant inner wall and a concomitant collapse of Schlemm's canal will *not* generate glaucomatous levels of flow resistance.

•Future Work

The network model has the capability to simulate many intriguing scenarios which have not been run in this study. One of the most powerful features of the

network model is that it allows for a non-symmetric distribution of the network parameters. Consequently, the interactions between different regions of the system can be studied as well as the interactions between different components (i.e., meshwork, canal and collector channels). Some of these scenarios are presented below:

1. A statistical variation of the meshwork stiffness would alter the P-R curve for a normal eye in the low pressure region (IOP=0–20 mmHg). Such a change would likely eliminate the 'dip' in the P-R curve (see figure 5.4) caused by the decrease in collector channel resistance without any accompanying increase in canal resistance as IOP increases beyond that range. The canal would collapse earlier in some sections than at others, thus producing a smoother resistance increase at low pressure.

2. The septae have been modeled in this study as uniformly distributed throughout the canal lumen. However, this is contrary to evidence which suggests that the septae are concentrated near the collector channels, possibly for the specific purpose of preventing their occlusion [16]. If a non-uniform septae distribution is incorporated into the model to account for this observation, it must be done in such a manner as to preserve the linear behavior of the P-R curve in the high pressure region. In a homogeneous eye, the septae would mostly be removed (or reduced in effective height) from the middle region between two collector channels. However, the overall effect is small because that region is contributing a small fraction to the total outflow under collapsed conditions. Post-trabeculotomy, this is no longer the case because of the enhanced circumferential flow through the canal. Canal collapse away from the incision could effectively seal it off at the regions between collector channels where septae support has been reduced.

3. The assumption that all of the change in resistance with increasing IOP is due to Schlemm's canal collapse can be tested against the alternative that some or all of the resistance generation is actually in the meshwork. For

example, the meshwork resistance could be made a linear function of the local pressure drop. If Schlemm's canal resistance is relatively small, the pressure-resistance curve of such a model would still be roughly linear. This modified network model could then be tested with cases such as trabeculotomy. If the discrepancy between the model predictions and the experimental data increased, this would suggest that the change in resistance should indeed reside mostly in the canal.

References

[1] K.W. Ascher. Aqueous veins. *American Journal of Ophthalmology*, 25:31–38, 1942.

[2] K.W. Ascher. Further studies on aqueous veins. *American Journal of Ophthalmology*, 29:1373–1387, 1946.

[3] K.W. Ascher and W.M. Spurgeon. Compression tests on aqueous veins of glaucomatous eyes. *American Journal of Ophthalmology*, 32:239–251, 1949.

[4] J. Battaglioli. *The role of vessel collapse on the flow of aqueous humor.* Master's thesis, Massachusetts Institute of Technology, 1981.

[5] A. Bill. Blood circulation and fluid dynamics in the eye. *Physiological Reviews*, 55(3):383–416, 1975.

[6] A. Bill. Further studies on the influence of the intra-ocular pressure on aqueous humor dynamics in cynomolgus monkeys. *Investigative Ophthalmology & Visual Science*, 6:364–372, 1967.

[7] A. Bill and B. Svedbergh. Scanning electron microscopic studies of the trabecular meshwork and the canal of schlemm–an attempt to localize the main resistance to outflow of aqueous humor in man. *Acta Ophalmologica*, 50:295–319, 1972.

[8] R.F. Brubaker. The effect of intraocular pressure on conventional outflow resistance in the enucleated human eye. *Investigative Ophthalmology & Visual Science*, 14(4):286–292, 1975.

[9] P.A. Chandler and W.M. Grant. *Glaucoma.* Lea & Fibiger, Philadelphia, 1979.

[10] S. Duke-Elder. *System of Ophthalmology, vol. II–The Anatomy of the Visual System.* Kimptom, London, 1961.

[11] B.A. Ellingsen and W.M. Grant. The relationship of pressure and aqueous outflow in enucleated human eyes. *Investigative Ophthalmology & Visual Science*, 10(6):430–437, 1971.

[12] W.M. Grant. Experimental aqueous perfusion in enucleated human eyes. *Archives of Ophthalmology*, 69:143–161, 1963.

[13] W.M. Grant. Further studies on facility of flow through the trabecular meshwork. *Archives of Ophthalmology*, 60:523–533, 1958.

[14] I. Grierson, W.R. Lee, and S. Abraham. Effects of pilocarpine on the morphology of the human outflow apparatus. *British Journal of Ophthalmology*, 62:302–313, 1978.

[15] J. Happel. *Low Reynolds Number Hydrodynamics*. Prentice Hall Inc., 1965.

[16] F. Hoffmann and L. Dumitrescu. Schlemm's canal under the scanning electron microscope. *Ophthal. Res.*, 2:37–45, 1971.

[17] M.C. Johnson and R.D. Kamm. The role of schlemm's canal in aqueous outflow from the human eye. *Investigative Ophthalmology & Visual Science*, 24(3):320–325, 1983.

[18] M.A. Johnstone. Pressure-dependent changes in nuclei and the process origins of the endothelial cells lining schlemm's canal. *Investigative Ophthalmology & Visual Science*, 18(1):44–51, 1979.

[19] M.A. Johnstone and W.M. Grant. Pressure-dependent changes in structures of the aqueous outflow system of human and monkey eyes. *American Journal of Ophthalmology*, 75(3):365–382, 1973.

[20] R. Levene and B. Hyman. The effect of intraocular pressure on the facility of outflow. *Exp. Eye. Res.*, 8(116), 1969.

[21] R.A. Moses. Circumferential flow in schlemm's canal. *American Journal of Ophthalmology*, 88:585–591, 1979.

[22] R.A. Moses. Review: the effect of intraocular pressure on resistance to outflow. *Survey of Ophthalmology*, 22(2):88–100, 1977.

[23] A.P. Nesterov. *Glaucoma.* Grune & Stratton, 1986. Chapter 17–Pathological Physiology of Primary Open Angle Glaucoma: The Aqueous Circulation.

[24] A.P. Nesterov, N.H. Hasanova, and Y.E. Batmanov. Schlemm's canal and scleral spur in normal and glaucomatous eyes. *Acta Ophthalmologica*, 52:634–645, 1974.

[25] J.W. Rohen and F.J. Rentsch. Uber den bau des schlemmschen kanals und seiner abflubwege beim menschen. *Albrecht v. Gaefes Arch. klin. exp. Ophthal.*, 176:309–329, 1968.

[26] R. Rosenquist, D. Epstein, S. Melamed, M.C. Johnson, and W.M. Grant. Outflow resistance with variations in perfusion pressure and extent of trabeculotomy. *in press*, 1988.

[27] A. Shapiro. Steady flow in collapsible tubes. *Journal of Bimechanical Engineering*, 99:126–147, 1977.

[28] V.L. Streeter. *Handbook of Fluid Dynamics.* McGraw-Hill, 1961.

[29] R. Tripathi. Aqueous outflow pathway in normal and glaucomatous eyes. *Brit. J. Ophthal.*, 56:157–175, 1972.

[30] S.L. Trokel. *YAG Laser in Ophthalmic Microsurgery.* Appleton-Century-Crofts, 1983.

[31] E.M. Van Buskirk. Anatomic correlates of changing aqueous outflow facility in excised human eyes. *Investigative Ophthalmology & Visual Science*, 22(5):625–632, 1982.

[32] E.M. Van Buskirk, V. Pond, R.C. Rosenquist, and T.S. Acott. Argon laser trabeculoplasty. *Investigative Ophthalmology & Visual Science*, 91(9):1005–1010, 1984.

[33] F.M. White. *Viscous Fluid Flow.* McGraw-Hill, 1974.

List of Symbols

CC	collector channel
D	diameter of the eye
E_{tm}	stiffness of trabecular meshwork (mmHg)
$\Delta\overline{F_i}$	normalized facility change after i-hour trabeculotomy
G_{cc_k}	conductance of the k^{th} collector channel (μl/min/mmHg)
$G\underline{p}$	conductance matrix
G_{sc_i}	canal conductance of the i^{th} element (μl/min/mmHg)
G_{tm}	total inner wall conductance (μl/min/mmHg)
G^*_{tm}	inner wall conductance per unit circumferential length (μl/(min·mmHg·m))
G_{tm_i}	inner wall conductance of the i^{th} element (μl/min/mmHg)
h_i	canal height at the i_{th} node
h_o	undeformed canal height
h_s	septae height
h(x)	local canal height
IOP	intraocular pressure
k	meshwork permeability
K_{sc}	septae stiffness parameter (μm/mmHg$^{\frac{1}{3}}$)
M	number of nodes between adjacent collector channels
$\underline{p}$	pressure vector
P(x)	pressure in the canal
P_i	pressure in the canal at the i^{th} node
ΔP_s	minimum pressure at which septae begin supporting canal
ΔP	pressure drop across inner wall (=IOP-P(x))
N	number of collector channels
$\underline{q}$	flowrate vector
Q(x)	volumetric flowrate in the canal (μl/min)
Q_{cc_i}	flowrate through the i^{th} collector channel element

Q_{sc_i}	flowrate through the i^{th} canal element
Q_{tm_i}	flowrate through the i^{th} meshwork element
Q_T	total flowrate throught the outflow network
r	radial coordinate in the eye
R	radius of the eye (μm)
R_{cc}	total collector channel resistance (mmHg/μl/min)
Re_h	flow Reynold's number in Schlemm's canal
R_M	model resistance with M number of nodes between adjacent CC's
R_{tm}	total inner wall resistance (mmHg/μl/min)
R_{10}	outflow resistance at IOP=10 mmHg
R_∞	asymptotic resistance with infinite number of canal
$\Delta\overline{R_i}$	normalized resistance change after i-hour trabeculotomy
Res	residual of the numerical iteration algorithm
t	thickness of the JCT and endothelial lining
$\vec{V}$	flow velocity vector in the meshwork
W	width of the canal (μm)
x_i	circumferential distance in Schlemm's canal
Δx_i	circumferential distance between nodes i and $i+1$ in canal
X_{cc}	circumferential distance between adjacent collector channels
α	fractional extent of trabeculotomy
β^2	ratio of undeformed canal resistance to total resistance
μ	absolute viscosity of aqueous humor (kg/m·s)
ν	kinematic viscosity of aqueous humor (m^2/s)
ρ	density of aqueous humor (kg/m^3)
θ	circumferential coordinate in Schlemm's canal in cylindrical coordinates

Table 1

Pressure-Resistance Data for Enucleated Human Eyes

IOP	Eye 1	Eye 2	Eye 3	Eye 4	Eye 5	$\overline{R}$	$\overline{(R/R_{10})}$
10	3.31	2.73	2.80	4.14	7.37	4.12±0.85	1.00
50	5.68	3.70	3.24	4.99	9.81	5.46±1.14	1.36±0.09
100	8.26	4.24	4.60	6.52	11.9	7.10±1.40	1.78±0.18

Resistances are measured in units of mmHg/μl/min. $\overline{(R/R_{10})}$ is the average of the normalized resistances for each of the 5 eyes, where R_{10} is the resistance at IOP=10 mmHg for a given eye.

$$\overline{(R/R_{10})} = \sum_{i=1}^{5} \left(\frac{R_i}{R_{10_i}} \right)$$

Table 2

Trabeculotomy Data: Experiments vs. Model

	Experiment		Model	
	7 mmHg	25 mmHg	7 mmHg	25 mmHg
$\overline{R_0}$	3.76±0.26	4.07±0.38	3.81	4.65
$\overline{R_1}$	2.64±0.20	2.87±0.37	2.62	2.62
$\overline{R_4}$	2.11±0.10	1.81±0.33	1.84	1.25
$\overline{R_{12}}$	1.84±0.16	1.15±0.16	1.80	1.20
$\overline{\left(\frac{R_0-R_1}{R_0-R_{12}}\right)}$	64±13%	43±6%	59%	59%
$\overline{\left(\frac{R_0-R_1}{R_0-R_{12}}\right)}$	100±22%	78±5%	98%	98%
$\frac{\overline{R_0}-\overline{R_1}}{R_0-R_{12}}$	58%	41%	59%	59%
$\frac{\overline{R_0}-\overline{R_4}}{R_0-R_{12}}$	86%	77%	98%	98%
$\overline{F_0}$	0.277±0.020	0.263±0.024	0.263	0.215
$\overline{F_1}$	0.396±0.028	0.396±0.046	0.381	0.382
$\overline{F_4}$	0.484±0.025	0.695±0.111	0.543	0.800
$\overline{F_{12}}$	0.571±0.042	1.000±0.131	0.556	0.833
$\overline{\left(\frac{F_1-F_0}{F_{12}-F_0}\right)}$	54±16%	19±5%	41%	27%
$\overline{\left(\frac{F_4-F_0}{F_{12}-F_0}\right)}$	99±32%	55±7%	96%	95%
$\frac{\overline{F_1}-\overline{F_0}}{F_{12}-F_0}$	40%	18%	41%	27%
$\frac{\overline{F_4}-\overline{F_0}}{F_{12}-F_0}$	70%	59%	96%	95%

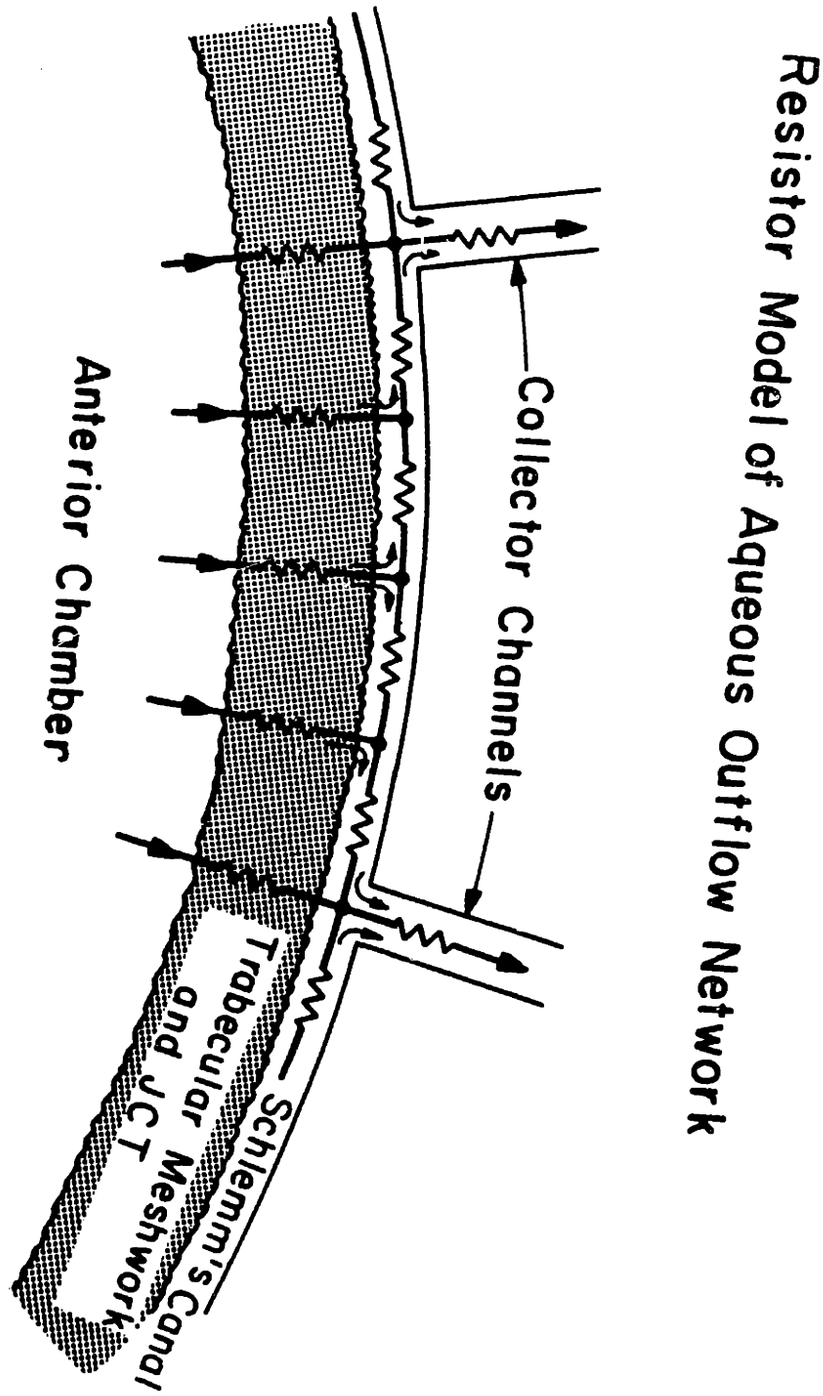

Figure 2.1—Schematic diagram of the network model for a representative section between adjacent collectors. The network has been simplified to M=4 for clarity.

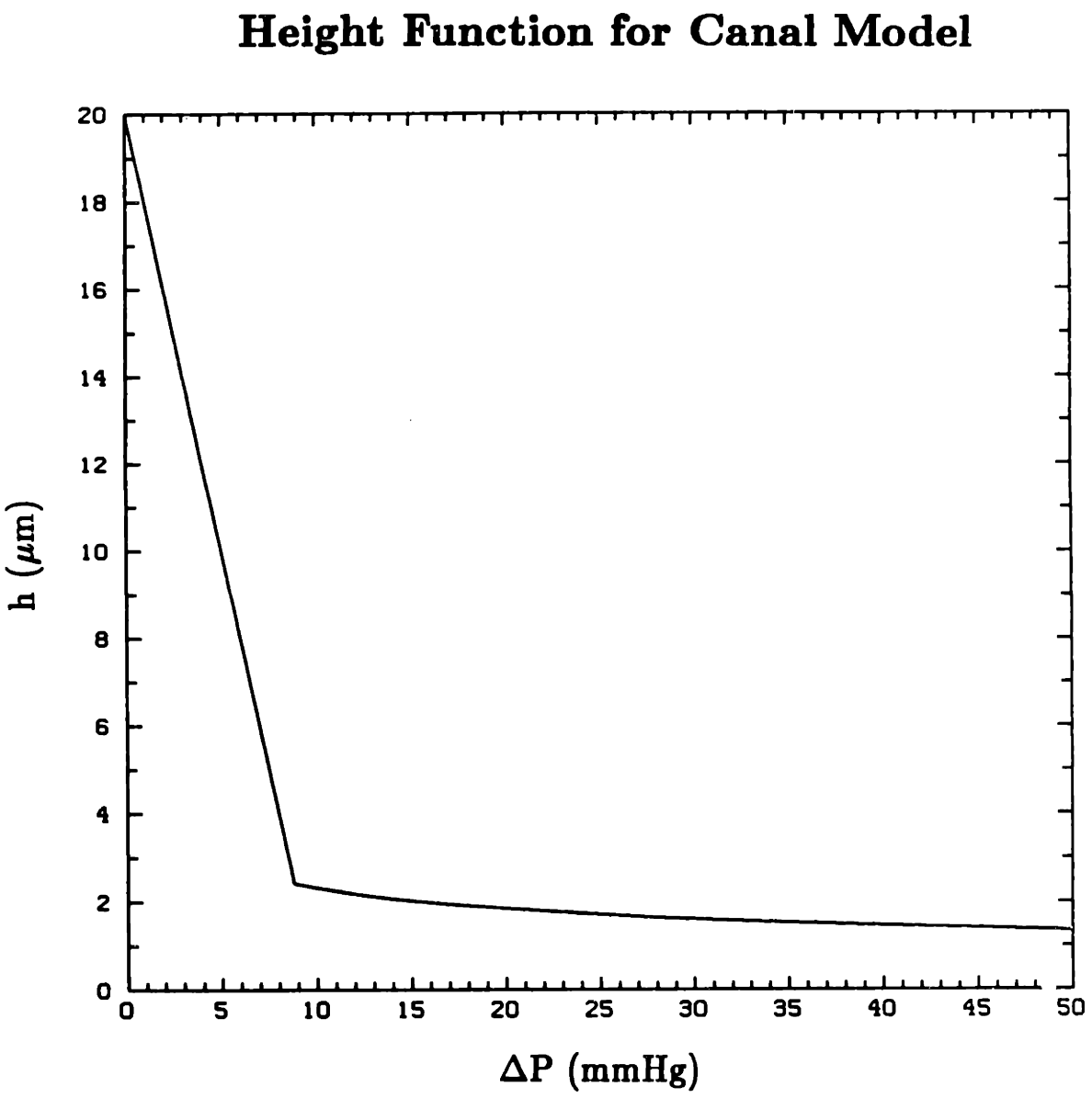

Figure 2.2—Canal Height (h) vs. Pressure Drop Across the Trabecular Meshwork (ΔP). E_{tm}=10 mmHg; h_0=20 μm; K_{sc}=5 $\mu m/mmHg^{\frac{1}{3}}$

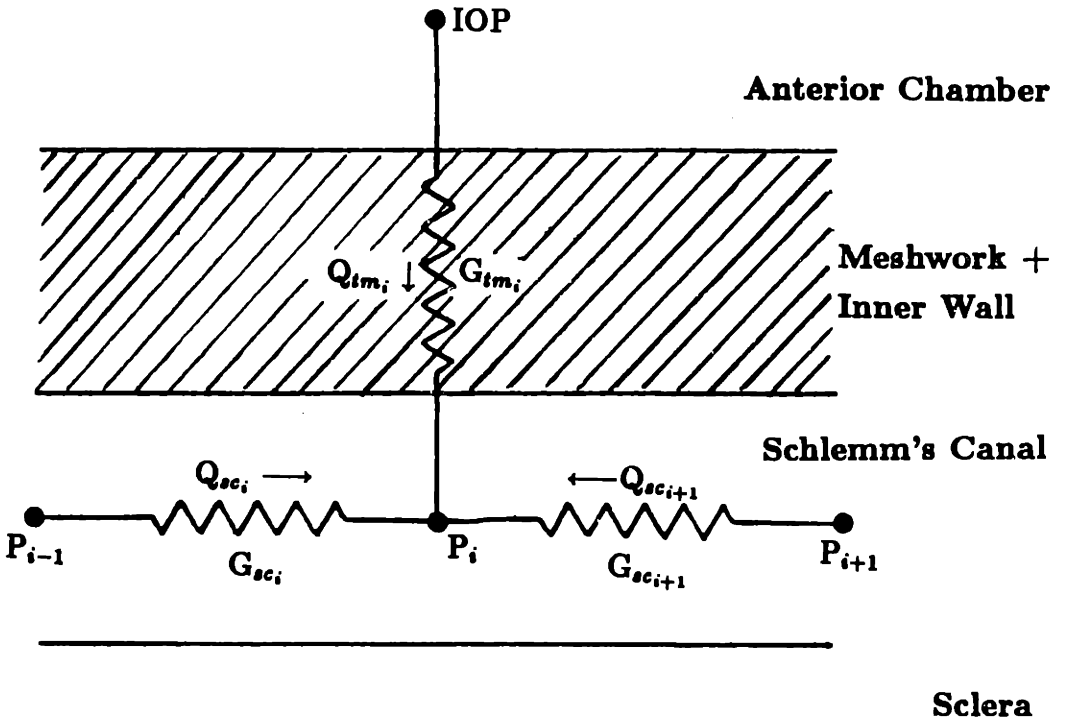

Figure 3.1—Schematic of flow resistors and pressure nodes.

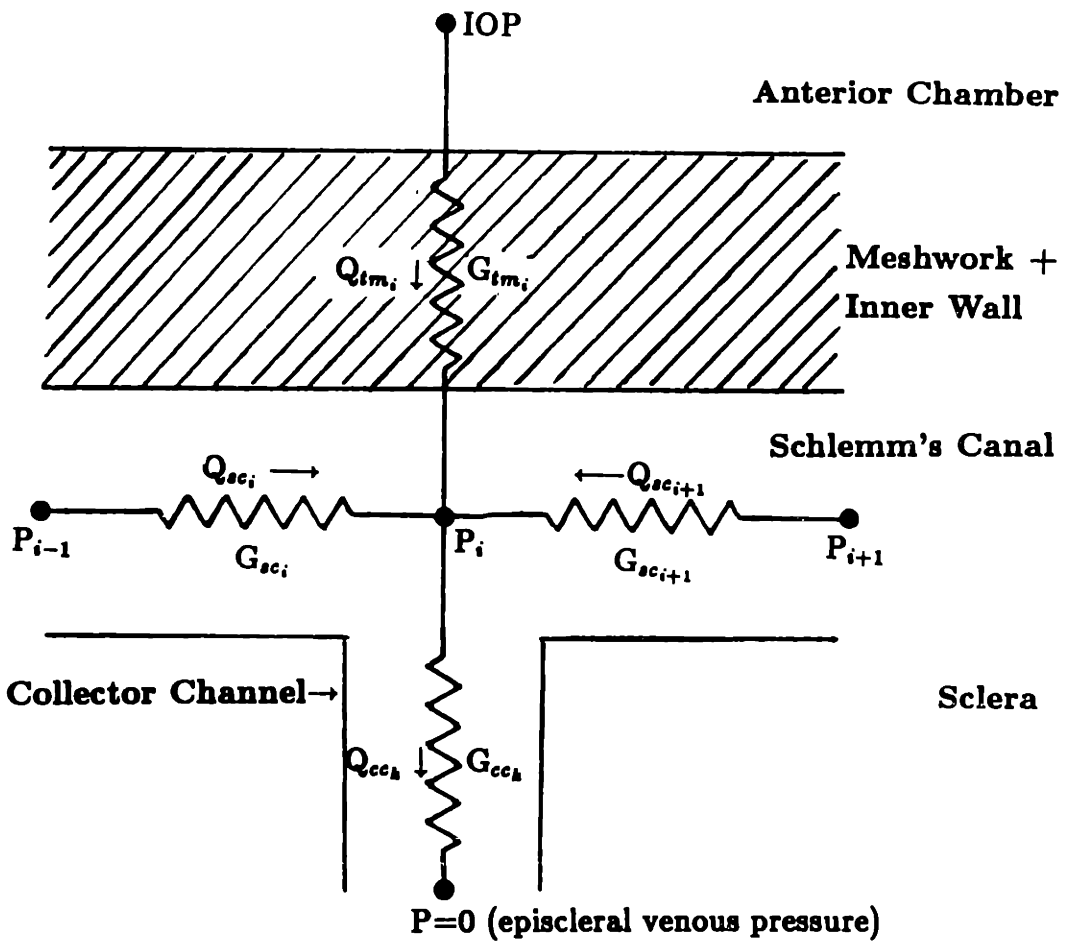

Figure 3.2—Schematic of flow resistors and pressure nodes at a collector channel opening.

$$\begin{bmatrix} G_{A_1} & G_{sc_2} & 0 & 0 & 0 & G_{sc_6} & G_{tm_1} \\ G_{sc_2} & G_{A_2} & G_{sc_3} & 0 & 0 & 0 & G_{tm_2} \\ 0 & G_{sc_3} & G^1_{B_3} & G_{sc_4} & 0 & 0 & G_{tm_3} \\ 0 & 0 & G_{sc_4} & G_{A_4} & G_{sc_5} & 0 & G_{tm_4} \\ 0 & 0 & 0 & G_{sc_5} & G_{A_5} & G_{sc_6} & G_{tm_5} \\ G_{sc_1} & 0 & 0 & 0 & G_{sc_6} & G^2_{B_6} & G_{tm_6} \\ G_{tm_1} & G_{tm_2} & G_{tm_3} & G_{tm_4} & G_{tm_5} & G_{tm_6} & \Sigma_1^6 G_{tm_i} \end{bmatrix} \begin{bmatrix} P_1 \\ P_2 \\ P_3 \\ P_4 \\ P_5 \\ P_6 \\ \text{IOP} \end{bmatrix} = \begin{bmatrix} 0 \\ 0 \\ 0 \\ 0 \\ 0 \\ 0 \\ Q_T \end{bmatrix}$$

$$G_{A_i} = -(G_{tm_i} + G_{sc_i} + G_{sc_{i+1}})$$

$$G^k_{B_i} = -(G_{tm_i} + G_{sc_i} + G_{sc_{i+1}} + G_{cc_k})$$

figure 3.3—System matrix representation of network model

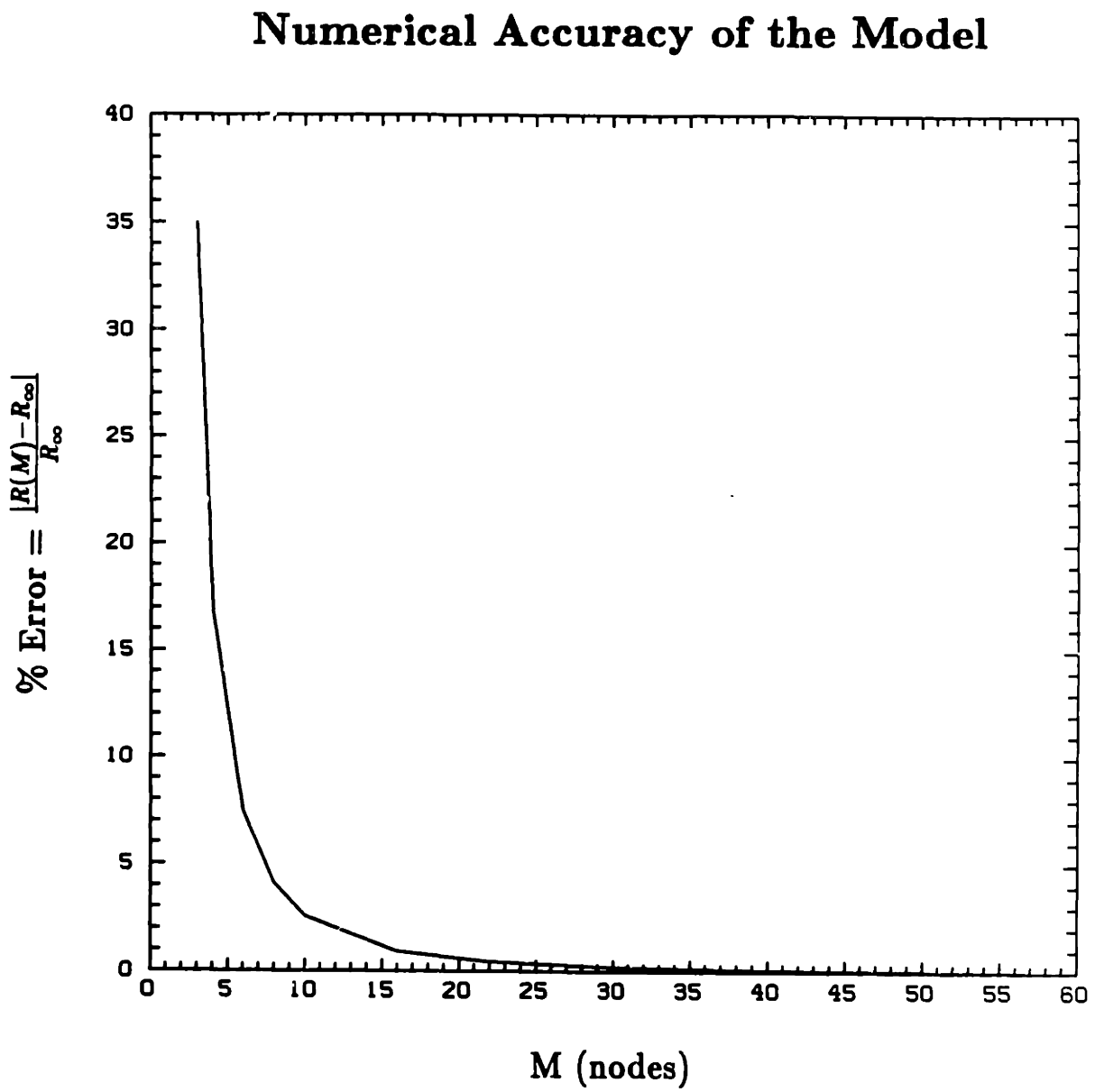

Figure 3.4—The relative error of a case with IOP=50 mmHg and all of the network parameters set to values as given in section 3.1. M is the number of nodes between adjacent CC's and R_∞ is the asymptotic resistance as M→∞.

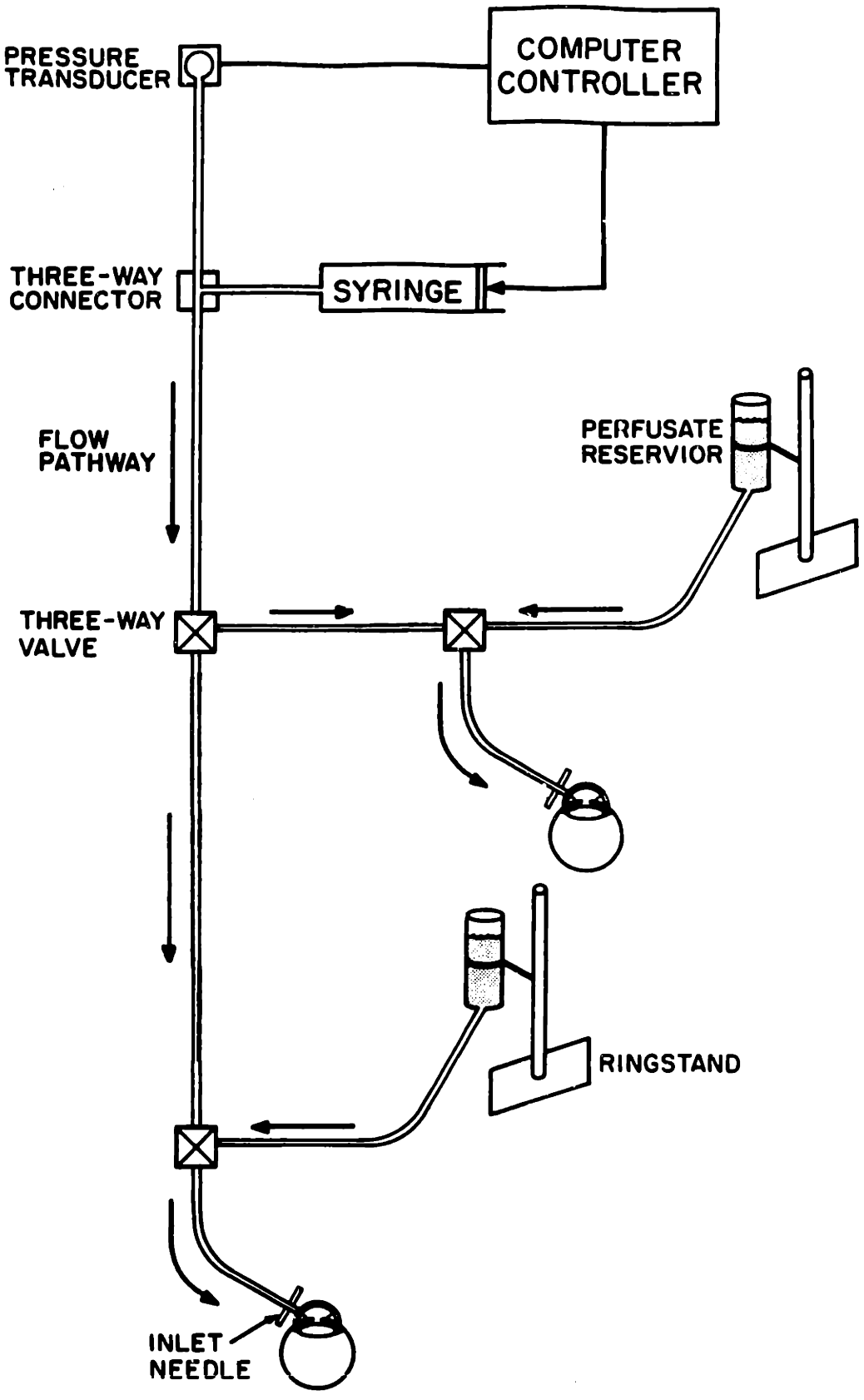

Figure 4.1—Schematic diagram of the perfusion apparatus set up to simultaneously run two eyes.

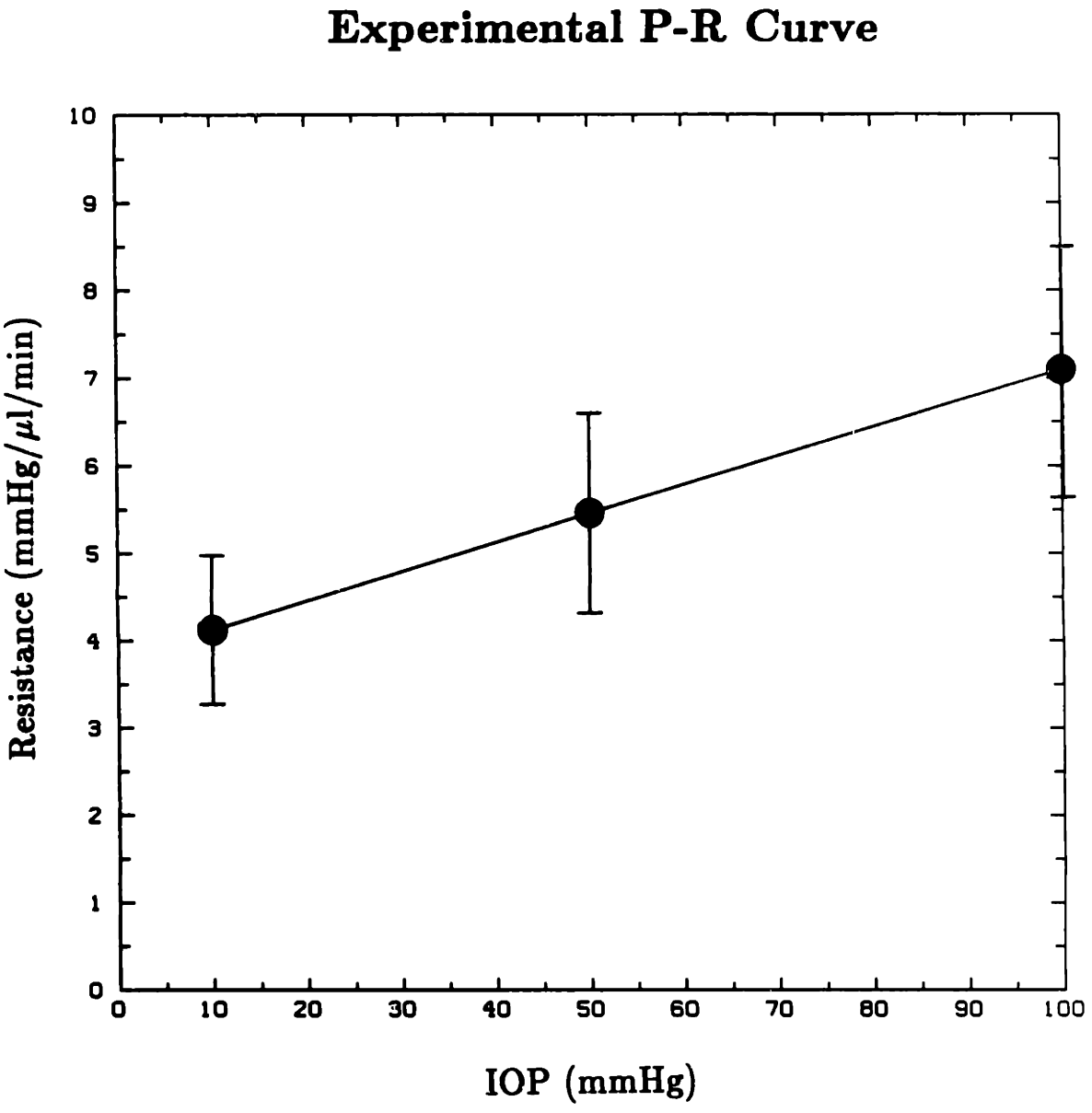

Figure 4.2—Experimental pressure-resistance results from the perfusion experiments. Standard error bars are plotted.

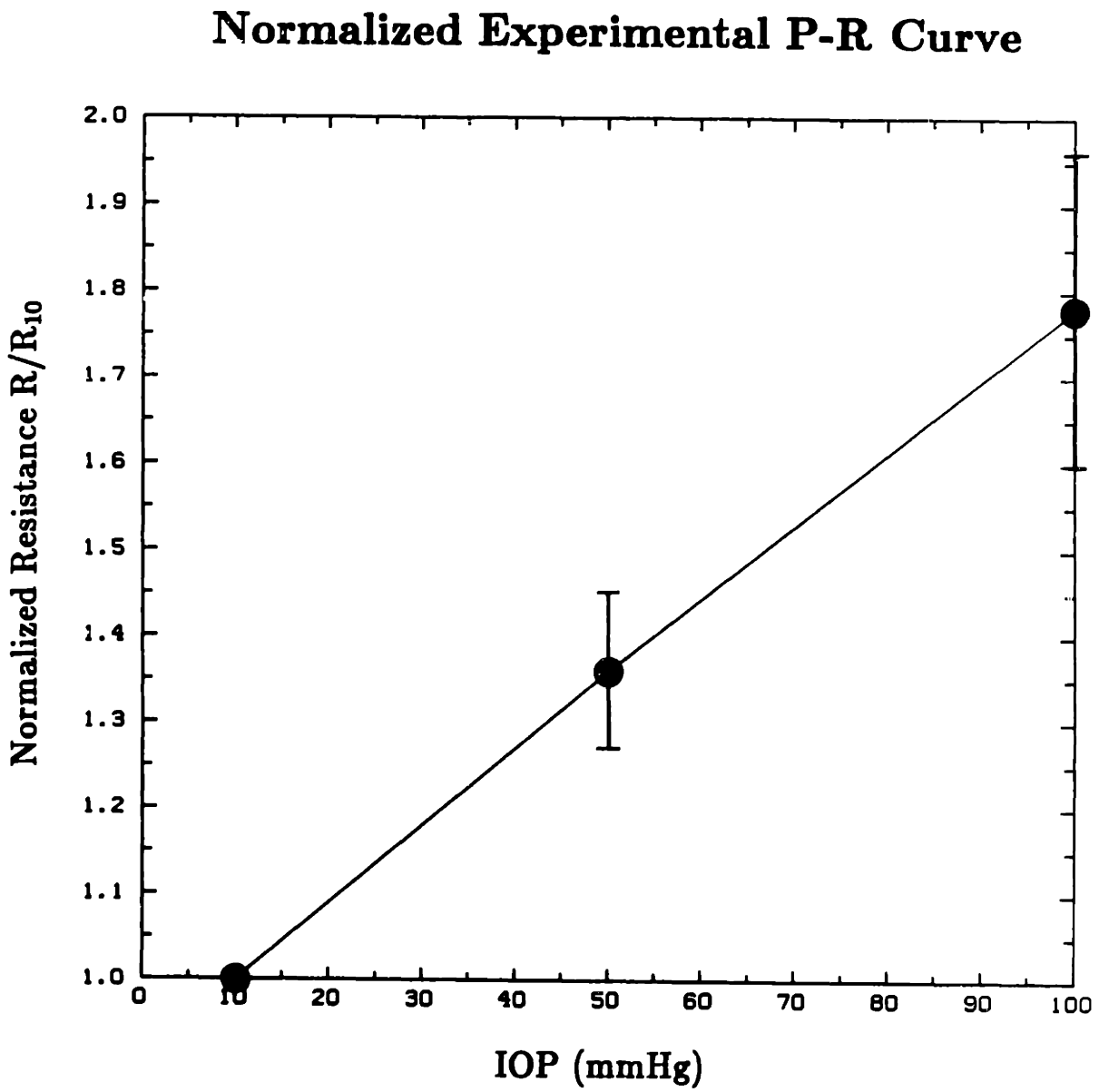

Figure 4.3—Experimental pressure-resistance data with the resistance normalized by R_{10}, the resistance at IOP=10 mmHg. Standard error bars are plotted.

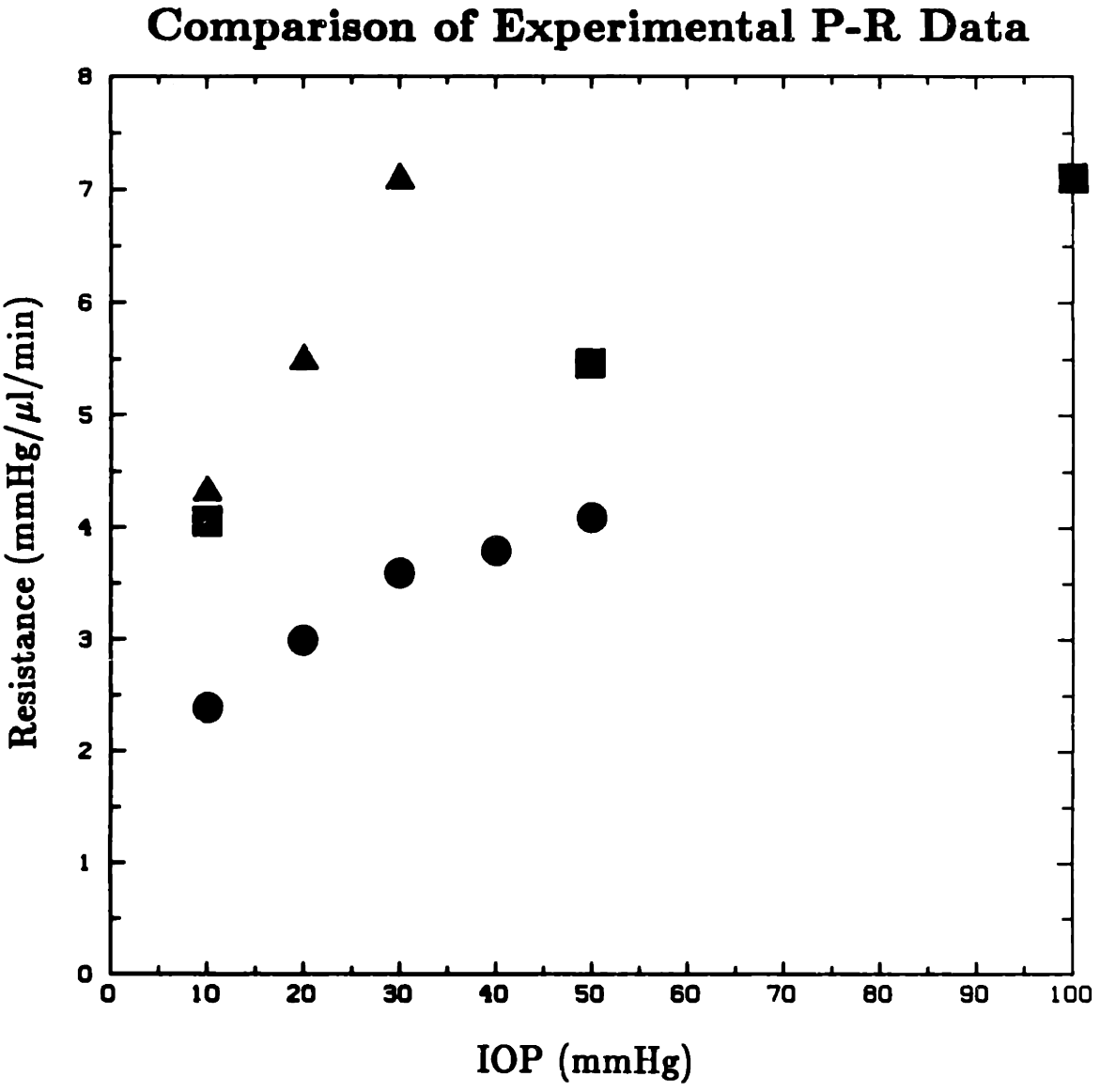

Figure 5.1—Compilation of the pressure-resistance data of various investigators. (●)–Brubaker[8], (▲)–Ellingsen & Grant[11], (■)–present study.

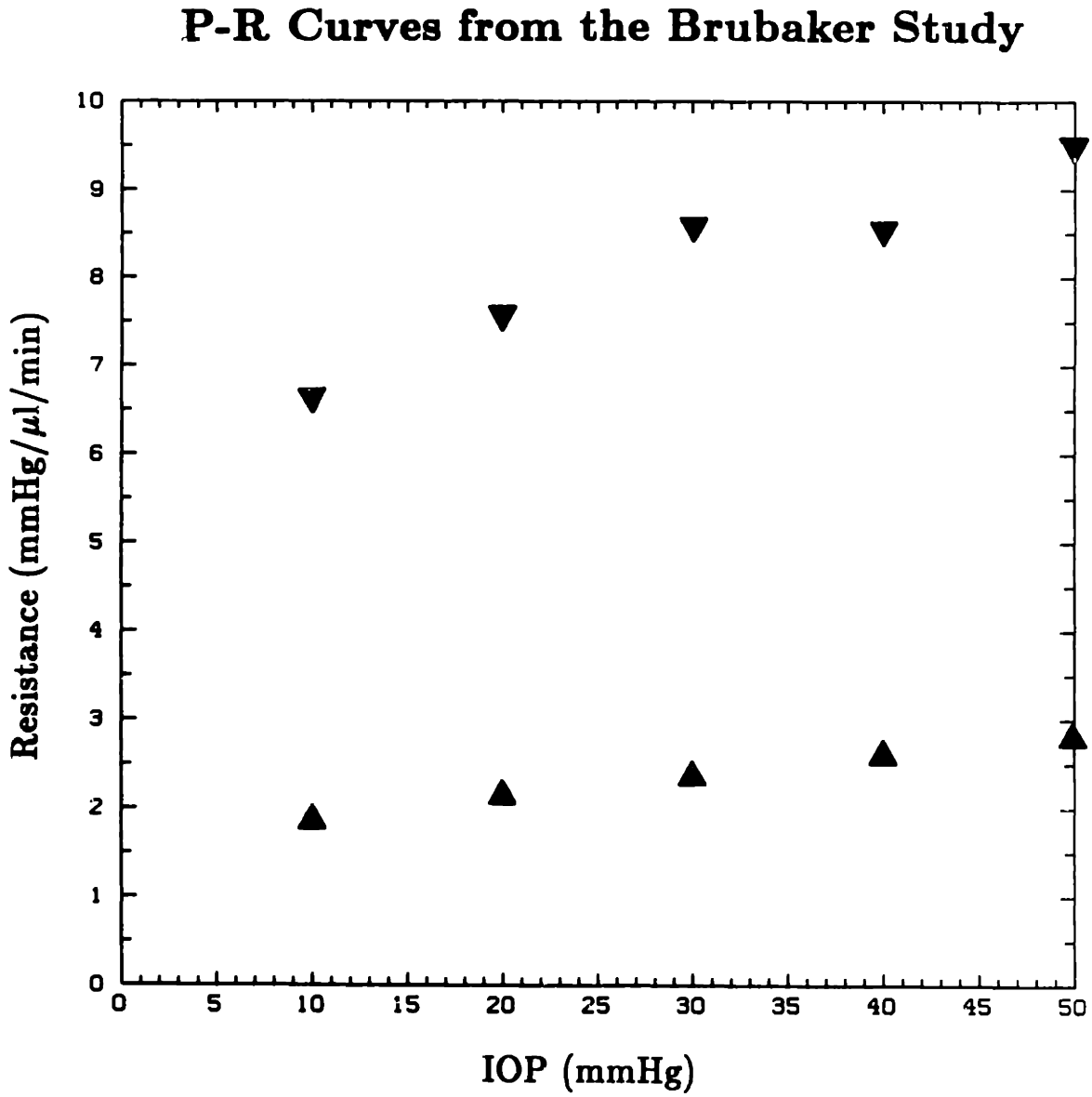

Figure 5.2—Pressure-Resistance data of Brubaker[8] with the 10 eyes divided into two groups of the 5 highest and 5 lowest resistances. (▼)–Highest resistance group, (▲)–Lowest resistance group.

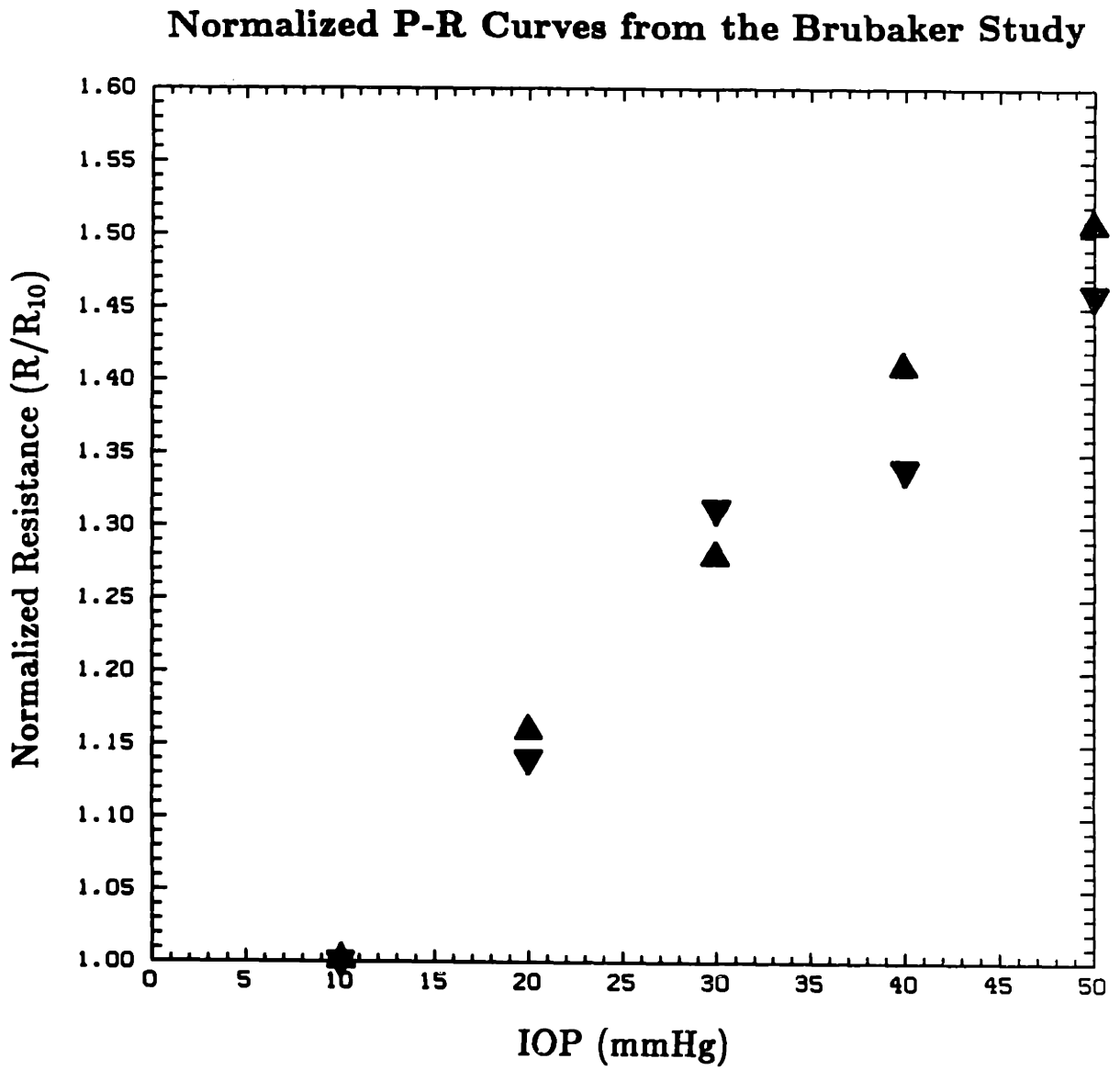

Figure 5.3—Pressure-Resistance data of Brubaker[8] normalized by the resistance at IOP=10 mmHg (R_{10}) with the 10 eyes divided into two groups of the 5 highest and 5 lowest resistances.
(▼)–Highest resistance group, (▲)–Lowest resistance group.

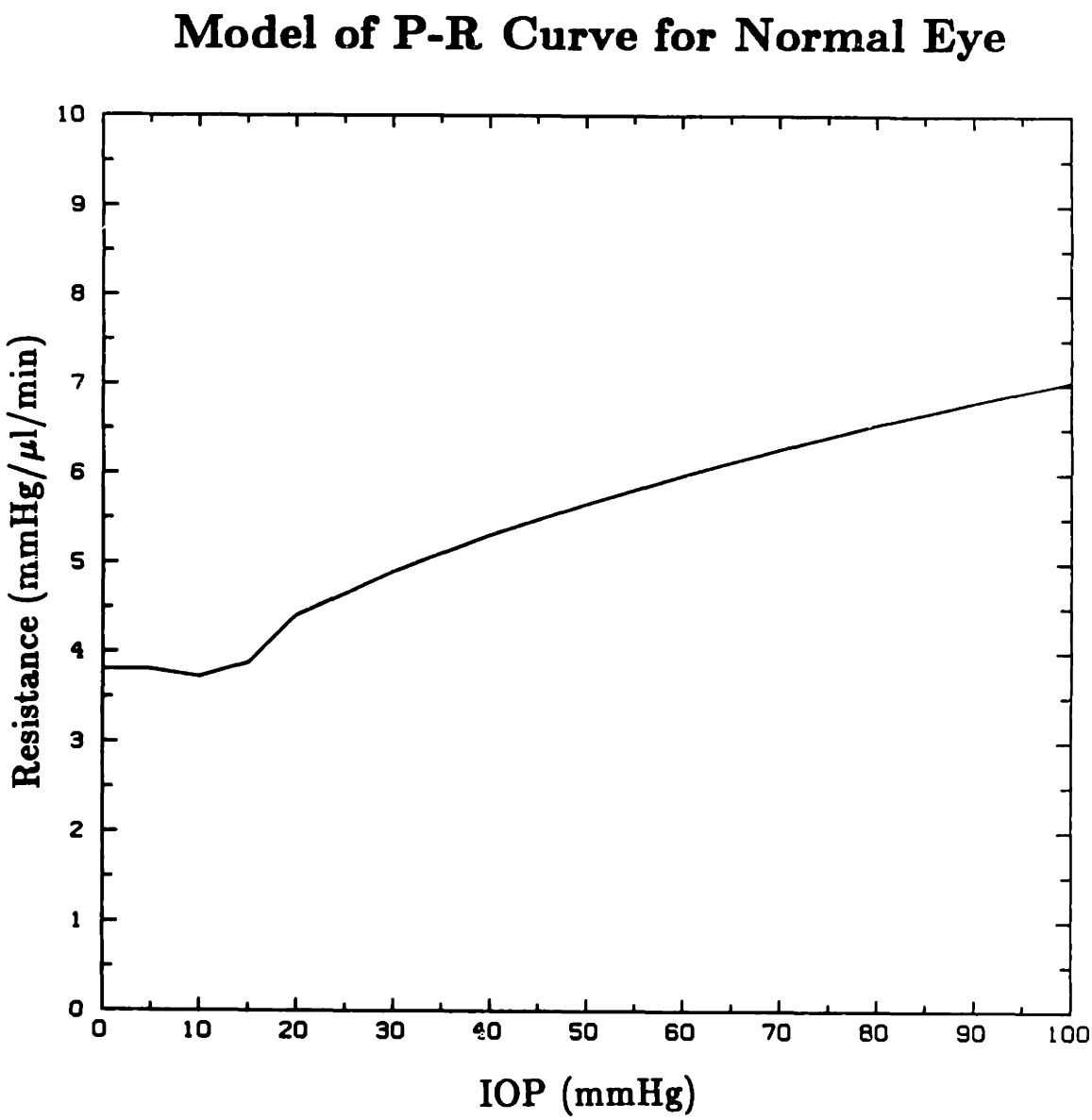

Figure 5.4—Network model of pressure-resistance curve for a normal eye, with all network parameters as given in section 3.1.

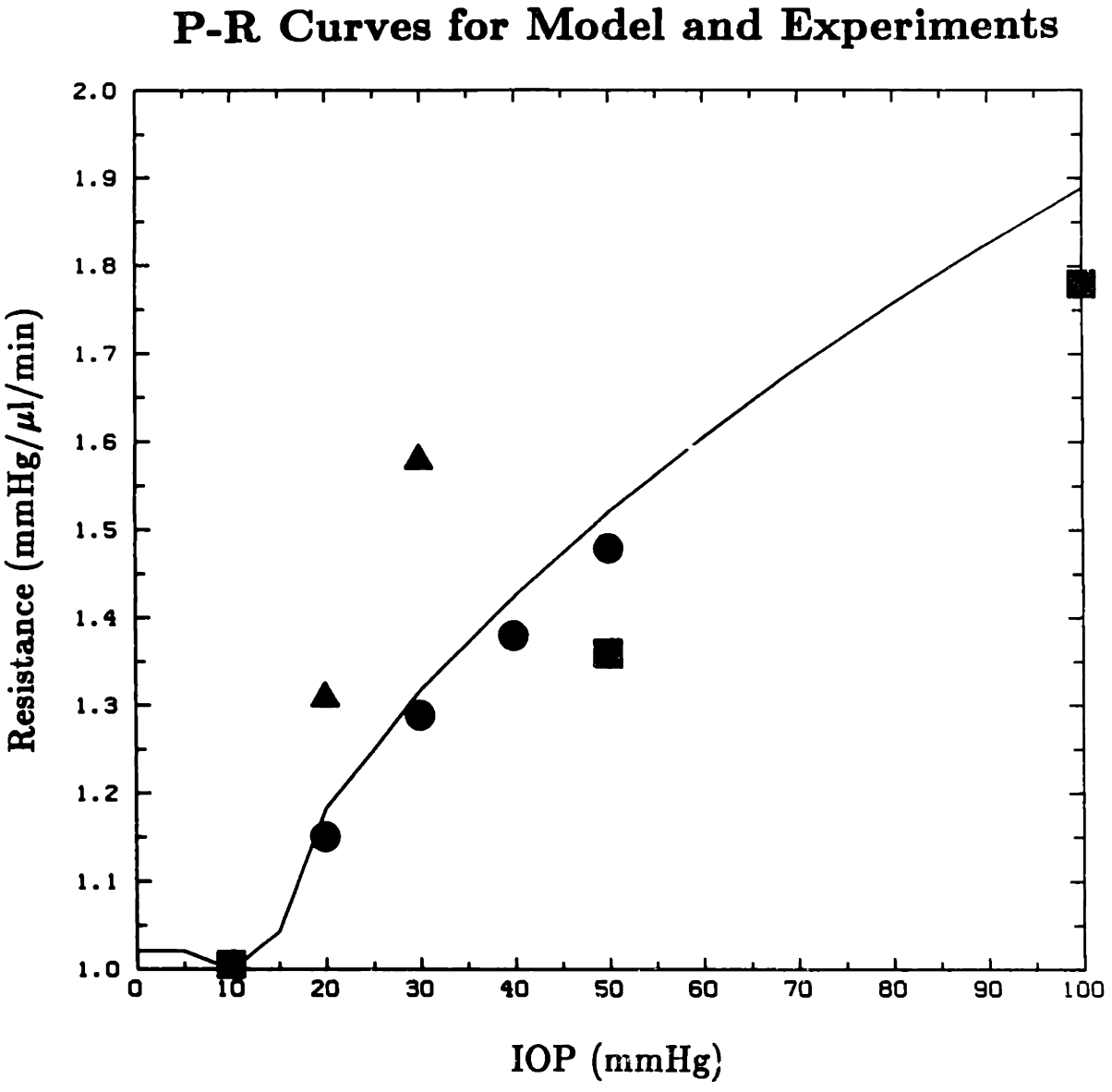

Figure 5.5—Normalized pressure-resistance data for experiments and the network model. Solid line is network model results. (●)–Brubaker[8], (▲)–Ellingsen & Grant[11], (■)–present study.

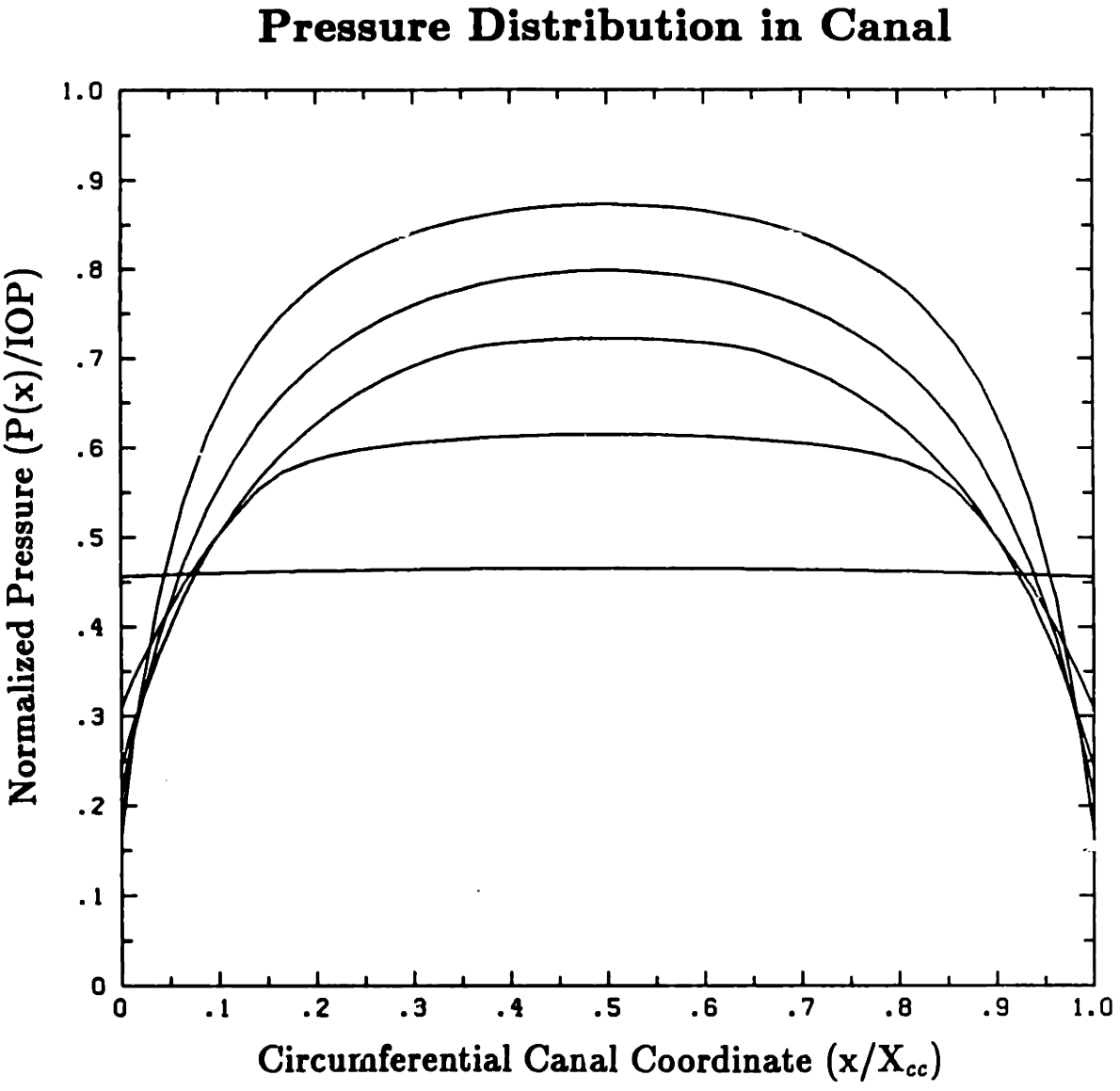

Figure 5.6—Pressure distribution in Schlemm's canal as a function of normalized distance between collector channels, which are located at 0 and 1. The pressure is normalized with respect to the IOP of each curve.

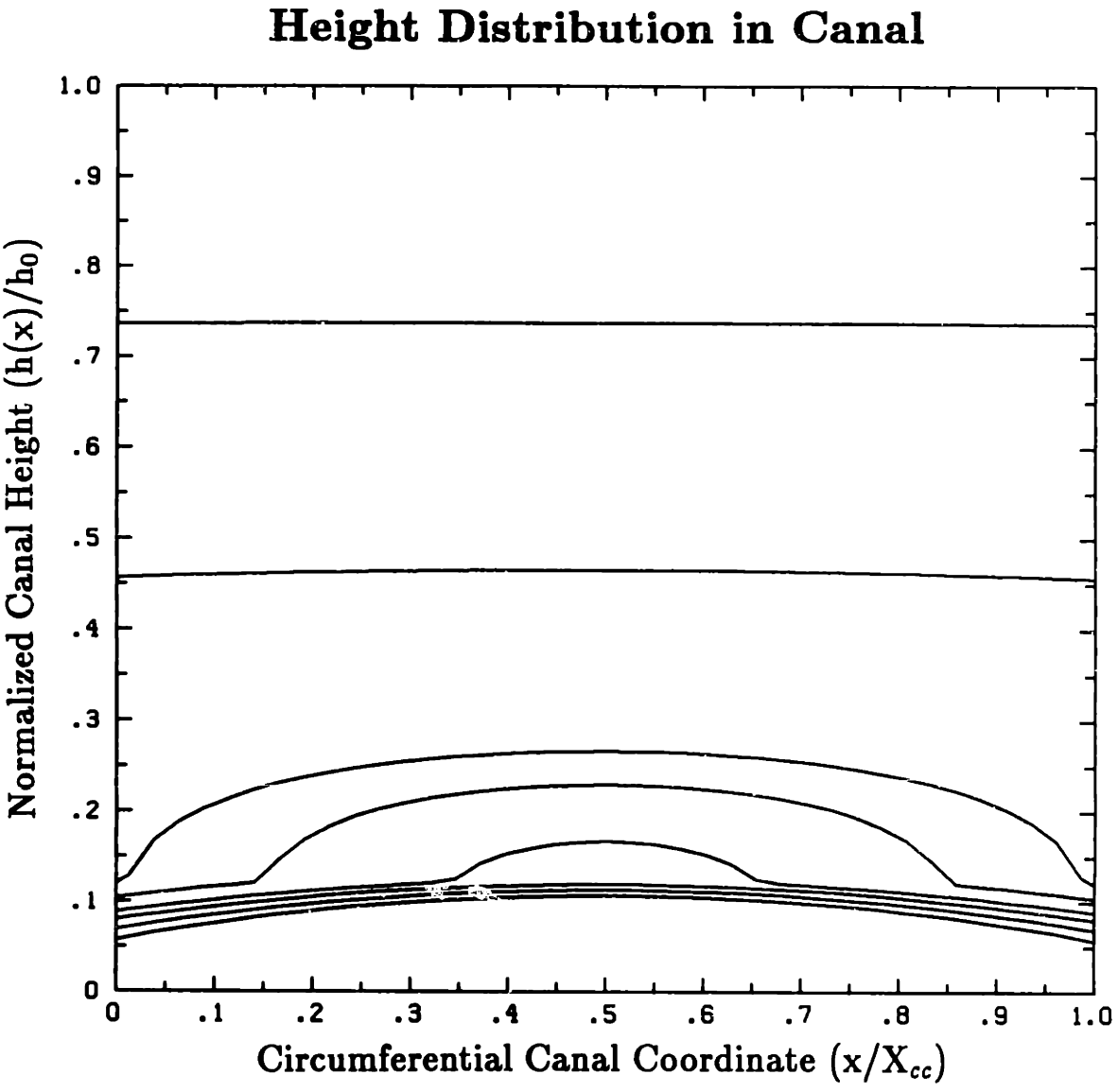

Figure 5.7—Schlemm's canal height distribution as a function IOP, plotted against the normalized distance between adjacent collector channels located at $x/X_{cc}=0$ and $x/X_{cc}=1$. The height is normalized with respect to the undeformed canal height $h_0=20$ μm.

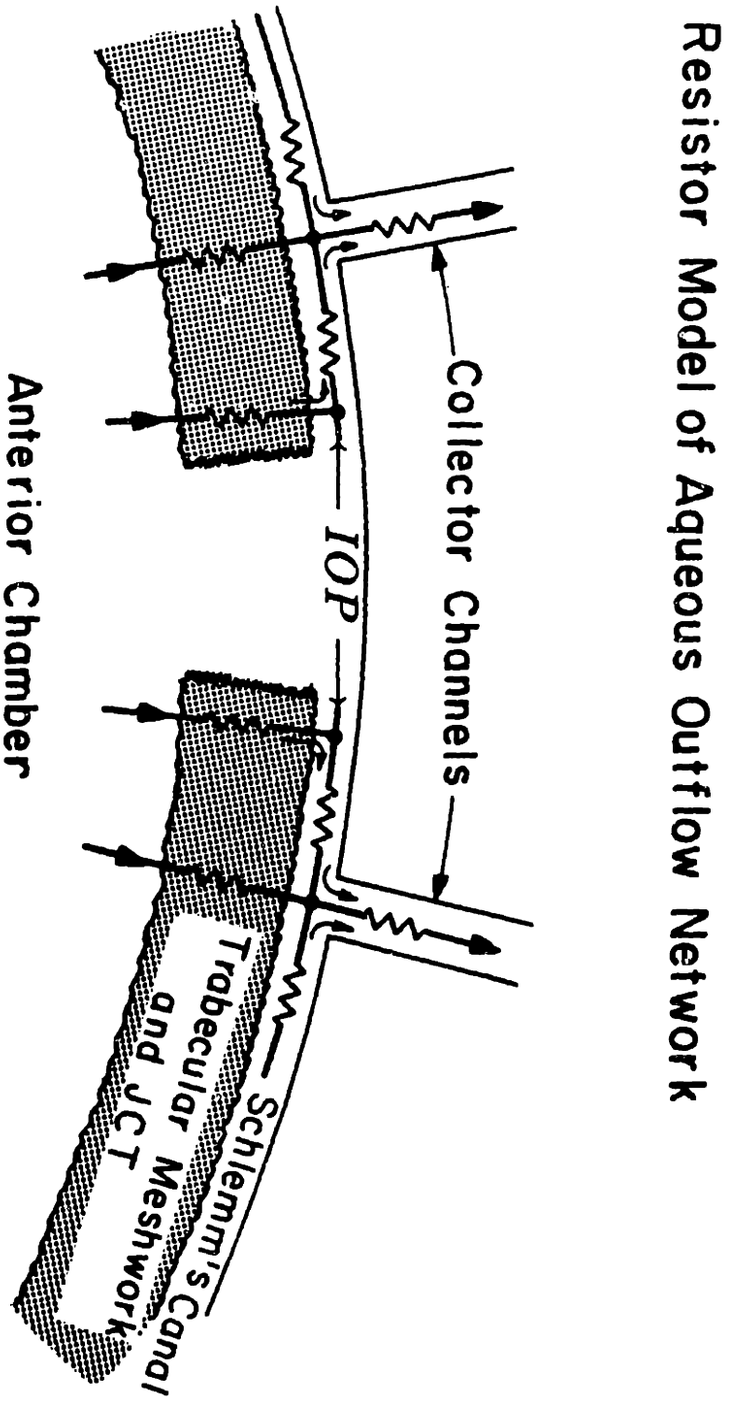

Figure 5.8—Schematic diagram of the network model after a trabecular incision has been performed. The extent of the incision is only $\sim \frac{1}{10}$ of a clock hour for clarity.

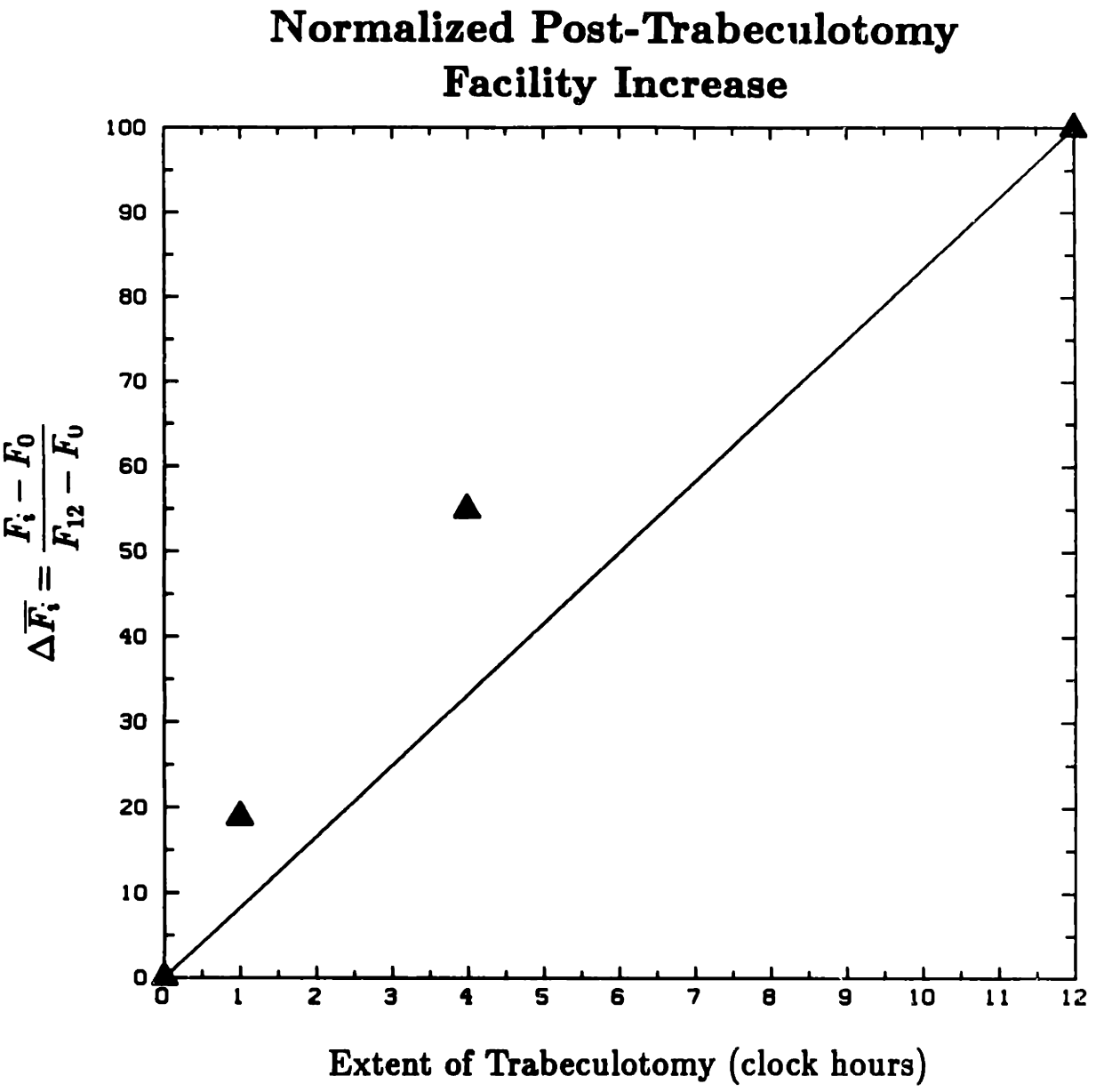

Figure 5.9—Plot of Rosenquist [26] trabeculotomy data at IOP=25 mmHg in terms of normalized facility increase. Solid line represents zero circumferential flow condition. i=0→baseline; i=1→1-hour trabeculotomy; i=4→4×1-hour trabeculotomy; i=12→complete trabeculotomy.

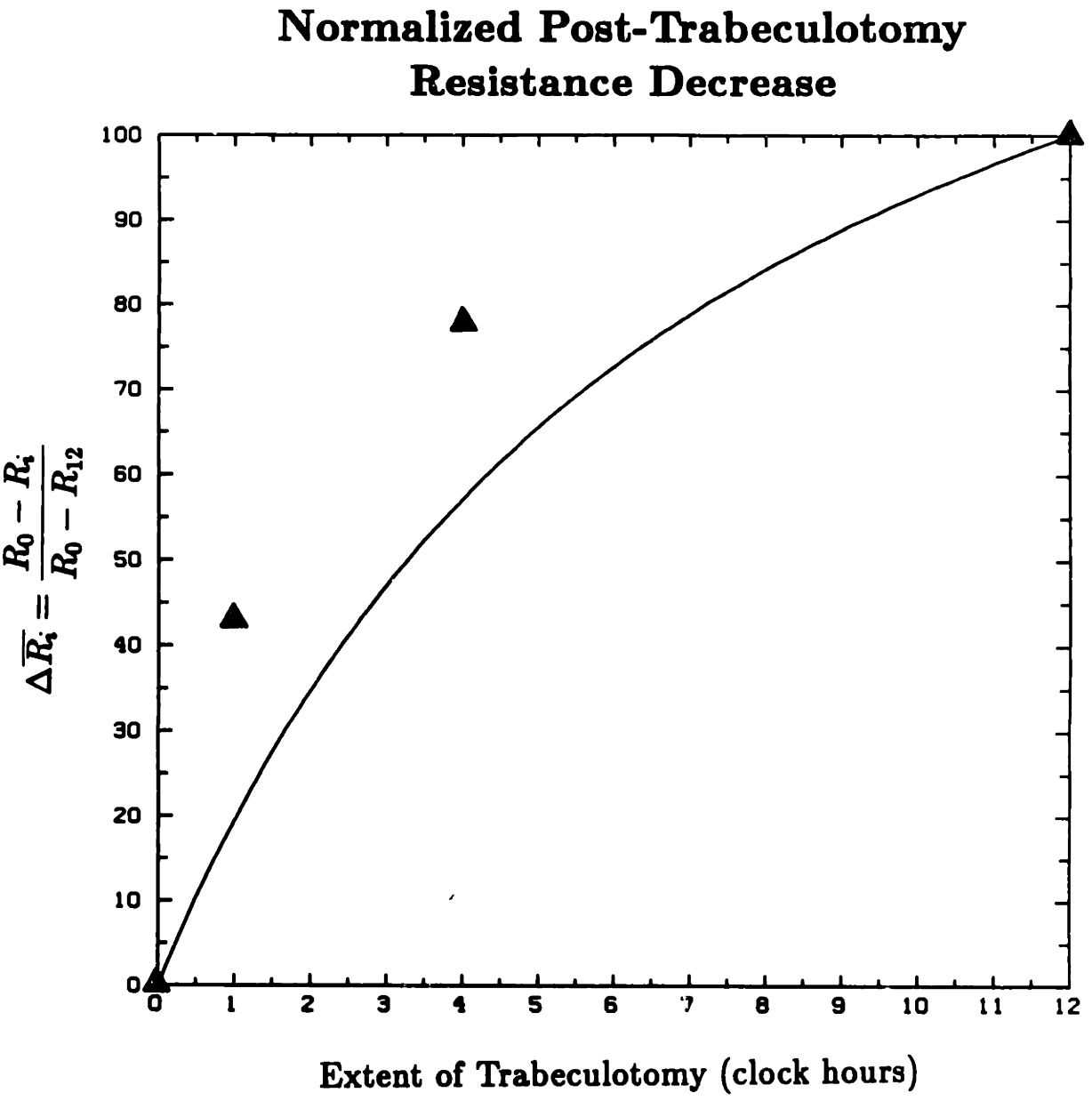

Figure 5.10—Plot of Rosenquist [26] trabeculotomy data at IOP=25 mmHg in terms of normalized resistance decrease. Solid line represents zero circumferential flow condition. i=0→baseline; i=1→1-hour trabeculotomy; i=4→4×1-hour trabeculotomy; i=12→complete trabeculotomy.

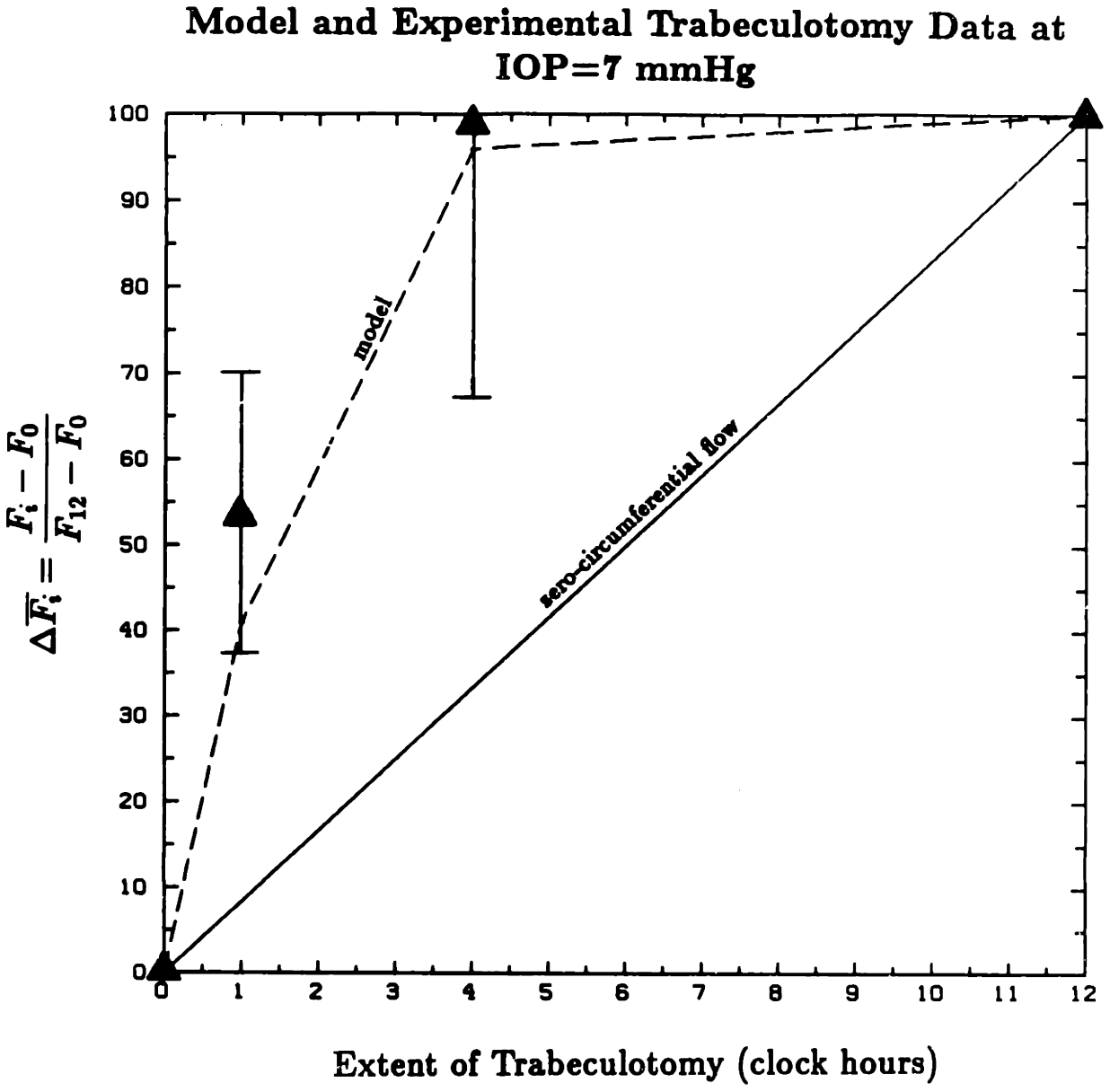

Figure 5.11—Trabeculotomy data for IOP=7 mmHg is plotted against the extent of trabeculotomy. Solid line is the zero-circumferential flow condition, dashed line is model results, and triangles are the Rosenequist data [26]. i=0→baseline; i=1→1-hour trabeculotomy; i=4→4×1-hour trabeculotomy; i=12→complete trabeculotomy.

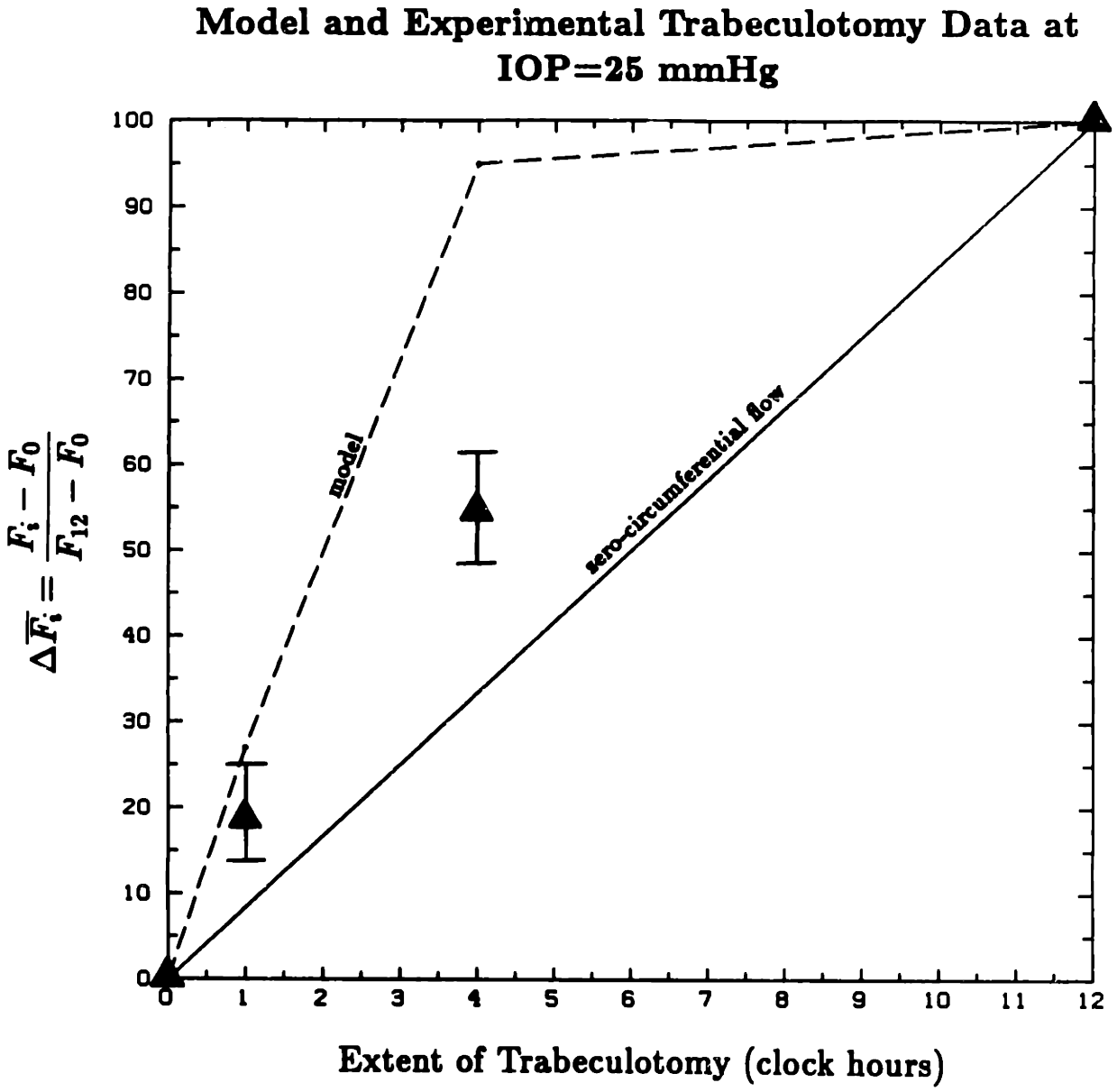

Figure 5.12—Trabeculotomy data for IOP=25 mmHg is plotted against the extent of trabeculotomy. Solid line is the zero-circumferential flow condition, dashed line is model results, and triangles are the Rosenequist data [26]. i=0→baseline; i=1→1-hour trabeculotomy; i=4→4×1-hour trabeculotomy; i=12→complete trabeculotomy.

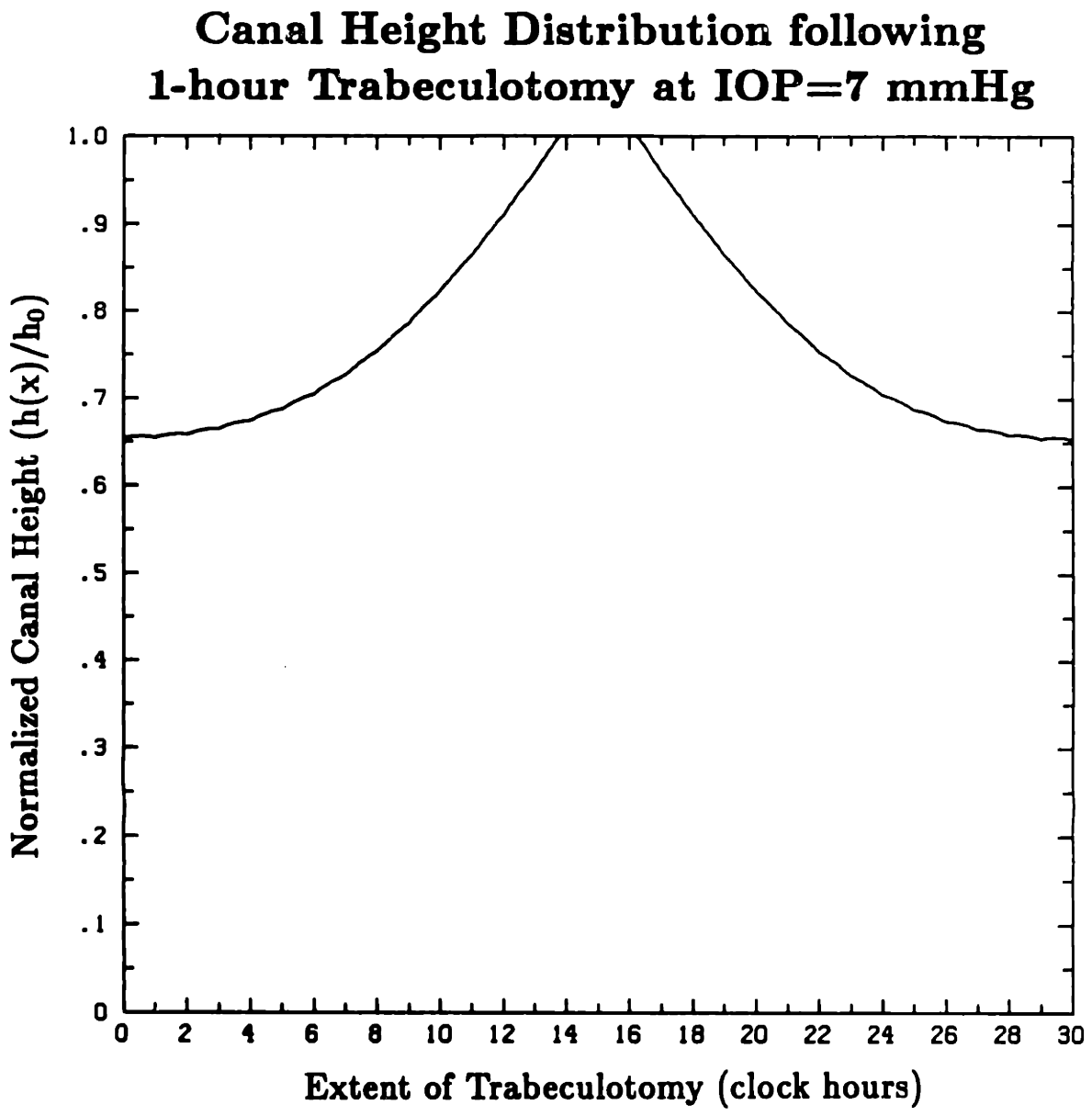

Figure 5.13—Model prediction of height distribution in Schlemm's canal as a function of circumferential coordinate for a 1-hour trabeculotomy performed at IOP=7 mmHg. The canal height is normalized by the undeformed height h_0=20 μm. The trabeculotomy incision is located from $13.75X_{cc}$ to $16.25X_{cc}$.

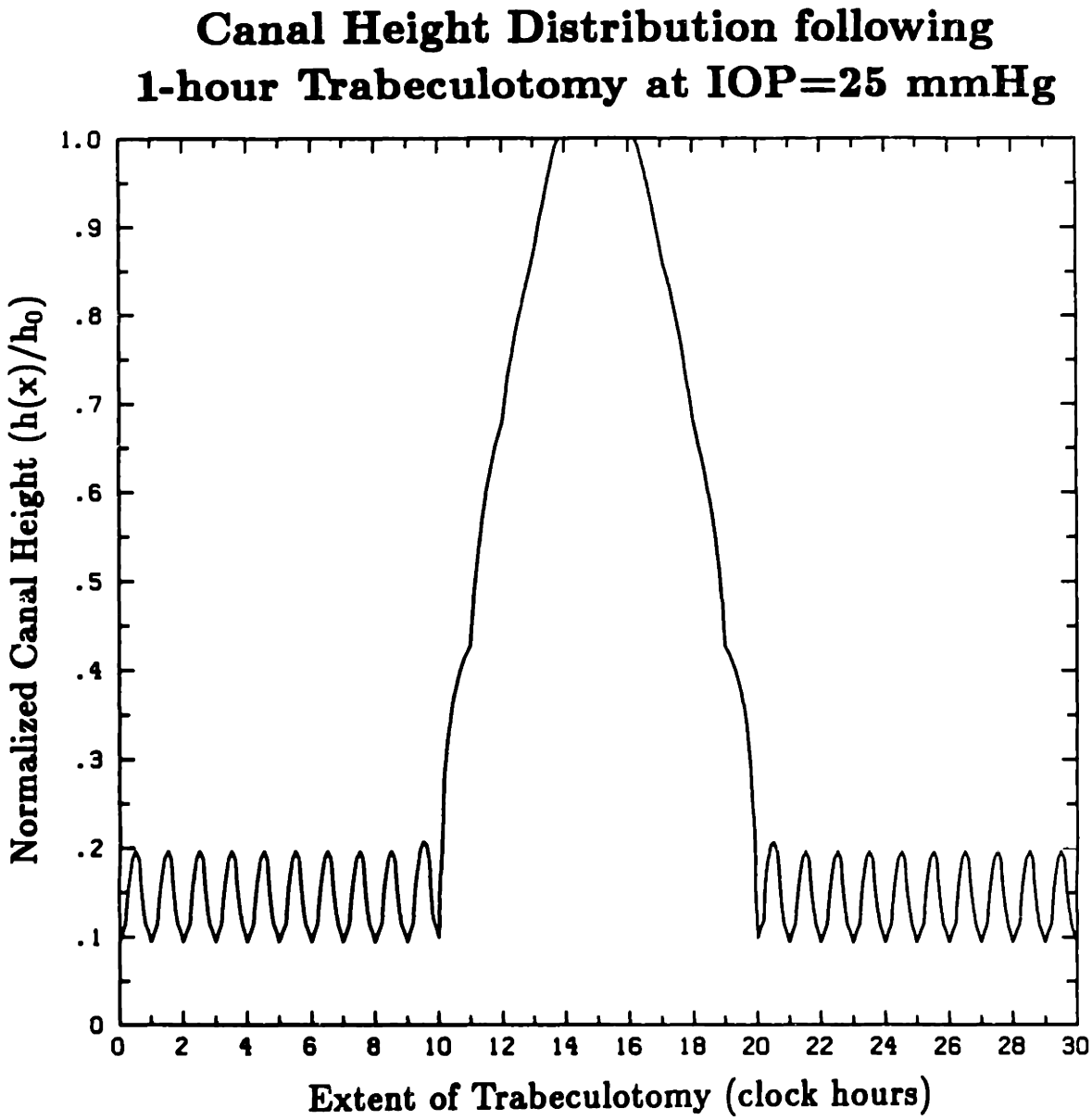

Figure 5.14—Model prediction of height distribution in Schlemm's canal as a function of circumferential coordinate for a 1 hour trabeculotomy performed at IOP=25 mmHg. The canal height is normalized by the undeformed height h_0=20 μm. The trabeculotomy incision is located from $13.75X_{cc}$ to $16.25X_{cc}$.

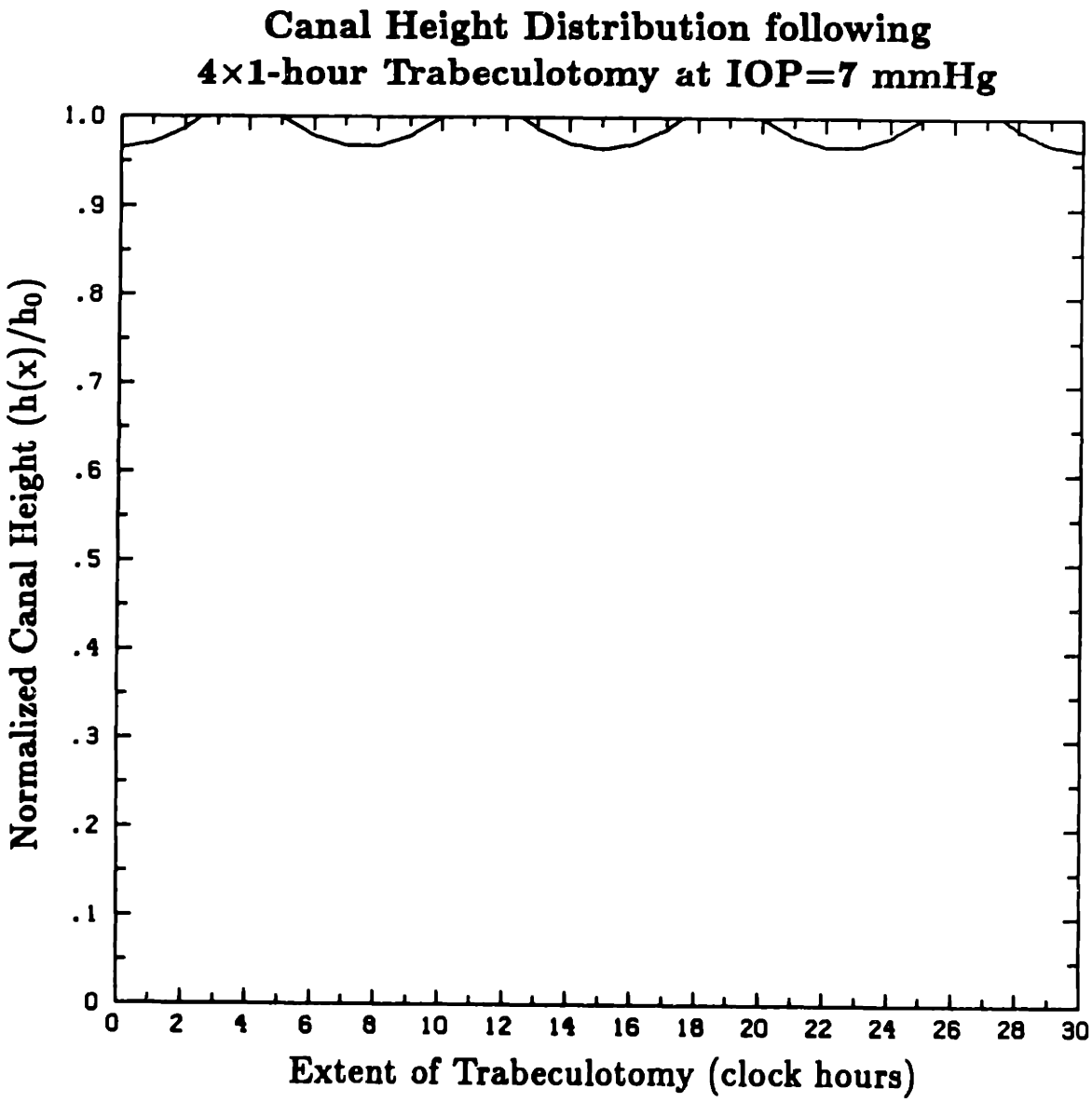

Figure 5.15–Model prediction of height distribution in Schlemm's canal as a function of circumferential coordinate for a 4×1-hour trabeculotomy performed at IOP=7 mmHg. The canal height is normalized by the undeformed height h_0=20 μm.

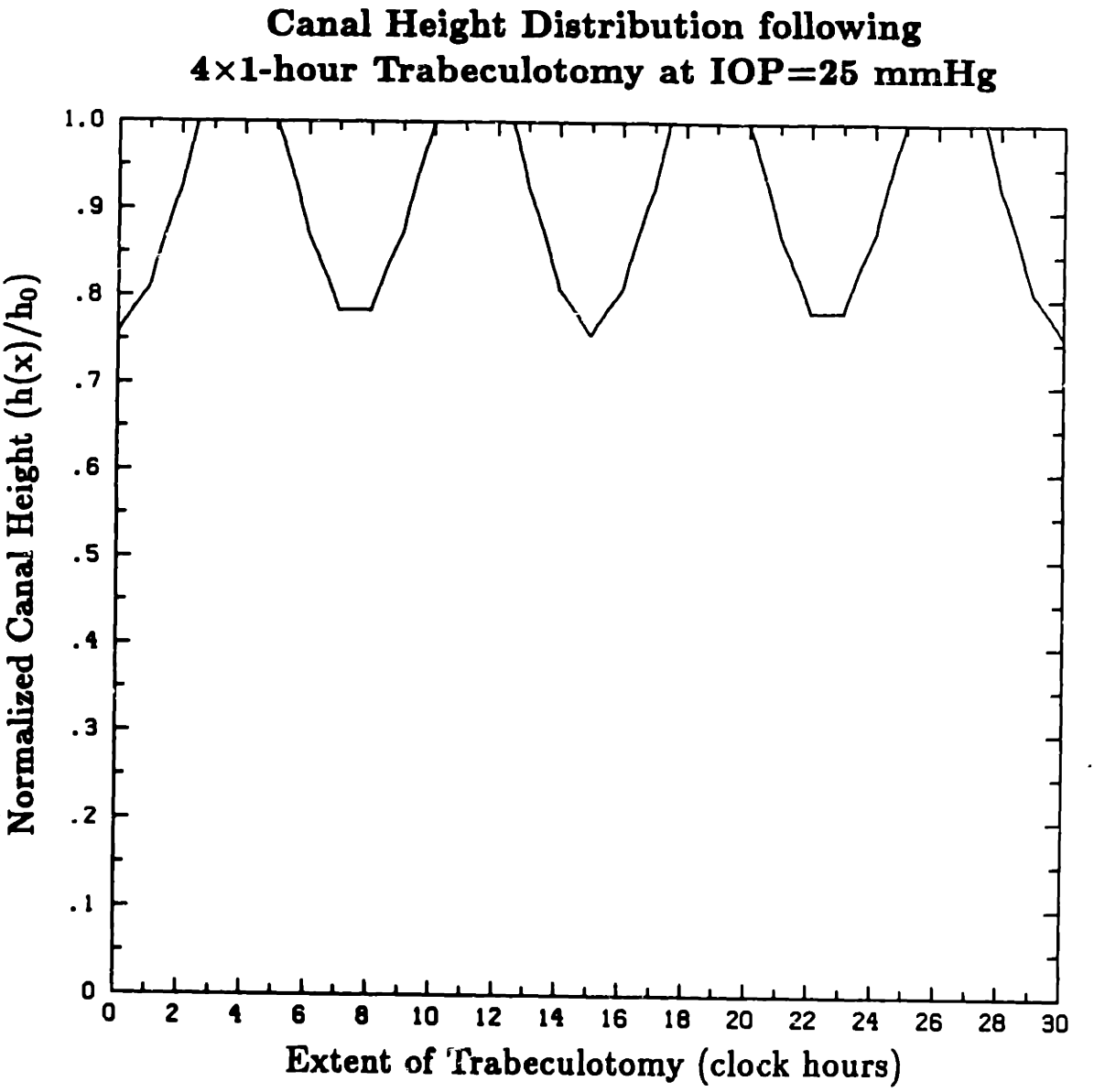

Figure 5.16—Model prediction of height distribution in Schlemm's canal as a function of circumferential coordinate for a 4×1-hour trabeculotomy performed at IOP=25 mmHg. The canal height is normalized by the undeformed height h_0=20 μm.

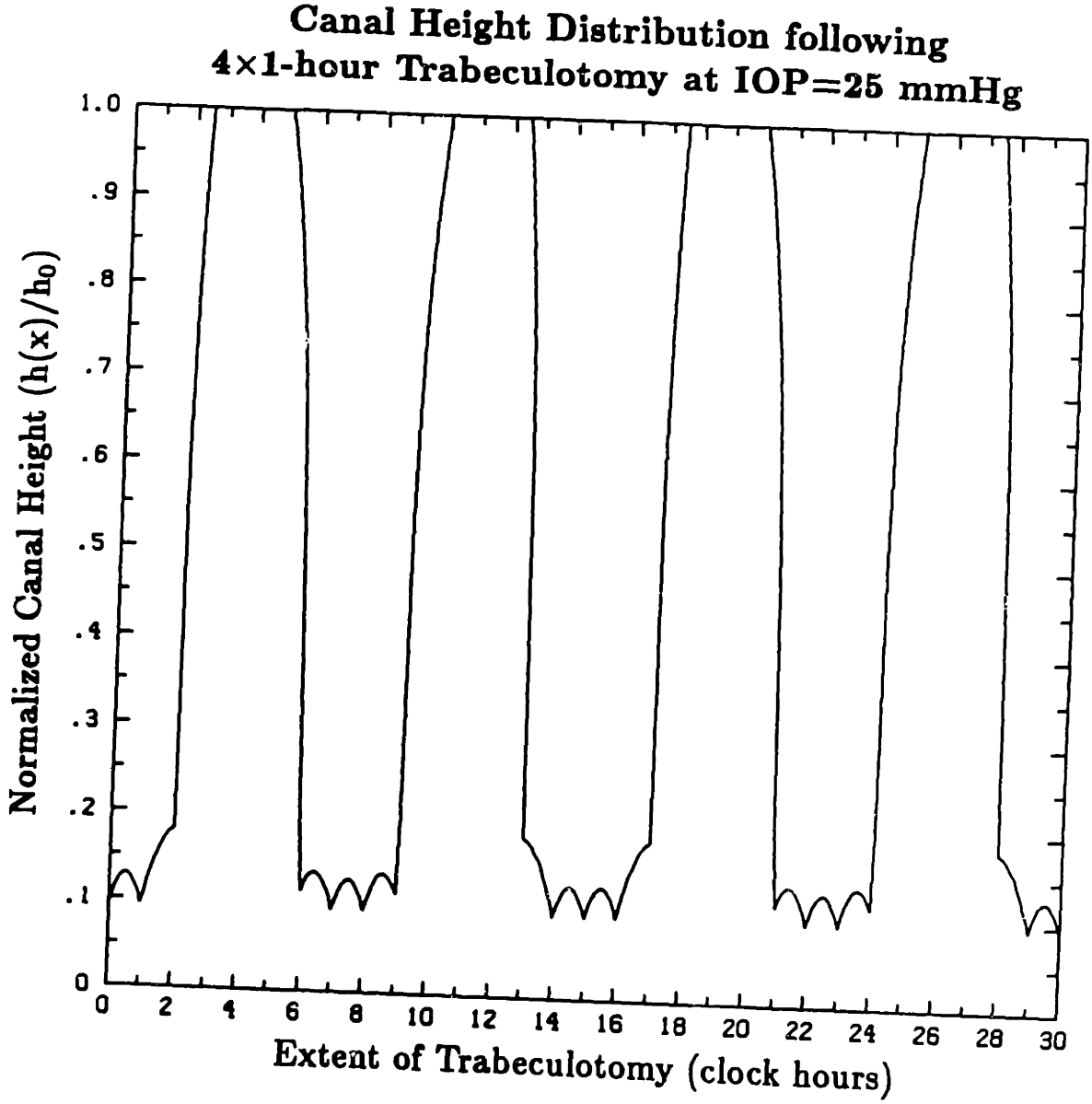

Figure 5.17—Model prediction of height distribution in Schlemm's canal as a function of circumferential coordinate for a 4×1-hour trabeculotomy performed at IOP=25 mmHg. The meshwork is weakened from E_{tm}=10 mmHg to E_{tm}=1 mmHg. The canal height is normalized by the undeformed height h_0=20 μm.

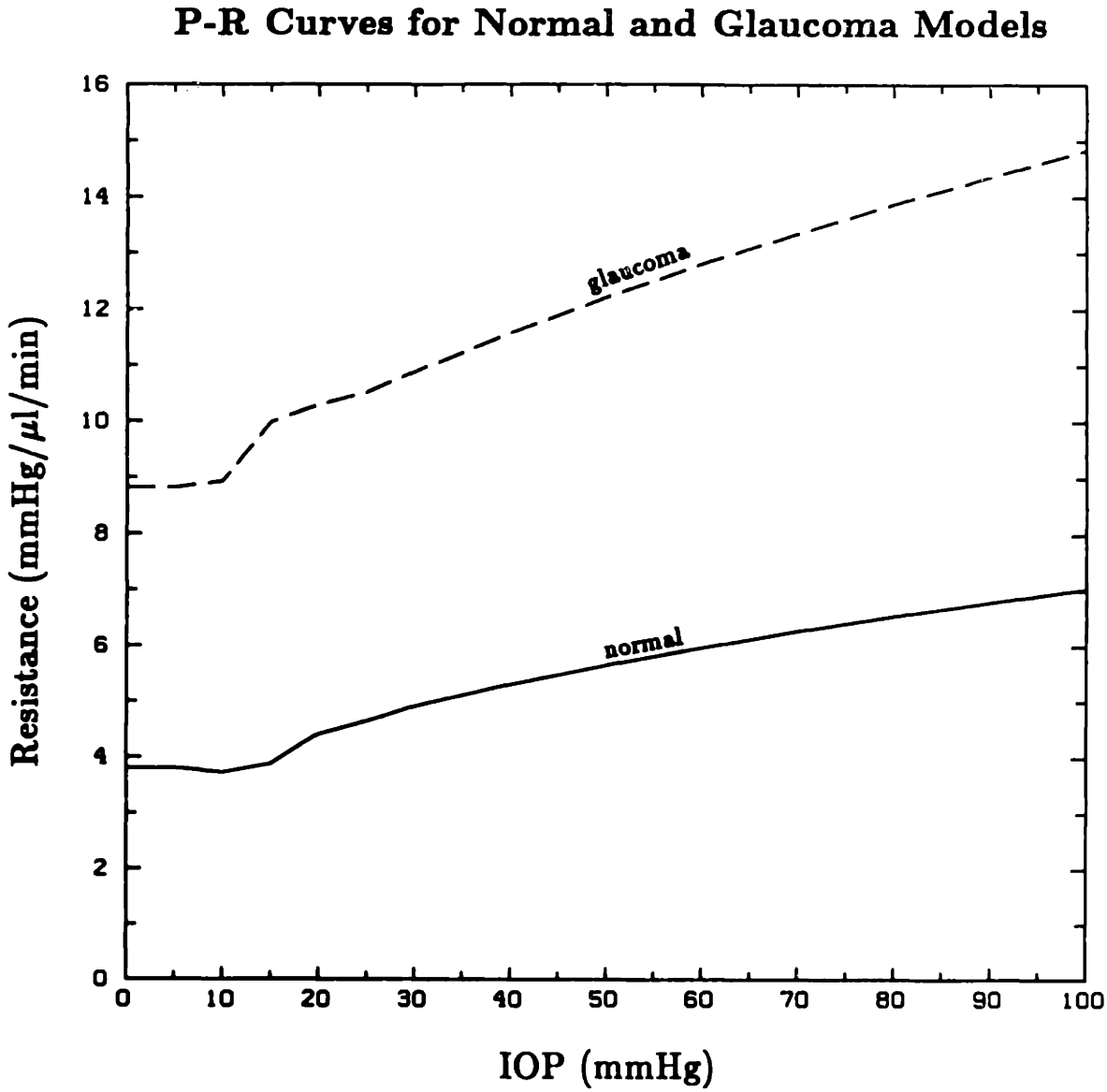

Figure 6.1—Model P-R curve for normal and glacomatous eyes. The glaucomatous eye model has an elevated meshwork resistance of R_{tm}=7 mmHg/μl/min.

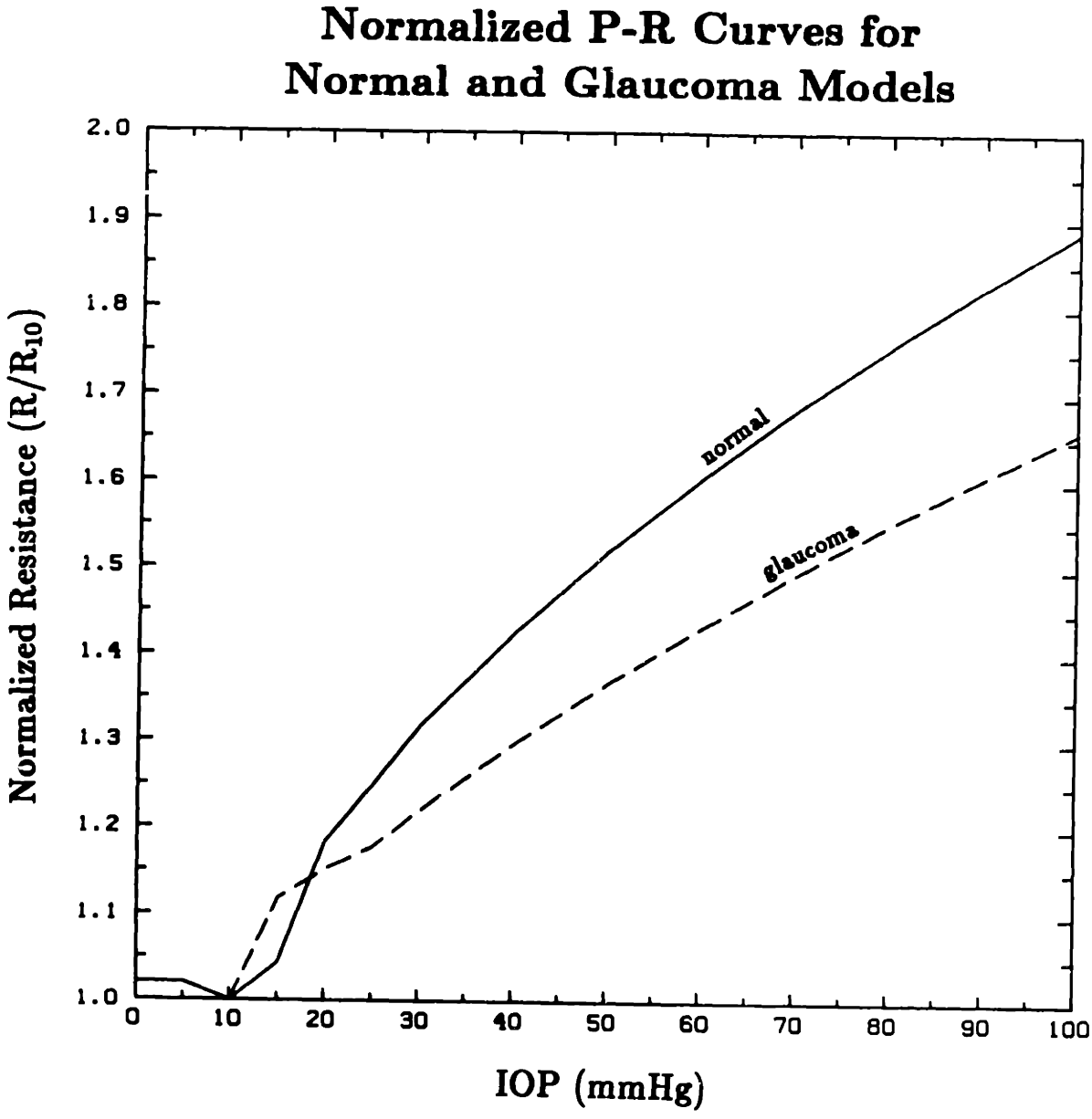

Figure 6.2—Normalized P-R curve for normal and glacomatous eyes. The glaucomatous eye model has an elevated meshwork resistance of R_{tm}=7 mmHg/μl/min. The resistances are normalized by the resistance at IOP=10 mmHg (R_{10}).

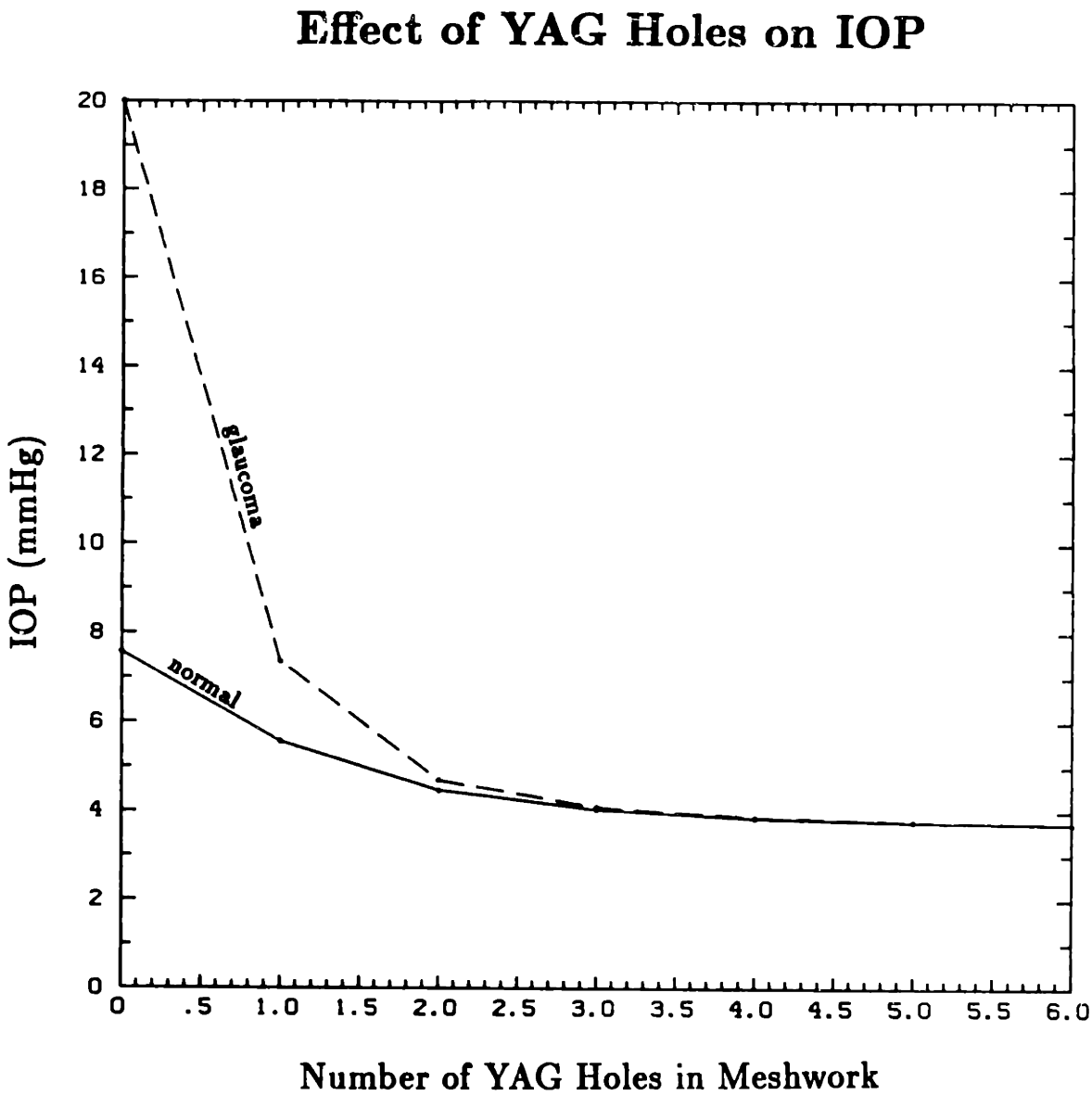

Figure 6.3—Intraocular pressure in normal and glaucomatous eye models as a function of the number of equidistantly spaced holes in the meshwork. The outflow rate Q is held constant at 2 μl/min.

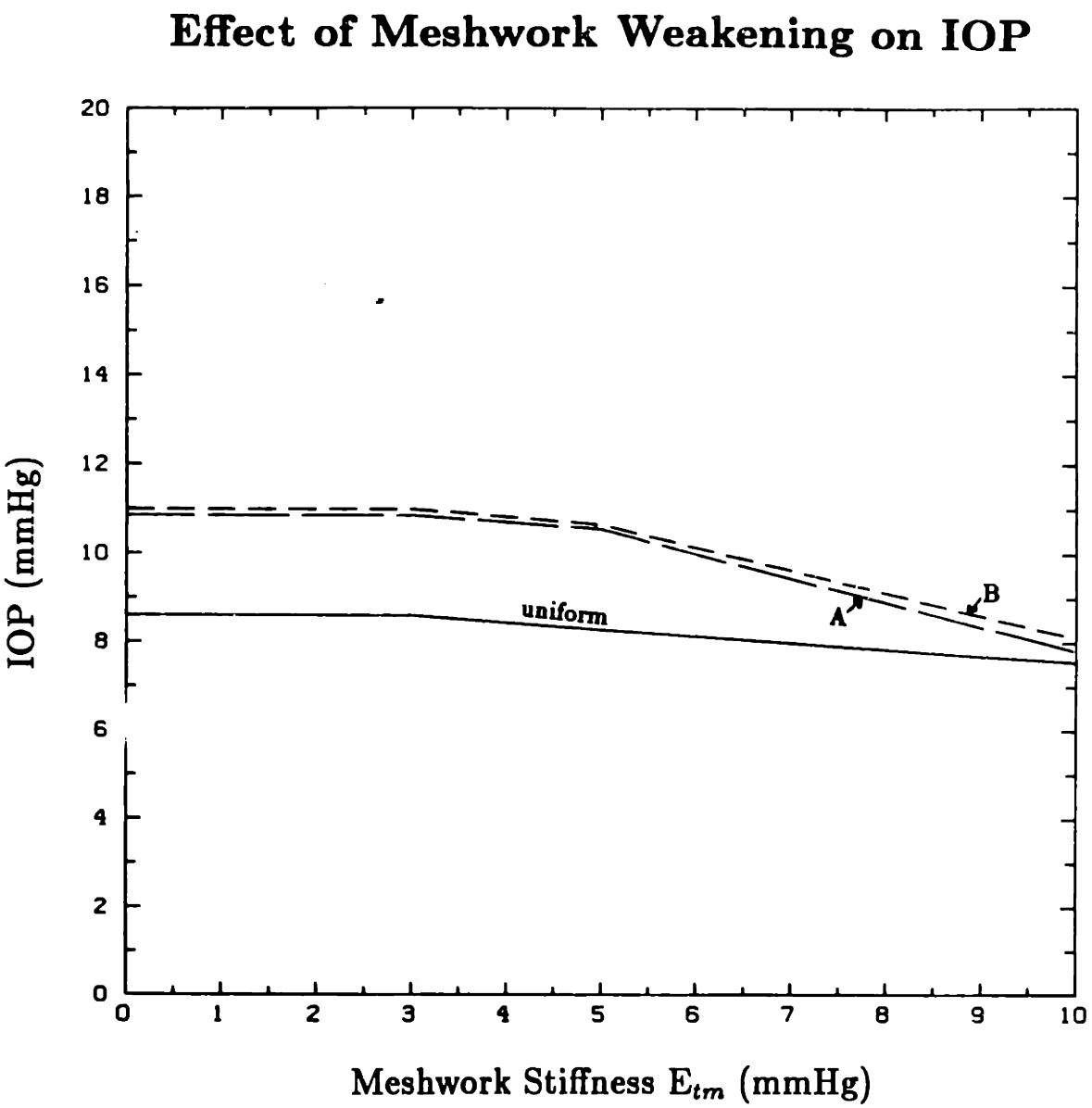

Figure 6.4—Intraocular pressure in the normal eye with various distributions of collector channels as a function of the meshwork stiffness E_{tm}. Distribution A is 5 large CC's and 25 small CC's, with the large ones spaced equidistantly $6X_{cc}$ apart. Distribution (B) is 5 large CC's concentrated in a group separated by $3X_{cc}$, $2X_{cc}$, $2X_{cc}$, and $3X_{cc}$. Flowrate Q is held constant at 2 μl/min.

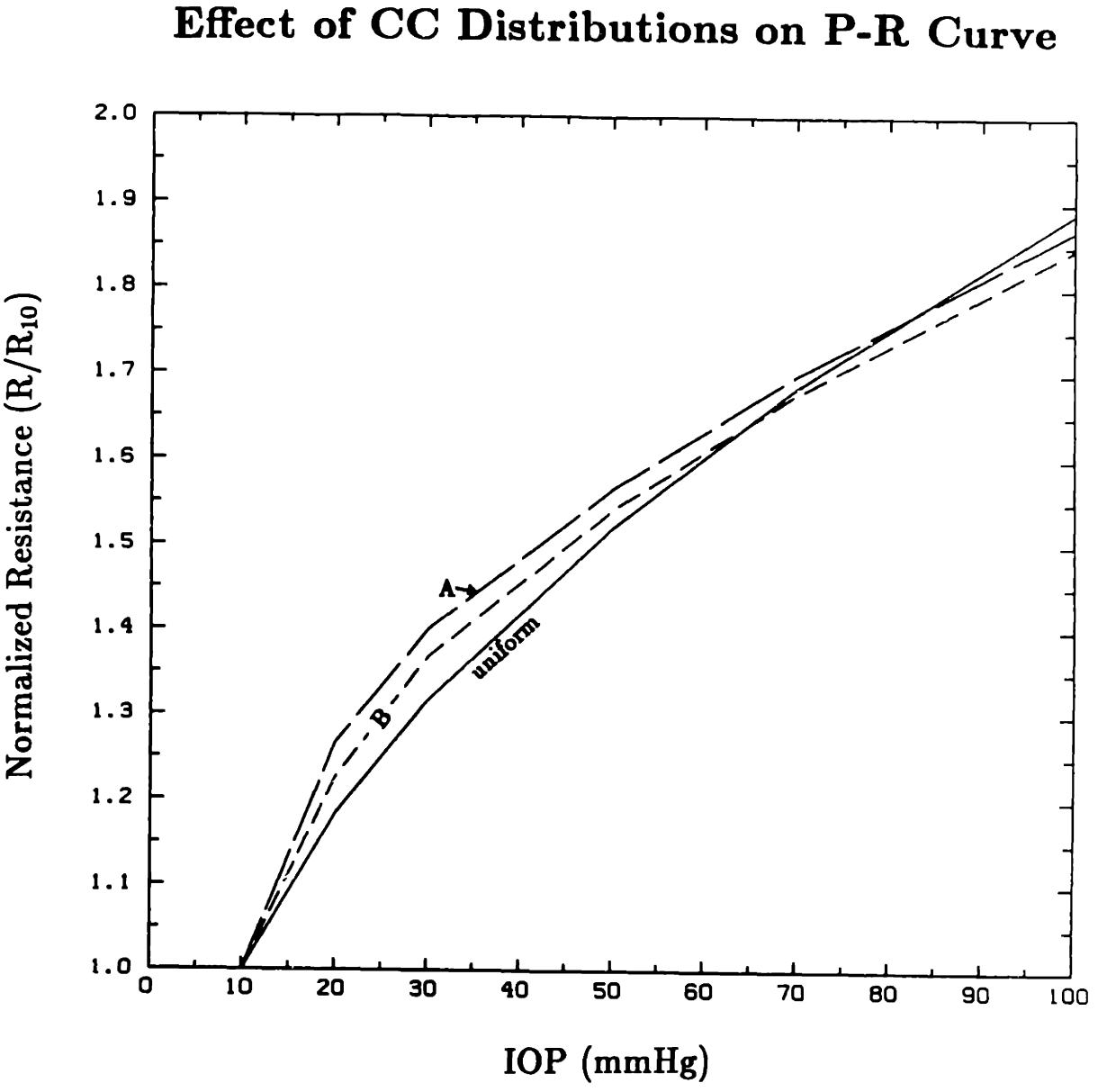

Figure 6.5—Normalized pressure-resistance curves for various collector channel distributions. Resistances are normalized by resistance at IOP=10 mmHg (R_{10}). Distribution A is 5 large CC's and 25 small CC's, with the large ones spaced equidistantly $6X_{cc}$ apart. Distribution (B) is 5 large CC's concentrated in a group separated by $3X_{cc}$, $2X_{cc}$, $2X_{cc}$, and $3X_{cc}$.